An Experiment to Test Gravity at Submillimeter Distances

Inaugural-Dissertation

zur

Erlangung des Doktorgrades der
Mathematisch-Naturwissenschaftlichen Fakultät
der Heinrich-Heine-Universität Düsseldorf

vorgelegt von
Luca Haiberger
aus Rom

Dezember 2006

Aus dem Institut für Experimentalphysik
der Heinrich-Heine Universität Düsseldorf

Gedruckt mit der Genehmigung der
Mathematisch-Naturwissenschaftlichen Fakultät der
Heinrich-Heine-Universität Düsseldorf

Referent:	Prof. Stephan Schiller, Ph.D.
Koreferent:	Prof. Dr. Klaus Schierbaum

Tag der mündlichen Prüfung: 03.02.2006

Dedicated to the memory of Wilhelm Röckrath (1950-2005)

Contents

List of Figures

Chapter 1

Introduction

The search for deviations from Newtonian gravity started in the 1970s. Its first theoretical motivation came from the attempt to determine if the universality of free fall is a fundamental principle as assumed in General Relativity [1, 2]. Moreover, the works of a number of authors suggested that a deviation from Newton's inverse-square law could be interpreted as the signature of new middle-range interactions mediated by light particles, that had not yet been observed (see for ex. [3]). These predictions gave rise to a first generation of experiments aiming to test gravity at laboratory distances. One of them, performed by Long, had great resonance, since he claimed to have detected an anomalous distance dependence of gravity over the distance range of 4 to 30 cm [4]. Several new laboratory experiments were set up to test these revolutionary results, but none of them could find any evidence of a non-Newtonian force [5, 6, 7, 8, 9, 10, 11, 12, 13]. Nevertheless the interest for experimental gravity at laboratory distances did not decline. A few years later Fischbach showed in a reanalysis of the Eötvos' experiment that the experimental knowledge of gravity at that time was still compatible with the existence of a macroscopic force, that could have a strength comparable to gravity [14]. The theoretical activity in this field grew further in the 90s, when it was clear that these kinds of experiments opened up the possibility to test some predictions of superstring-based models [15, 16, 17]. This provided the impetus for a second generation of experimental tests of the gravitation law at distances smaller than one millimeter [18, 19]. In the most sensitive among them, performed by Adelberger *et al.*, gravity was detected for the first time at distances as small as 200 μm, but no deviations from Newton's Law were found [20].

In this work we present an experiment performed at the University of Düsseldorf to detect and test gravity in the submillimeter range with a high Q mechanical oscillator.

This dissertation has the following structure. In the next chapter the theoretical motivations for our experiment are discussed. A string-based model, relying on the existence of spatial extra dimensions and their influence on gravity, is reviewed. Some other theoretical proposals are briefly introduced and their experimental relevance is discussed. Next, the constraints from recent laboratory experiments are presented. For the sake of completeness the limits to the existence of a non-Newtonian force derived from high energy and astrophysical experiments are shortly presented. In Chapter 3, after having introduced the principle on which our experiment relies, a theoretical description of its major components is given. Particular attention is paid to the sensor, a silicon torsional oscillator, and to its Brownian motion, which is the fundamental limit to the sensitivity of our apparatus. The second part of the thesis is devoted to a detailed description and characterization of the experiment. In Chapter 4 an extensive description of the procedure for the microfabrication of the silicon torsional oscillator is given. The properties of this resonant structure are then presented and compared to the results published by other authors [21, 22]. A detailed experimental characterization of the Brownian noise of such oscillators, as well as the first implementation, to our knowledge, of their laser control, is provided. Finally, the possibility of using a metal oscillator as a possible alternative to single-crystal sensors is investigated. Chapter 5 describes the gravitational excitation scheme we developed. The results of numerical simulations performed to optimize the dimensions of the source mass are also given. Next, a detailed description of the experimental apparatus and of the data acquisition routine is outlined in Chapter 6. Great attention is also paid to the crucial alignment and positioning procedure of the oscillator and the source masses. The experimental results are then presented in Chapter 7. Their compatibility with the theoretical expectation is investigated through various consistency checks and the use of three different sets of source masses. Limits to the existence of a new gravity-like force derived from the experimental results presented here are then compared to the present best limits to be found in literature [19]. Further improvement to the present setup are also suggested. Finally, a new experiment is proposed in Chapter 8, which is designed to improve the present best limits in the distance range between 0.1 and 100 μm.

Chapter 2

Theoretical background

In the picture of the world given to us by modern theoretical physics there are two fundamental energy scales. The electroweak scale $m_{EW} \sim 10^3$ GeV and the Planck scale $M_{Pl} = G^{-1/2} \sim 10^{19}$ GeV (here it is assumed that $\hbar = c = 1$). The existence of this large energy gap, also known as the hierarchy problem, has no explanation in the frame of the Standard Model, the most successful theory, to date, in high energy physics[1]. The attempts to solve the hierarchy problem have so far been based on two different theoretical approaches. Theories based on Supersymmetry, whose existence has not yet been experimentally proven, lead to the solution of this problem [23]. An alternative approach is based on the change of the geometry of space-time. This technique was applied for the first time in the 1920s by T. Kaluza and O. Klein [24, 25], who tried to unify gravity and electromagnetism postulating the existence of an additional spatial dimension[2]. The need for a higher dimensional space–time as a condition to formulate a more fundamental theory (often referred to as unified theory) was rediscovered about half a century later in the framework of the string-based model, that are considered to be very good candidate for overcoming the inadequacies of the Standard Model[3]. Generally, the existence of the extra dimensions, with a size R, of the order of the Planck length ($R \sim \frac{1}{M_{Pl}} \sim 10^{-35}$ m), is assumed. Because of their extension, there is no experimental method suited to test this assumption. Nevertheless, there have been new prospects for

[1] The Standard Model, in spite of its good agreement with the experimental results is far from being a complete theory. It contains a number of arbitrary parameters like, for example, the masses of known particles, the electric charge of the electron, the number of particle generations.

[2] The introduction of time-like extra dimensions would affect deeply well tested physics laws (e.g. no defined dynamics [26]).

[3] At present Superstring theory is neither complete nor a single theory, but rather a collection of different theories. It has been recently shown that they are aspect of a single theory, known as M-theory [27].

proving the existence of spatial extra dimensions. Some theoretical models suggest that the extra dimensions, or at least some of them, could be larger than the Planck scale and could even be of macroscopic size. This modified geometry of the space-time significantly affects the nature of gravity, which is expected to have a power law deviating from the inverse-square law at distances comparable to the size of the extra dimensions. The following sections are mainly devoted to the description of two models that predict the existence of extra spatial dimensions, and significantly modify Newton's law. Moreover, a review of some other modern theories, predicting the existence of deviations from the Newtonian gravitational law, will be given. In the last section we will briefly review the most significant experiments performed to test the previously cited theoretical models. In doing so we will focus our attention only on the most recent ones (a detailed review of experiments performed before 1998 can be found in two books by Fischbach [28], and by Chen and Cook [29]).

2.1 Compactified large extra dimensions

Superstring theory can be consistently formulated only in a nine-dimensional space. The contradiction between this statement and the number of observable dimensions is solved by postulating that the extra dimensions are very small, as small as the Planck length, which cannot be probed by any experiment. Based on these ideas, Arkani-Hamed, Dimopoulos, and Dvali developed a model, where at least some of the extra dimensions are much larger than the Planck scale [15, 16, 17]. In this section we will show how this prediction affects gravity.

In this scenario the world, as we know it, can be pictured as a 3-dimensional subspace (often referred to as brane), which is embedded in a higher-dimensional space. One special property of the brane is that all the Standard Model fields are confined on it. This can be seen as a consequence of the fact that particles are described by the vibrational modes of one-dimensional strings that can be open or closed. Open strings (e.g. photons) have their ends attached to the brane, while closed strings (e.g. gravitons) can move in the complete $(3+n)$-dimensional space, where n is the number of extra dimensions[4]. Since Newton's Law is a natural result of the dimensionality of space, it is to be expected that gravity's power law is changed by the existence of the extra dimensions. A well-known property of a 3-d space is that the integral of the gravitational field over a closed

[4]It has been shown that electrical charge cannot exist in the extra dimensions. It is a consequence of the fact that photons are confined on the 3-dimensional brane and no single charge can exist in a part of the space which is not accessible to the electric field [15].

surface is a constant (Gauss' Theorem). Let us assume the validity of this property also in a space with $3+n$ dimensions. The gravitational field exerted by a mass M on a test mass m then obeys the following equation

$$F = -G_{(4+n)}\frac{Mm}{r^{2+n}}, \tag{2.1}$$

where $G_{(4+n)}$[5] is the generalized gravitational constant in the higher-dimensional space. This result shows that the presence of the extra dimensions dramatically changes gravity. If one imagines that the extra dimensions have an infinite extension, Eq. (2.1) has to be valid at any distance, which contradicts the results of gravity measurements at terrestrial and planetary distances [28].

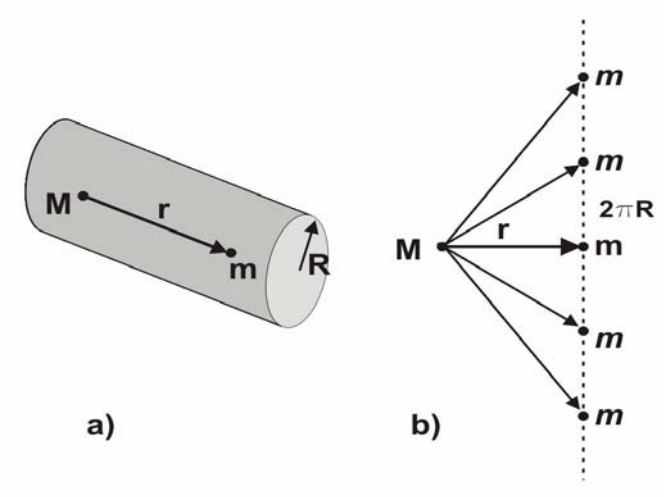

Figure 2.1: a) Model of a 2-d space consisting of an ordinary dimension (in the picture it is represented by a line, which contains the Standard Model fields, masses and charges) and one large extra dimension that is curled up and has the radius R. b) The image method: the compactified dimension is unrolled. The resulting flat space has a $2\pi R$ periodicity. (Picture adapted from Ref. [30].)

Following the proposal of Arkani-Hamed, Dimopoulos and Dvali, we will assume now that the extra dimensions are curled up and have a radius R, as shown in Fig. 2.1(a) for the subspace made of one 'normal dimension' of infinite extension, plus an extra compact dimension. In order to investigate the effect of the size of R on gravity, it is convenient to use the method of the images. Two masses, M and m, are at the distance r and rest both on the 3-d brane (in the picture it is represented by a line). Unrolling the extra

[5] The subscript $(4+n)$ takes into account the existence of one time dimension.

dimension on a plane of infinite extension, one gets a space with a $2\pi R$ periodicity as shown in Fig. 2.1(b). The interaction of the mass M with m and its images is then given by

$$F(r) = -\sum_{k\in\mathbb{Z}^n} G_{(4+n)} \frac{Mm}{\left(r^2 + \sum_{i=1}^{n} (2\pi R k_i)^2\right)^{\frac{n+2}{2}}} \frac{r}{\sqrt{r^2 + \sum_{i=1}^{n} (2\pi R k_i)^2}}. \tag{2.2}$$

If we assume now that the distance between the masses is much smaller than the radius of the extra dimensions ($r << R$), the contributions due to image masses are much smaller than the term for $k_i = 0$ (which corresponds to the direct attraction between the two real objects) and Eq. (2.2) reduces to Eq. (2.1).

In the limit $r >> R$ the distance between the masses is so large that the distribution of the images can be approximated by a continuum and Eq. (2.2) becomes

$$\begin{aligned} F(r) &\simeq -G_{(4+n)} Mm \int_{-\infty}^{+\infty} d^n k G_{(4+n)} \frac{r}{\left(r^2 + \sum_{i=1}^{n} (2\pi R k_i)^2\right)^{\frac{n+2}{2}}} \\ &= -G_{(4+n)} \frac{Mm}{r^2} \left(\frac{1}{2\pi R}\right)^n \int_{-\infty}^{+\infty} d^n x \frac{1}{\left(1 + \sum_{i=1}^{n} x_i^2\right)^{\frac{n+3}{2}}} = -G_{(4+n)} \frac{C_n}{R^n} \frac{Mm}{r^2}, \end{aligned} \tag{2.3}$$

where

$$C_n = \frac{1}{(2\pi)^n}^n \int_{-\infty}^{+\infty} d^n x \frac{1}{\left(1 + \sum_{i=1}^{n} x_i^2\right)^{\frac{n+3}{2}}} \tag{2.4}$$

is a constant.

If $r \sim R$, it can be shown that the gravitational force has the following form

$$F = -G_{(4+n)} \frac{Mm}{r^2} \left[1 + \alpha(1 + \frac{r}{\lambda}) e^{-\frac{r}{\lambda}}\right], \tag{2.5}$$

where α and λ depend on the fundamental constants n and R, and on the topology of the space[6]. Assuming a toroidal compactification, for example, it is found that $\alpha = 2n$ and $\lambda = R$, while $\alpha = n + 1$ and $\lambda = R/\sqrt{n}$ in the case of a spherical compactification.

Using Eq. (2.3) and $M_{Pl_{(4)}}^2$, it can be found that[7]

$$M_{Pl_{(4)}}^2 \sim R^n \left(M_{Pl_{(4+n)}}^2\right)^{n+2}, \tag{2.6}$$

[6] This correction is often referred to as the Yukawa correction.

[7] The exponent of $M_{Pl_{(4+n)}}$ is chosen in such a way that $M_{Pl_{(4)}}^2$ and $M_{Pl_{(4+n)}}$ have the same physical dimensions.

where $M^2_{Pl_{(4+n)}}$ is (4+n)-dimensional Planck constant, which corresponds to the energy scale at which gravity is unified with the Standard Model fields. The authors of this model assume then that the unification takes place at the electroweak scale (∼1 TeV) in the (4+n)-dimensional space. Using Eq. (2.6), it is possible to calculate values for R as a function of the number of extra dimensions, n, as shown in Table I.

Table I. Size of the compactification radius vs number of extra dimensions.

n	1	2	3	4	5	6
R (m)	$\sim 10^{13}$	$\sim 10^{-3}$	$\sim 10^{-8}$	$\sim 10^{-11}$	$\sim 10^{-13}$	$\sim 10^{-14}$

While the scenario with one large extra dimension is ruled out by gravity measurements at planetary distances, for $n \geq 2$ the existence of the extra dimensions cannot be excluded. This is a consequence of our poor experimental knowledge of gravity at distances smaller than 1 mm [28]. Taking this into account, gravity measurement at laboratory distances gives us, in principle, the possibility to prove the existence of extra dimensions.

The solution to the hierarchy problem proposed by Arkani-Hamed, Dimopoulos and Dvali can be summarized as followed:

Assuming the electroweak scale as the only fundamental energy scale in a space with compactified extra dimensions, gravity is expected to be stronger than experiments show; the apparent weakness of gravity is due to the fact that it is diluted in the extra dimensions.

Actually, this is not a complete solution to the hierarchy problem, because a new fundamental scale, R, is incorporated into the theory. Nevertheless this approach gives the possibility, for the first time, to perform a test of some predictions of superstring theory at low energies.

2.2 Warped extra dimensions

An alternative perspective has been proposed by Randall and Sundrum [31]. In this model, space is made of two 3d-branes connected by a warped extra dimension. The metric of this non-factorizable space is given by

$$ds^2 = e^{-2\pi k y}\eta_{\mu\nu}dx^\mu dx^\nu + \pi r dy^2, \tag{2.7}$$

where k is a constant of the order of the Planck scale and describes the curvature of the extra dimension ($e^{-2\pi k y}$ is referred as to warp factor), x^μ is the coordinate of the

known 4-dimensional space, r is the size of the extra dimension, and $0 \leq y \leq 1$ is the coordinate of the warped extra dimension. The brane at $y = 0$ is known as Planck brane, while the other, at $y = 1$, is the brane where the Standard Model fields are confined. Gravity is concentrated ("quasilocalized") on the Planck brane and its strength decreases exponentially as it propagates through the extra dimension. Because of the warp factor, it reaches the experimentally measured strength on the second brane. This condition is fulfilled if $kr \sim 10$, and since $k \sim 10^{18}$ GeV, the extra dimension is much smaller ($\sim 10^{-33}$ m) than in the model with large extra dimensions.

The solution of the hierarchy problem given by Randall and Sundrum is the following:

The source of the large hierarchy between the observed Planck and the weak scale is the warp factor.

In analogy to the previous model, also in this case the proposed solution still contains two different scales: the electroweak scale and the size of the extra dimension.

Under the assumption of a very small k (~ 0.1 mm), Chung *et al.* showed that experimental tests of Newtonian gravity could distinguish this scenario from the model by Arkani-Hamed, Dimopoulos, and Dvali, since the correction to the newtonian potential has, in the Randall-Sundrum scenario, the following form

$$V(r) = -\frac{GMm}{r}\left(1 + \frac{2}{3k^2r^2}\right), \tag{2.8}$$

for $kr \gg 1$ [32].

2.3 Predictions from other theories

The scientific value of the experimental tests of Newton's Law is not limited to the search for extra dimensions. In this section we will briefly review some other modern theories that predict the existence of new fields that couple to mass.

Several string-based models require the existence of gravitationally-coupled scalars, known as moduli. These particles are massless at the Planck scale and they obtain a mass as a consequence of Supersymmetry breaking. Assuming that supersymmetry breaking takes place at low energy, for example in the range $(H)^{1/2}$ = 1-10 TeV, the mass of the moduli is given by

$$m \cong \frac{H}{M_{Pl}} \sim 10^{-4} - 10^{-6}\text{eV}. \tag{2.9}$$

This mass corresponds to a Compton wavelength in the range of 1 mm to 10 μm and is the source of deviations from Newton's Law at this distance range [33].

Antoniadis, Dimopoulos and Dvali proposed a theory in which supersymmetry breaking takes place at the electroweak scale in the presence of one extra dimension [34]. A modulus, known as radius modulus, is associated with the size of the large compact dimension of the order of the weak scale ($\sim 10^{-19}$ m). This scalar field is essentially given by the logarithm of the radius of the large extra dimension and its strength is expected to be 1/3 of gravity at sub-mm distances.

Another modulus that couples to mass is the dilaton [35]. Veneziano and Taylor [36] calculated that it can lead to a force with a strength 2000 times larger than gravity.

In strong interaction, non-perturbative effects induce the violation of parity (P) and charge conjugation-parity (CP), which has not yet been observed. Peccei and Quinn developed a model in which a light-mass boson, the axion, mediates a short-range mass-mass interaction. The present upper bounds to the CP violation, derived from measurements of the neutron electric dipole moment, do not rule out the existence of an axion-mediated interaction with a strength of about one thousandth of that of gravity at distances of the order of 200 μm [37, 38, 39, 40].

In the frame of loop quantum gravity, G. G. Kirilin and I. B. Khriplovich [41] calculated the correction to the Newton potential due to two-graviton interaction between two masses m_1 and m_2 obtaining:

$$V(r) = -G_{(4)}\frac{m_1 m_2}{r}\left(1 + \frac{763}{30\pi}\frac{G_{(4)}\hbar}{c^3 r^2}\right). \tag{2.10}$$

The correction in this case is about 10^{60} times smaller than gravity at a distance of 0.1 mm, still far beyond the present sensitivity of experimental tests.

2.4 Laboratory tests

Since the first gravitational measurement by H. Cavendish, the torsion pendulum has played a central role in experimental gravitational physics [42]. This device is one of the most sensitive force sensors that has been developed so far. In most experiments its sensitivity is limited by the seismic noise background because of its sub-Hz resonance frequency. A modern version of this experiment was performed by Adelberger and coworkers in 2001 with the aim to detect the deviation from Newton's Law predicted by the large extra dimensions model [20]. The torsion pendulum consists of a 1 mm thick aluminium anulus (radius approx. 50 mm), provided with an array of ten equally spaced holes, while the source mass consists of two copper disks provided with a similar array of holes. The source mass is rotated with a frequency of about 10^{-4} Hz. This experiment presents two interesting features. The detection of the torque is performed at the tenth

harmonic of the source mass rotation frequency in order to reduce the influence of the vibrations associated with the torque drive. Moreover, adjusting the relative position of the two disks in the source mass stack, it is possible to cancel the torque due to the Newtonian background. Any signal measured under this condition would come from a non Newtonian interaction. This experiment attained a torque sensitivity of 10^{-16} Nm and made it possible for the first time to detect gravity at distances as small as 210 μm. However, no deviations from the expected Newtonian signal were observed. A lower bound of 4 TeV for the unification energy (see Eq. (2.6)) was set. Because of low frequency seismic noise, the gap between the test masses could not be reduced further.

An alternative experimental approach was suggested by J. Price [18]. Since the sensing element is, in this case, a mechanical oscillator with a frequency in the kHz range, the sensitivity of the experiment is not limited by seismic noise, but by Brownian noise. A torsional oscillator made of tungsten and having an area of 1 cm^2, a thickness of about 250 μm, and a resonance frequency of about 1 kHz, is used to detect the gravitational field produced by a 305 μm thick tungsten plate driven at the oscillator resonance frequency. A thin conducting shield is set between the test masses in order to eliminate possible electrostatic disturbances. To date the existence of new fields with a strength 3 times larger than gravity at the distance of 108 μm has been ruled out [43]. A low temperature version of this experiment is planned to improve the sensitivity to non-Newtonian forces.

Another high frequency experiment was performed by A. Kapitulnik and coworkers. In this case a microfabricated cantilever (250 μm in length, 50 μm in width, and 0.335 μm thick) with a 50 μm gold cube mounted on its top is used as a resonant sensor. The source mass consists of an array of alternating parallel strips of gold and silicon, that are periodically moved in the direction orthogonal to their long side. In this way a mass modulation in front of the sensor is produced. The sensor and the source masses are separated by a 3 μm thick electrostatic shield, while the gap between the masses is 20 μm. The present sensitivity of this experiment is limited by an unknown disturbance, which is three times larger than the thermal noise level.

Bounds to the existence of non-Newtonian mass-coupled fields can be set also by experiments aiming to measure the Casimir and van der Waals interaction [44, 45]. Fig. 2.2 shows a comparison between the limits derived from the Casimir force measurement by Lamoreaux [46] and from the others works presented in this section.

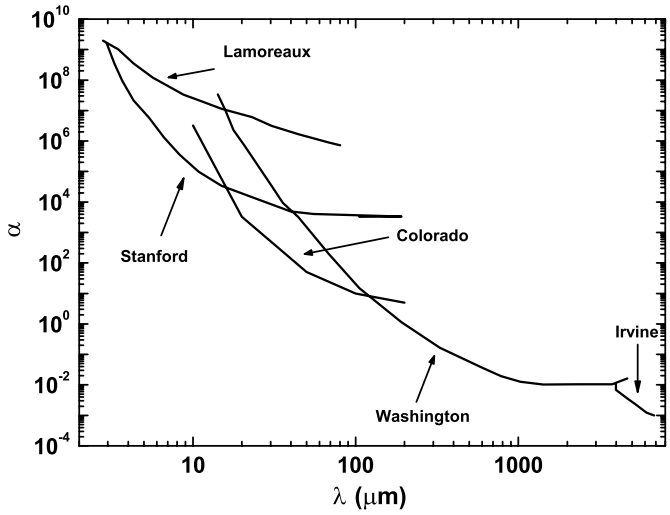

Figure 2.2: Upper limits to the strength of a non Newtonian interaction of the form given by Eq. 2.5. The region above the curves is excluded by the experiments [11, 20, 43, 46, 47]. (Picture adapted from Ref. [47].)

2.5 Constraints from high energy physics, astrophysics and cosmology

Measuring gravity at laboratory distances is not the only way to test the theories presented in this chapter. Limits on the radii of the extra dimensions can be set via high energy experiments. For example, in the collision of a proton and an antiproton some energy can escape into the bulk (extra dimensions) in the form of gravitons. The present limit to the unification energy derived from collider measurement is of 1.1 TeV [48]. Measurements of the missing energy in positronium decay at LHC should provide better constraints to the size of the extra dimensions [17].

The present best limits are derivable from astrophysical and cosmological observations. An example is the anomalous cooling of supernovae due to the emission of gravitons into the extra dimensions [49]. The observation based on the neutrinos from supernova SN1987A measured by the Kamiokande experiment [50] put some constraints on the size of the extra dimensions. In the case of two extra dimensions $R \leq 7.1 \cdot 10^{-7}$m is obtained, while for $n = 3$ $R \leq 8.5 \cdot 10^{-10}$ m. The lower limit for the unification energy is 30 TeV.

Chapter 3

Principle of the experiment

Experimental tests of Newton's law at laboratory distances can enable us to gain an insight into the fundaments of physics and, as shown in the previous chapter, to shed light on the hierarchy problem. This ambitious goal can be reached, in such an experiment, only by continually reducing the distance between the test masses, for example below 1 mm. In order to measure gravity at this distance range the dimensions of the test masses cannot be arbitrarily large, since the accuracy of their alignment depends on their size. To a first approximation, their typical dimension should be comparable to the distance scale that is going to be probed [43]. In 1798 Cavendish measured the gravitational attraction of masses put at a distance of 0.1 m [51]. His apparatus had a force sensitivity of about 10^{-5} N. Modern experiments designed to measure gravity at distances of the order of 10^{-4} m need typically to be able to measure a force as small as 10^{-14} N, which corresponds to the order of magnitude of the force that the Sun would exert on a mass of 1 kg at the distance of 10 light years. This comparison gives an idea of how measuring gravitation at small distances can be challenging. In order to overcome this problem, it is crucial to place as much mass as possible within the required distance. We will show that this can be achieved by choosing a planar geometry for the test masses. In fact, an infinite plane slab offers the advantage of producing a gravitational field whose strength does not depend on the separation (Newtonian null source) [28]. This limit can be reproduced, at a good approximation level, in the laboratory by choosing masses with an extension much larger than their mutual separation. In this configuration their gravitational interaction is given by

$$F_G = -2\pi G\rho_1\rho_2 L^2 D^2, \tag{3.1}$$

where ρ_1 and ρ_2 are the densities of the masses, L^2 is their area, and D is their thickness. Eq. (3.1) is valid in the limit $D << L$, in which the edge effects can be neglected. Any deviation from Newton's law would then introduce a distance dependence of the measured force. A Yukawa type interaction as in Eq. (2.5) would have the form

$$F_Y = -2\pi\alpha\lambda^2 G\rho_1\rho_2 L^2 \left(1 - e^{-D/\lambda}\right) e^{-d/\lambda} \approx -2\pi\alpha\lambda^2 G\rho_1\rho_2 L^2 e^{-d/\lambda}, \tag{3.2}$$

where d is the separation between the two plates. Calculating the ratio between Eq. (3.1) and Eq. (3.2), it yields

$$\frac{F_Y}{F_G} \simeq \alpha \left(\frac{\lambda}{D}\right)^2 e^{-d/\lambda}. \tag{3.3}$$

Assuming $\alpha \sim 1$ and $d \sim \lambda$, the relative strength of the correction term to gravity is reduced by the the factor $\left(\frac{\lambda}{D}\right)^2$. Whereas the whole mass generates the gravitational attraction, the Yukawa correction is mainly due to a slice of mass with a thickness of the order of λ. In the light of this consideration, the planar geometry proves to be the one that maximizes the non-Newtonian interaction as shown in Fig. 3.1. It follows from these considerations that the best configuration to search for non-Newtonian components of gravity is given by two planar test masses with a thickness of the order of the gap between them. Moreover, if the gap is much smaller than the square root of the masses' surface the Newtonian background does not depend on their mutual distance. Therefore, every distance dependence of the observed force has to be due to a non-Newtonian component, if all other possible interactions are accurately shielded.

In principle it is possible to implement this geometry in a Cavendish-like experiment, i.e. a thin plate, attached to a fine wire, placed in front of a second planar mass used as a source of static gravitational field. The sensitivity of this apparatus would be limited by seismic noise, since it is extremely difficult to attenuate vibrations at low frequencies (the frequency of such a pendulum would not exceed 1 Hz). Moreover, stray gravitational force due to objects nearby would represent a further disturbance, which cannot be shielded. An alternative approach is to perform an a.c. measurement in which one mass is part of an oscillator with resonance frequency in the kHz-range, where effective vibration isolation is achievable and stray gravitational signals are unlikely. Moreover the amplitude response of the oscillator is not affected by disturbances at frequencies far away from the resonance. In this case the sensitivity of the apparatus is limited by the Brownian (thermal) noise of the sensor. The history of dynamic measurement of gravity started with an experiment performed at the University of Maryland in 1967 by Sinsky, who used a resonant bar, designed to detect gravitational waves, as a detector for an

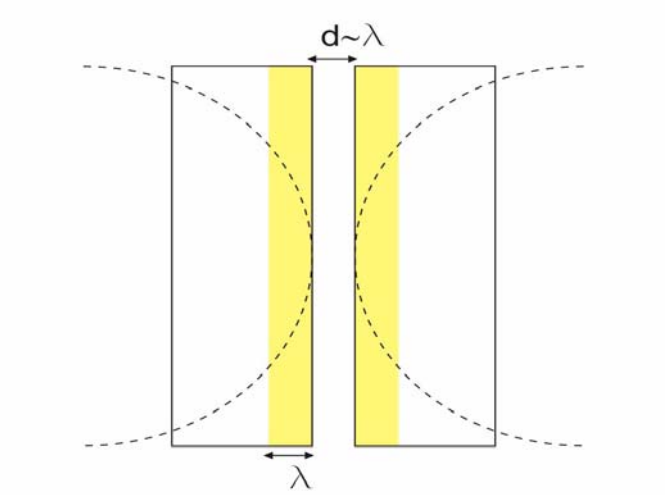

Figure 3.1: Comparison between two possible geometries for the test masses: the planar and the spherical geometry. Since only a λ-thick slice of each mass contributes to the Yukawa correction term, a larger effect can be measured using planar masses instead of spheres, as in the classic experiment by Cavendish.

a.c. gravitational field [52]. Price was the first to suggest to use an ac gravitational experiment based on the use of planar masses to detect deviations from Newton's Law [18].

Our experiment combines the advantages of a flat geometry with the increased sensitivity of a resonant detection. The sensitive element is a harmonic oscillator with resonance frequency, ν_R, that can be pictured as a thin plate attached to a spring, whereas the excitation is provided by a plate parallel to the sensor driven at the sensor's resonance frequency. Measuring the sensor's amplitude response for different values of the distance sensor-source mass, it is possible to infer the nature of the excitation force. Assuming that all external disturbances are eliminated, the fundamental limit to the sensitivity of this experiment is given by Brownian noise. In the following we will show that in this regime the sensitivity to a non-Newtonian force of the type given by Eq. (2.5) scales like $A^{-1}(Q \cdot \Delta t)^{-1/2}$, where Q is the mechanical quality factor of the sensor, A its sensitive area, and Δt the integration time. A consequence of this is that the use of a sensor with a high Q-factor is convenient. To date, the highest quality factors have been achieved by single-crystal silicon oscillators ($\simeq 10^5$). Assuming an integration time of 1000 s, the thermal noise force of such a sensor is of the order of 10^{-14} N in vacuum and at room temperature (see Section 3.2). This value also corresponds to the minimum

detectable force, that can further be improved by increasing the integration time. Fig. 3.2 shows the goal sensitivity of our experiment compared to previously published works.

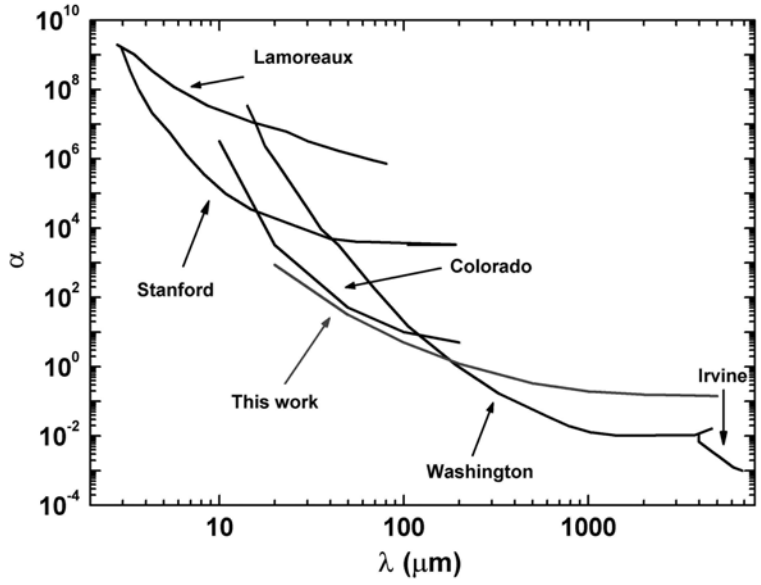

Figure 3.2: Expected sensitivity of our experiment compared to the existing limits. The parameter of this simulation $Q = 10^5$, Δt =1 day.

In the following sections we will outline the harmonic oscillator's theory, in order to determine the parameters that define the sensitivity of the experiment. Moreover, two fundamental noise sources, Brownian and shot noise, will be reviewed and experimental strategies to reduce their influence on the measurement will be presented.

3.1 Mechanical harmonic oscillator

The sensing element in our experiment is a mechanical torsional oscillator. The equation of motion of a torsional oscillator is given by

$$\left(I\frac{d^2}{dt^2} + \beta\frac{d}{dt} + D_{sp} \right) \vartheta = 0, \tag{3.4}$$

where $I = 2mr^2/3$ is the moment of inertia around the torsion axis, r is the half width of the oscillator, and β is the friction coefficient. The general solution of this equation

is an exponential decaying harmonic oscillation

$$\vartheta(t) = \vartheta_o e^{-\frac{\gamma}{2}t} \cos(\omega_d t + \Psi), \tag{3.5}$$

which is characterized by a damping coefficient $\gamma = \beta/I$, by the oscillator decay frequency $\omega_d = \sqrt{\frac{D_{sp}}{I} - \frac{\gamma^2}{4}}$, and by the integration constants ϑ_0 and Ψ. The amplitude of the periodic motion typical of the undamped case is now decreased by the exponential factor. This decay can be characterized by defining the (amplitude) damping time $\tau = 2/\gamma$. For weakly damped systems ($\gamma/\omega_d << 1$), as the one used in our experiment, it is possible to approximate $\omega_d \approx \omega_R = \sqrt{\frac{D_{sp}}{I}}$.

The resonant efficiency of the oscillator is specified in terms of the quality factor Q, which is defined by

$$Q = 2\pi \frac{\text{total elastic energy}}{\text{energy loss per cycle}}. \tag{3.6}$$

In the case of weak damping, it is possible to show that the relationship $Q \approx \omega_R/\gamma = \pi\nu_R\tau$ holds.

If the oscillator is driven by a time-dependent torque of the form $\Gamma(t) = \Gamma_0 \cos(\omega t)$ the steady state response is given by

$$\vartheta(t) = \Theta(\omega) \cos(\omega t + \delta(\omega)) \tag{3.7}$$

with $\Theta(\omega) = \frac{\Gamma_0}{I\sqrt{(\omega_R^2-\omega^2)^2+(\frac{\beta\omega}{I})^2}}$, and $\tan\delta(\omega) = \frac{\beta\omega}{I(\omega^2-\omega_R^2)}$. In the approximation of weak damping the line shape $\Theta(\omega)$ can be written in a simpler form, assuming that it vanishes for all the frequencies except for a small range around the resonance frequency. It is then possible to approximate ω by ω_R and the term $(\omega_R^2 - \omega^2)$ by $2\omega_R(\omega_R - \omega)$ obtaining

$$\Theta^2(\omega) = \frac{M_0^2}{4I^2\omega_R^2} \frac{1}{(\omega_R - \omega)^2 + (\frac{\gamma}{2})^2}, \tag{3.8}$$

which has the form of a Lorentian function. Since the full width of the curve at half maximum can be easily calculated to be $\Delta\omega = \gamma$, the quality factor can be expressed as $Q = \omega_R/\Delta\omega$. At resonance ($\omega = \omega_R$) Eq. 3.8 becomes

$$\Theta^2(\omega_R) = Q^2 \frac{M_0^2}{D_{sp}^2}. \tag{3.9}$$

This result shows that the resonant response of the oscillator to an external perturbation is proportional to the amplitude force and the proportionality coefficient is given by the ratio of quality factor over spring constant. In order to measure weak forces, it then is necessary to maxime this ratio, i.e. using a mechanical oscillator with a high

quality factor and as small as possible spring constant. Whereas the first condition is compatible with the measurement strategy of this work, reducing the spring constant, i.e. the resonance frequency, makes the implementation of the vibration isolation more difficult and for this reason will be not considered.

In order to be able to predict the mechanical losses in a vibrating oscillator, it is necessary to distinguish between ideal and real solids. In the first case mechanical vibrations produce a process which is fully reversible from the thermodynamical point of view. On the other side, considering an imperfect crystal or an amorphous body the situation changes drammatically. While the solid is vibrating, a part of its mechanical energy is used to rearrange its lattice imperfections. Several different mechanims contribute to dissipation in solid state matter. In this section, we will focus our attention on just one of them, the thermoelastic dissipation, which will be used in the forthcoming chapters to characterize the sensor used in this experiment. In a solid, vibrations are accompanied by changes in its volume (compression or decompression) producing spatial inomogeneous temperature changes, that cause energy dissipation [53]. As an example, the quality factor of a longitudinally oscillating bar, in which thermoelastic dissipation is the main source of loss, is given by [54]

$$Q = \varsigma \frac{C^2}{\kappa T \alpha \Lambda^2 \omega \rho V}, \tag{3.10}$$

where ς is a numerical constant, ω is the vibrational angular frequency, T is the bar's temperature, ρ is the density of the bar's material, C is the specific heat capacity, Λ is the thermal expansion coefficient, κ is the thermal conductivity, and V is the volume of the bar. Eq. (3.10) is valid for frequecies of up to 10 GHz. In contrast, the energy of a pure shear vibration is not dissipated by this process, because no volume change takes place during this kind of vibration. This is the case of a torsion pendulum, where no contraction or expansion is involved in the oscillation. Considering this fact, the optimum sensor for weak force measurement should be a torsional oscillator made of a single crystal material, which shows low dislocation damping.

Other loss mechanims due to the environment are to be considered. If the oscillator vibrates in a gaseous medium, it generates a sound wave, which removes part of its energy. The quality factor of such an oscillator depends on the gas pressure p, on the

temperature T as follows[1]

$$Q \sim \frac{T^{1/2}}{p} \tag{3.11}$$

under the assumption that the mean free path of the gas molecules is much shorter than the wavelength of the sound waves in the gas. In the case of oscillators with a resonance frequency of the order of 10 kHz, Eq. (3.11) is valid for pressure larger than 10^{-2} mbar, while mechanical loss due to gas friction becomes very small, often smaller than thermoelastic dissipation, at lower pressure. Further dissipation effects can arise from surface defects and absorbed molecules (e.g. water and organic compounds), whose presence introduces many different relaxation processes [53].

3.2 Internal Brownian noise of an elastic body

One of the first measurements of the Brownian motion of a mechanical oscillator goes back to Gerlach in 1927, who measured the rotational Brownian noise of a small mirror attached to a very fine wire [56]. A theoretical analysis of this phenomenon was then provided by Uhlenbeck and Goudsmith in 1929 [57]. A deeper understanding of the origin of Brownian noise was developed by Nyquist, who pointed out the existence of a connection between stochastic motion and the internal mechanical loss of the material [58]. A further generalization of this concept was given by Callen and Welton, through the Fluctuation-Dissipation Theorem [59].

In the last decade the relevance of mechanical oscillators for precision measurement of weak forces grew steadily [60]. The detection of the Casimir force [61], 3-d microscopy with sub-nm resolution [62], attogram mass detection [63] are some of the most recent examples of the results achieved by the use of mechanical oscillators in high precision experiments. Particularly challenging applications of ultrasensitive force sensors are tests of Newton's law at short distances [10, 20, 43, 47, 64, 65] and optical measurement of small displacements [66, 67]. In many cases, Brownian noise of the detector represents the desirable ultimate limit to their sensitivity. A review of the measurement and data analysis strategies, developed to improve the sensitivity of these detectors, can be found in the work by Ritter *et al.* [42].

[1] R. Buser calculated the exact pressure dependence for another torsional structure, which is given by [55]

$$Q = \frac{\sqrt{2\pi}}{4}\frac{\omega\rho h}{p}\sqrt{\frac{R_{gas}T}{M}},$$

where h is the thickness of the oscillator, M its mass, and R_{gas} is the *ideal gas constant*.

A simple model can describe the angular fluctuations of a torsional oscillator due to Brownian noise, and is suitable for characterizing the sensitivity of a variety of precision experiments, e.g. weak force sensors and gravitational wave detection [68].

The equation of motion of a harmonic torsional oscillator driven by Brownian noise is

$$I\ddot{\vartheta} + \beta\dot{\vartheta} + D_{sp}\vartheta = \Gamma(t), \tag{3.12}$$

where I is the moment of inertia around the torsion axis, ϑ is the angular deflection of the oscillator, β is the damping coefficient, D_{sp} is the spring constant, and Γ is a fluctuating torque. Eq. (3.12) is a generalization of the Langevin equation for a simple harmonic oscillator. We assume that $\Gamma(t)$ has the following properties:

i) zero mean value,

ii) its variance is a constant in time: $\overline{\Gamma^2(t)} = const.$,

iii) its values at two different times are uncorrelated.

The angular fluctuations of an oscillator excited by such a stochastic torque do not obey exactly the statistics of pure random noise. This is a consequence of the correlations introduced by the oscillator. If the oscillator's deflection at time t_0 is $\vartheta(t_0)$, the probability distribution of its angle at a later time t is given by [69]

$$P[\vartheta(t) \mid \vartheta(t_0)] = \frac{\vartheta(t)}{\overline{\vartheta^2}(1-e^{-2t/\tau})} I_0\left(\frac{\vartheta(t)\vartheta(t_0)e^{-t/\tau}}{\overline{\vartheta^2}(1-e^{-2t/\tau})}\right) \exp\left[-\frac{\vartheta^2(t)+\vartheta_0^2(t)e^{-t/\tau}}{2\overline{\vartheta^2}(1-e^{-2t/\tau})}\right], \tag{3.13}$$

where $\tau = 2I/\beta$ is the mechanical relaxation time of the oscillator, $\overline{\vartheta^2}$ is the mean square of the oscillation amplitude, and I_0 is the modified Bessel function.

If the oscillator is excited by an external harmonic torque at the oscillator's resonance frequency, $\Gamma = \Gamma_0 \sin(\omega_R t)$, the minimum detectable torque amplitude can be derived using Eq. (3.13) and is given by [69, 70, 71]

$$(\Gamma_0)_{\min} = \pi\sqrt{\frac{Ik_BT}{\tau\Delta t}} = \pi\sqrt{\frac{Ik_BT\omega_R}{2Q\Delta t}}, \tag{3.14}$$

if the measurement time Δt is smaller than the oscillator relaxation time τ. Here, the Q-factor has been introduced through $\tau = 2Q/\omega_R$. The improvement of torque sensitivity with increasing measurement time can easily be pictured. During the measurement time the response of the oscillator to the external force increases steadily due to the phenomenon of resonance, whereas the response due to Brownian noise fluctuates. This is the regime in which, for instance, the most sensitive torsion pendulums, that have relaxation times of the order of $10^6 \div 10^9$ s, operate [71]. A detailed analysis of the sensitivity of torsion pendulums can be found in the book by Chen and Cook [29].

Increasing the measurement time beyond $\Delta t = \tau$ does not lead directly to an improved torque sensitivity unless an appropriate data analysis is performed [42, 29]. Following Uhlenbeck and Goudsmit [57], it is necessary to develop the measured angular displacement in a Fourier series like $\vartheta(t) = \sum_k \vartheta_k(t)$, where the index $k = 0...\infty$ corresponds to the frequency $\omega_k = 2\pi k/\Delta t$. We first consider the oscillator motion in absence of external torque. The term of the series at the oscillator's resonance frequency is the one of interest. Its mean square depends on the measurement time as follows [68]

$$\overline{\vartheta_k^2} = \frac{8 k_B T Q}{I \omega_R^3 \Delta t}. \tag{3.15}$$

Each quadrature amplitude of $\vartheta_{k'}$ then also averages to zero, as $(\Delta t)^{-1/2}$ for $\Delta t \gg 4Q/\omega_R$. A similar result can be obtained applying Nyquist's theorem [68]. The potential energy of the oscillator, in absence of external excitation, can be calculated from Eq. (3.15) and, as shown in Ref. [57], is constant and independent of the observation time as expected from the equipartion theorem.

The signal-to-noise ratio is defined as the ratio between the corresponding steady-state oscillator amplitude and the Brownian noise amplitude given by Eq. (3.15). Setting this ratio equal to unity yields the minimum detectable torque in the case $\Delta t \gg \tau$,

$$(\Gamma_0)_{\min} = \sqrt{\frac{4 k_B T I \omega_R}{Q \Delta t}}. \tag{3.16}$$

Thus, the minimum detectable torque decreases with the square root of the measurement duration. The validity of this analysis is limited to the case of noise with white spectrum. An example of weak (gravitational) force detection using detection of the oscillator amplitude at the resonance frequency is given in ref. [10].

It is interesting to consider the statistical properties of the oscillator's response. In the following analysis we assume that the deflection of the oscillator at resonance frequency is measured by a lock-in technique. This yields the slowly varying amplitude $r(t)$, and phase $\psi(t)$ of the oscillator's response $\vartheta(t) = r(t)cos(\omega_R t - \psi(t))$. The quadrature amplitudes $X(t) = r(t)\cos\psi(t)$ and $Y(t) = r(t)\sin\psi(t)$ are calculated. In steady-state, the probability distribution function for these two quantities is given by $W(X,Y) = W(X)W(Y)$, where [72]

$$W(X) = \left(\frac{I\omega_R^2}{2\pi k_B T}\right)^{\frac{1}{2}} \exp\left(-\frac{I\omega_R^2}{2k_B T} X^2\right). \tag{3.17}$$

From Eq. (3.17) it follows that both quadratures have vanishing mean value, while their variance is equal to $k_B T/I\omega_R^2$, as expected from the equipartion theorem.

3.3 Sensitivity requirements of the detection system

Besides Brownian noise, there is another fundamental phenomenon that could affect the sensitivity of the experiment described here: laser shot noise. In this section we will describe the conditions that have to be fulfilled in order to avoid that the use of a simple optical detector, similar to those used for atomic force microscopy [73], could degrade the accuracy of our measurements. In this setup a laser beam is directed onto a cantilever and is reflected to a split photodiode. The angle variation due to the deflection of the device shifts the position of the laser beam on the photodetector. This position can be measured monitoring the difference photocurrent of the two illuminated areas. The use of a split photodiode instead of a normal photodetector enhances the sensitivity of this system, because in this case variations of the optical power on the detector area do not produce any signal (common mode rejection). The ultimate limit for this detection scheme is (when all other noise are negligible) the quantum (shot) noise of the used laser light. The shot noise current in both photodetector areas is uncorrelated so that it does not subtract to zero. The quantum noise is a result of the Poisson statistics of the laser photon number n with $\sqrt{<\Delta^2 n>} = \sqrt{<n>}$. The quantum noise power for a fixed laser power can be obtained by using the relation

$$P =< n > \frac{\hbar c}{\lambda t} \tag{3.18}$$

and is given by

$$\sqrt{<\Delta^2 P>} = P_N = \sqrt{\frac{hc}{\lambda}}\sqrt{<P>} \tag{3.19}$$

where λ is the wavelength of the laser light. It has to be noted that P_N is expressed in $W/\sqrt{Hz}$. For the sake of simplicity, the spatial distribution of optical power impinging on the photodetector is assumed to be rectangular. The beam has a gaussian distribution in reality, but the detector cannot distinguish between gaussian and rectangular distribution if each area is illuminated by 50% of the total laser intensity. Under this approximation the optical power density per unit length in the illuminated area results in being constant and is given by

$$< P(l) >= \frac{< P >}{2w} l, \tag{3.20}$$

where w is the width of the rectangular beam profile, which is roughly the waist of a gaussian laser beam. A shift of the illuminating beam causes an inequal distribution of the power between the sensor areas. The difference average power can be expressed as

$$< P_- >=< P_R > - < P_L >= \frac{< P >}{w} l_R - \frac{< P >}{w} l_L = \frac{< P >}{w} \delta l. \tag{3.21}$$

In order to determine the minimum detectable displacement of the laser beam $\delta l_{\min}$, the ratio of this quantity to the shot noise P_N has to be equal to 1. The result of this calculation is given by

$$\delta l_{\min} = w\sqrt{\frac{hc}{\lambda}}\frac{1}{\sqrt{< P >}}. \tag{3.22}$$

For a sensor, such as the one presented in this work, an angular motion makes the laser beam move on the photodiode surface. Assuming that there is a distance z between the sensor and the photodetector, the minimum detectable angular displacement is

$$\delta\phi_{\min} = \frac{\delta l_{\min}}{z}. \tag{3.23}$$

This quantity is proportional to the width of the laser beam (see Eq. (3.22)). For gaussian beam the waist is a function of the position and can be expressed as

$$w(z) = w_0\sqrt{1 + \left(\frac{\lambda z}{\pi w_0}\right)} \tag{3.24}$$

where the width at the waist is $w_0 = \lambda/\pi\theta$ and θ is the divergence angle of the beam. For large distances (far field) the expression reduces to

$$w_\infty = \frac{\lambda z}{\pi w_0}. \tag{3.25}$$

Using these expressions, the minimum detectable angular motion becomes

$$\delta\phi_{\min} = \frac{w(z)}{z}\sqrt{\frac{hc}{\lambda}}\frac{1}{\sqrt{< P >}}. \tag{3.26}$$

In the near-field approximation the optimum place to position the detector is the focus of the beam, where $w = w_0$. Assuming the spot size being U, it is easy to obtain

$$\delta\phi_{\min} = \frac{2}{\pi U}\sqrt{hc\lambda}\frac{1}{\sqrt{< P >}}. \tag{3.27}$$

On the other hand, using the far-field approximation it turns out that

$$\delta\phi_{\min} = \frac{1}{\pi w_0}\sqrt{hc\lambda}\frac{1}{\sqrt{< P >}}. \tag{3.28}$$

From these results, it follows that the sensitivity of the setup does not depend on the distance between sensor and photodetector, i.e. there is nothing like an optical lever arm.

Chapter 4

The double-paddle oscillator

Single-crystal mechanical oscillators have proven to be a powerful tool for different applications, such as magnetic force microscopy [74], the characterization of thin films at low temperature [75], the study of metallic films at high temperature [76], torque magnetometry [77], and the investigation of quantum effects [67]. The key property is the very small damping (high quality factor) of these oscillators. In 1978 McGuigan and coworkers [78] measured a quality factor of about $2{\cdot}10^9$ for a longitudinal mode of a single-crystal silicon cylinder of mass 4.9 kg at 3.5 K. This result stimulated further efforts to improve the mechanical performances of microfabricated structures. An important development in this field was the double paddle oscillator (DPO) by Kleiman and coworkers [79]. A further improvement in the quality factor of single-crystal oscillators was obtained by Pohl and coworkers at Cornell University, who produced and used DPOs to study elastic properties of thin metal films [75]. A typical DPO is shown in Fig. 4.1. Six different eigenmodes of this type of oscillator have been experimentally identified in the frequency range between 0.1 and 6 kHz [22]. One of them, an antisymmetric torsion mode, exhibits very small losses and its mechanical properties do not appear to be influenced by aging. Its quality factor was found to be about $3 \cdot 10^5$ at 300 K and on the order of $8 \cdot 10^7$ at 4 K [80]. The difference between this result and the values reported by McGuigan and coworkers suggests that there could still be room for further improvements of the DPOs. Moreover recent studies of the thermoelastic effect in single crystal micromechanical oscillators [81] have confirmed that the internal friction observed below 60 K cannot be explained in terms of thermoelastic losses.

In the present chapter we report on the fabrication of DPOs using a different procedure from the standard one used in the previously cited works. We evaluate our fabrication method with respect to the oscillators' performance. Particular attention is

paid to the measurement of the Brownian noise of a DPO. Next, we also show actuation of DPOs by means of a laser beam and control of their torsional constant. Optical actuation of resonant microstructures has previously been applied by different groups [82]. To our best knowledge this technique has not yet been reported for DPOs, and is a natural candidate for applications, in which an actuation method is required, that does not need any metallic coating on the DPO, unlike the electrostatic excitation method.

4.1 Theoretical background

As shown in Fig. 4.1, a DPO consists of two paddles, denoted by head and wings, that are connected by a torsion rod, the neck.

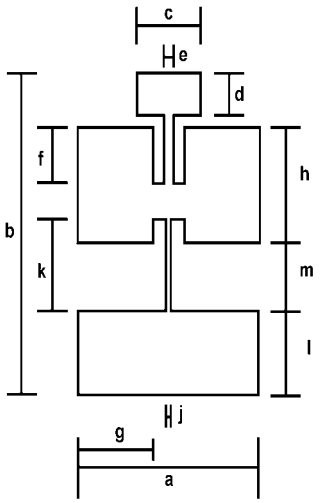

Dimension (mm)	
a	19.63
b	28.00
c	6.85
d	3.65
e	1.09
f	4.88
g	8.13
h	10.05
k	7.95
j	0.54
l	7.32
m	5.95
Thickness	0.30/0.50

Figure 4.1: Dimension of the DPOs used in this work.

The wings are connected to the base, the foot, by another torsion rod, the leg. This system can be modeled as a coupled oscillator consisting of two masses (head and wings) and of two springs (neck and leg). Since each spring can be twisted or bent in different directions, several vibration modes exist. In the present work we will restrict attention to an antisymmetric torsion mode, known in literature as AS2 [22]. It consists of a twist of the neck around its length and a synchronous oscillation of the wings around an axis

orthogonal to the DPO symmetry axis. The oscillations of head and wings are out of phase [83], as shown in Fig. 4.2. This mode is particularly interesting because of its very low internal losses.

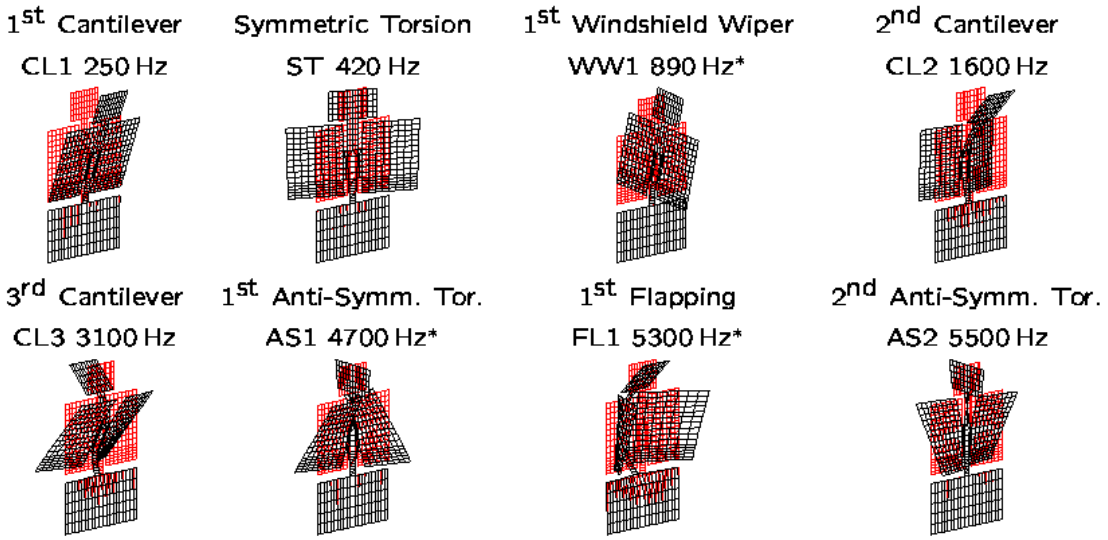

Figure 4.2: Model plots of the first eight oscillation modes of a DPO resulting from FEM calculations. The last mode is the one of interest here. The displacements are exaggerated to make the sketches intelligible. (Courtesy of C. L. Spiel.)

The resonance frequency of the mode AS2 is given, to first approximation, by [84]

$$\nu_0 = \frac{\sqrt{3}}{\pi}\sqrt{\frac{S}{c^3 d}t_s^2\frac{\Phi}{\rho f'}e} \tag{4.1}$$

where c is the full width of the oscillator head, t_s the oscillator thickness, $f' = f + b - (h + l + m)$ the neck length, e the neck width, d the height of oscillator head, g the shear modulus of silicon for a wafer with a (100) orientation, and Φ is a parameter, that depends weakly on the ratio t_s/e and is of the order of unity. The shear modulus of silicon around the torsion axis of the DPO, <110> direction, is $S = 61.7$ GPa at room temperaure [85]. In our calculations Φ is equal to 0.25 [86].

4.2 Material and technology

The unit cell of silicon crystal is of the type F.C.C. (face centered cubic) with two atoms in the positions (0, 0, 0) and (1/4, 1/4, 1/4). The resulting crystal structure is diamond-like with a lattice constant a = 5.43 Å. Crystal planes are characterised by the Miller indices, that describe vectors normal to the crystal plane in question, e.g. (100), while the crystallographic directions are indicated by <...>, e.g. <100>. The knowledge of the crystallographic directions is of great importance, since the etch rates of the used etchant depend on this.

There are different procedures to grow silicon single crystals. In the Czochralski method, polycrystalline silicon is melted by high-frequency heating in a crucible and heated up to 1440 °C to destroy crystallization seeds. Then the temperature is stabilized at about 1425 °C (sightly above the melting point). A single crystal is immersed in the melt and then slowly pulled upwards so that the solid-liquid interface is just above the level of liquid silicon. This is the most common method to obtain large dimension wafers (up to 300 mm in diameter), but it is not suited to the production of high purity material. In spite of the fact that the procedure is performed in high vacuum conditions, the melt can be contaminated by impurities contained in the crucible (typical resistivity is the range between 50 Ω·cm and 0,01 Ωcm). An alternative technique is the so-called float-zone crystal growth. In this scheme a circular rod of polycrystalline silicon is converted into single crystal material by zone melting starting from a plane in which a crystallization seed is contained. Crystals grown according to this method have resistivities, which exceeds 1 kΩ·cm. A high resistivity is a sign of a good crystal structure, because it corresponds to a low level of dopant (impurities), that degrade the mechanical quality of the crystal. Insufficient control of the growth parameter is responsible for the presence of crystal lattice defects, such as point defects (interstitial, substitutional, selfinterstitial and vacancies) and dislocations [87]. The silicon wafers used in the present work were grown according to this second method.

4.2.1 Fabrication technique

The DPO design we implemented is similar to the one developed by Pohl and coworkers [22]. Its dimensions are shown in Fig. 4.1. The procedure decribed in this section was developed by the author of this work in the clean room facilities of the group of Prof. D. Jäger at the University of Duisburg-Essen.

The oscillators were fabricated from a 300 μm (or 500 μm) thick, float zone refined, double-side polished, <100> oriented, and p-doped silicon wafer, with a room-

temperature specific resistance larger than 10 kΩ·cm. On each side a 80 nm thick silicon nitride layer (deep-etch-stop layer) had been thermally grown [88]. The process flow, described in this section, is summarized in Fig. 4.3 and in Table II.

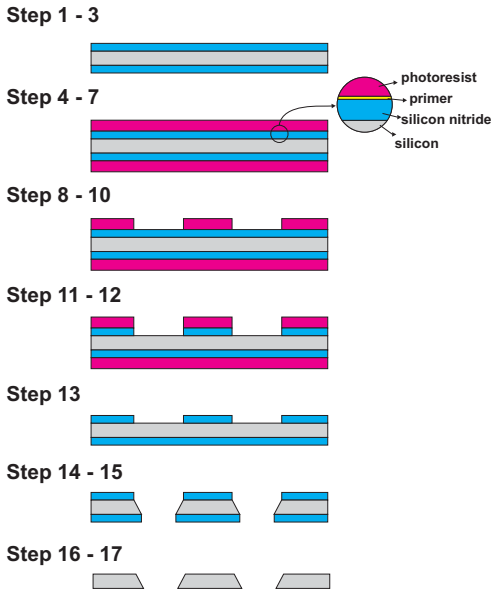

Figure 4.3: DPO fabrication procedure.

Table II. Steps used for microfabricating the DPOs.

	Fabrication Process
1	Wafer cleaving
2	Sample cleaning
3	Annealing at 230 °C for 30 minutes
4	Coating with primer (AR 300-80)
5	Annealing at 170 °C for 3 minutes
6	Coating with photoresist (AR 4040)
7	Annealing at 95 °C for 3.5 minutes
8	Photolithography
9	Development (AR 3035)
10	Annealing at 110 °C for 10 minutes
11	Stripping of silicon nitride in H_3PO_4 at 140 °C
12	Probe cleaning
13	Photoresist removal
14	KOH etching at 99 °C
15	Probe cleaning
16	Silicon nitride removal in HF
17	Structure cleaning

The wafer was laid on a clean room wipe and a small notch was scratched with a diamond scriber in the direction parallel to the crystal axis <100>. The scriber tip was then put in the notch and pressed firmly. In this way the wafer was split into more samples, each having an edge parallel to the crystal direction <100> [89]. For cleaning, the sample was then immersed in boiling acetone and afterwards in boiling propanol for a few minutes. After blow-drying with nitrogen, the sample was put on a hot plate at 230°C and at ambient pressure for 30 minutes (dehydration bake), in order to eliminate solvent residuals, that could degrade the quality of the sample surface.

The following steps (6-10 in Table II) were performed in a class 10 yellow clean room, in which the UV light was filtered out (photoresists are very sensitive to short wavelenghts) and less than 10 particles larger than 0.5 microns were present in each cubic foot of air space. It was essential that during this procedure the relative humidity was at least 35% and the temperature was kept constant within 1 °C. This condition, guaranteed by the air conditioning of the clean room, was monitored for the whole duration of the fabrication. Since most photoresists have bad adhesion on silicon nitride, a primer (Allresist, AR 300-80) was spun on each side of the sample at a spinning speed

of 4000 rpm. These thin layers were annealed at 170 °C for 3 minutes. Next, a positive photoresist (Allresist, AR 4040) was spun on both sides. The thickness of each layer was 1.4 μm. Baking at 95°C for 3.5 minutes was required in order to temper the photoresist. To reproduce the oscillator pattern on the photoresist layer, the sample was then put in contact with a chrome coated glass mask[1], on which the shape of the oscillator had been previously printed via scanning laser lithography. In order to minimize the mechanical losses of the DPO, it was important to align the sample carefully, so that the crystal axis <110> was parallel to the symmetry axis of the DPO [22]. The sample was then exposed for 12 s to light from a mercury short-arc lamp, which produced a radiation in the wavelength range between 350 and 550 nm. The intensity required for the exposure of the resist layer was 70 mJ/cm^2. After developing in a 60% solution (by weight) of AR 3035 (Allresist) for 4 minutes, the sample was rinsed, blow-dried and annealed at 110°C for 10 minutes (postbake). The bare silicon nitride was then stripped in a H_3PO_4 solution (concentration 85% by weight) at 140°C. Under these conditions an etch rate of about 1 nm/min was measured. At this point, the nitride layer had been etched except in the area corresponding to the oscillator. In order to eliminate the residual photoresist, the sample was then put in boiling N-methylpyrrolidone (NMP) for about 15 minutes. The silicon etching was then performed in a KOH solution (30% concentration by weight) at 99°C. Since the KOH etch rate in the <100> direction is much higher than in the <111> direction, holes in a silicon wafer with surface orientation (100) can be easily etched. The measured etch rate was about 3 μm/min. Next, the silicon nitride layer on the free standing structure was removed by HF solution (concentration 20% by volume) for five minutes. The oscillator was then rinsed and blow-dried. The total time required to fabricate a DPO was about 5 hours. Two oscillators of different thicknesses, produced following the aforementioned procedure, are shown in Fig. 4.4. As it takes longer to etch the thicker oscillators, the etch-stop can be damaged. This is the reason why the DPO in Fig. 4.4(b) shows slightly irregular edges.

[1] Observing the sample at the mask aligner, it was possible to see that the photoresist, because of its viscosity, formed a bulge at the border of the plate. In this case, since the mask contact with the sample was not perfect, the image fidelity was reduced. This was a crucial problem for the reproduction of micrometer-sized structures. In our procedure it did not represent a major problem because of the macroscopic size of our structure.

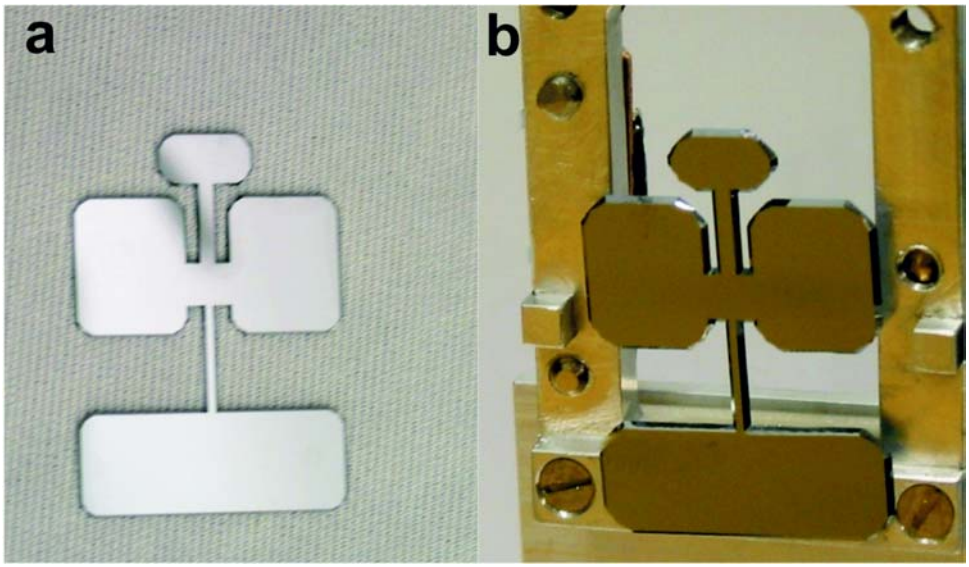

Figure 4.4: (a) 300 μm thick DPO; (b) 500 μm thick DPO

4.3 Measurements and results

4.3.1 Oscillator characterization

Since any coupling of the oscillator to the external environment would introduce mechanical losses, fastening it without degrading its mechanical properties is crucial. As suggested in Ref.[83], a small displacement during the oscillation takes place in the upper part of the foot. For this reason, in our setup only the lower half of the oscillator foot was carefully glued with Stycast 1260 on an aluminium holder[2], as shown in Fig. 4.4(b). The oscillator holder was mounted onto a piezoelectric transducer resting on a passive vibration isolation system to reduce the influence of seismic noise. This setup was operated in a high vacuum chamber (typical pressure 10^{-6} mbar and room temperature). In order to characterize the mechanical properties of the DPOs, an optical detection system, similar to the one described in the previous chapter, was set up. A He-Ne laser beam (0.9 mW optical power) was reflected by the DPO onto a split photodiode, which generated a photocurrent proportional to the amplitude of the angular displacement of the oscillator. This setup could detect a laser beam displacement of the order of 10^{-11} m in a bandwidth of 1 Hz. As a comparison, the mininum detectable angular motion due to shot noise of the laser, as from Eq. (3.28), was $2{\cdot}10^{-12}$ m. The measured signal,

[2] We also experimented with an alternative clamping method for the DPOs. In this case the foot was clamped between two metallic plates. Both techniques were found to be comparable.

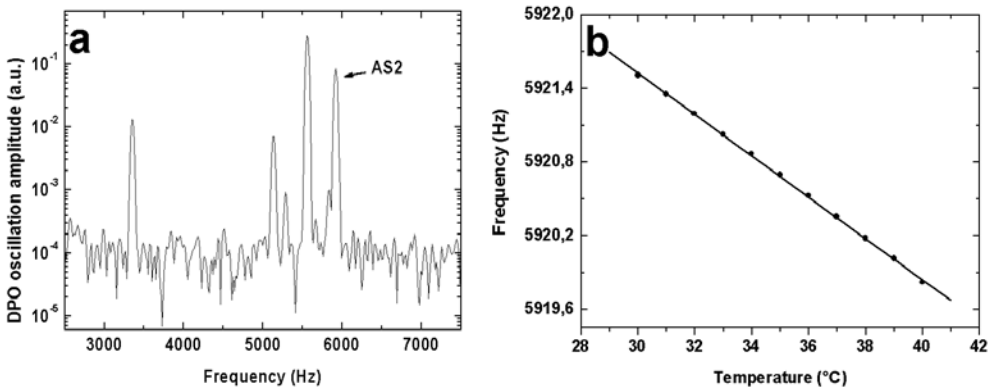

Figure 4.5: (a) Spectrum of a 300 μm thick oscillator driven by white vibrational noise; (b) Dependence of the resonance frequency on the temperature.

u_{sp}, could then converted into the DPO's angular displacement ϑ, using the following relation

$$\vartheta = \frac{u_{sp}}{2l\Omega}, \tag{4.2}$$

where l is the distance between the DPO and the split photodiode, and Ω is the sensitivity of the split photodiode. In this work, l is equal to (64.4±2.0) cm and Ω to (167.0±0.2) kV/m.

An electrical heater, mounted on the DPO support, enabled us to control the oscillator temperature. The temperature could be stabilized using an analog PID-controller. The measured temperature instability (in vacuum) was smaller than 10 mK over several hours.

Applying a white noise voltage source, it was possible to record the spectrum of a 300 μm thick DPO, shown in Fig. 4.5(a), in which, besides the AS2, three other modes can be clearly recognised. Following the abbreviation introduced by Spiel in Fig. 4.2, they should be the FL1, AS1, and CL3. While the AS2 can be identified by its high quality factors, the others have to be characterized directly, for example via scanning laser vibrometry [90]. It was not possible to perform this kind of measurement in our laboratory.

The resonance frequency (and consequently the spring constant) is a function of the temperature of the oscillator. The temperature dependence of the resonance frequency was measured, as shown in Fig. 4.5(b). The frequency-temperature coefficient, obtained from a linear fit, was found to be -169 mHz/K for a 300 μm thick oscillator.

In order to determine the quality factor of the mode AS2, the oscillator was driven at resonance by the piezoelectric transducer. The excitation was then turned off. Using a lock-in amplifier the amplitude decay was measured. The result of a typical measurement is shown in Fig. 4.6(a). The experimental data was fitted by a single exponential function with a ring-down time $\tau = 23$ s, which corresponds to Q $=7.7{\cdot}10^5$ (oscillator thickness 500 μm, see Fig. 4.4). Fig. 4.6(b) shows the resonance curve of the same DPO fitted to a Lorenz function with a width at $2^{-1/2}$ of its maximum amplitude of 0.013 Hz. This value corresponds to a quality factor of $8{\cdot}10^5$ in accordance with the ring-down measurement. In every case, the measured Q-factor exceeds any measurement previously reported in literature. Houston *et al.* [81] have developed a model in which the quality factor of the mode AS2 is calculated assuming that the internal friction is due to the thermoelastic losses associated with a vibrational flexural component of this mode. Under this assumption the quality factor is given by

$$Q = \left[p_1 \frac{E\Lambda^2 T}{c_{sp}} \frac{\omega_R \delta}{1 + (\omega_R \delta)^2} \right]^{-1}, \tag{4.3}$$

where p_1 is the modal participation factor and is equal to the ratio of vibrational flexural energy relative to total modal energy, E is the Young's modulus, Λ is the thermal expansion coefficient, c_{sp} the specific heat, ω_R is the angular frequency of the mode AS2, and δ the thermal relaxation time is given by

$$\delta = \frac{t^2 c_{sp}}{\pi^2 \kappa} \tag{4.4}$$

with κ as the thermal conductivity. Substituting the material properties of silicon [91] in Eq. (4.3) and using Eq. (4.1), it is easy to show that the quality factor of the mode AS2 scales as t_s^{-3} (t_s, DPO's thickness) and is about $2{\cdot}10^5$ for a 300 μm thick DPO. This value fits with our results for the thin oscillators. For the thicker oscillators the measured values are significantly higher than expected from Eq. (4.3). A possible explanation is a strong reduction in the modal participation factor with increasing thickness, a reasonable assumption, which overcompensates the factor t_s^{-3}.

Table III summarizes the results of the characterization of different oscillators. The discrepancies between the calculated and measured resonance frequency are due to variations in the fabrication process (for example photoresist underetching due to different duration of the etching steps.) The quality factors were measured several times and they increased in the first days after the oscillators had been put under high vacuum conditions. This was probably due to a thin water layer on the DPOs surface, that slowly evaporated. The average increase was found to be of the order of 5% for all the tested oscillators.

Table III. Experimental characterization of different DPOs. The theoretical resonance frequencies are derived from Eq. (4.1).

Oscillator	1	2	3	4	5
Thickness (μm)	300	300	500	500	500
Measured res. freq. (kHz)	5.9	5.2	8.6	8.9	10.6
Calculated res. freq. (kHz)	5.3	5.3	8.9	8.9	8.9
Q factor at 300 K and 10^{-6} mbar	$1.9{\cdot}10^5$	$1.3{\cdot}10^5$	$2.6{\cdot}10^5$	$3.0{\cdot}10^5$	$7.7{\cdot}10^5$

A few oscillators, that were not been tested in our laboratory, were provided for the group of Prof. Samwer (University of Göttingen) to be used for measuring the internal friction in thin metallic and organic films in the range of temperature between 300 and 650 K [76].

Concerning the dissipation of the mode AS2, the oscillator produced with our manufacturing procedure, proved to be, at least, comparable to others reported in literature [21, 22]. In one case (oscillator #5) the quality factor achieved is, to our best knowledge, the highest demonstrated so far at room temperature. Fig. 4.7 shows a comparison of our best results with others previously published [21, 22].

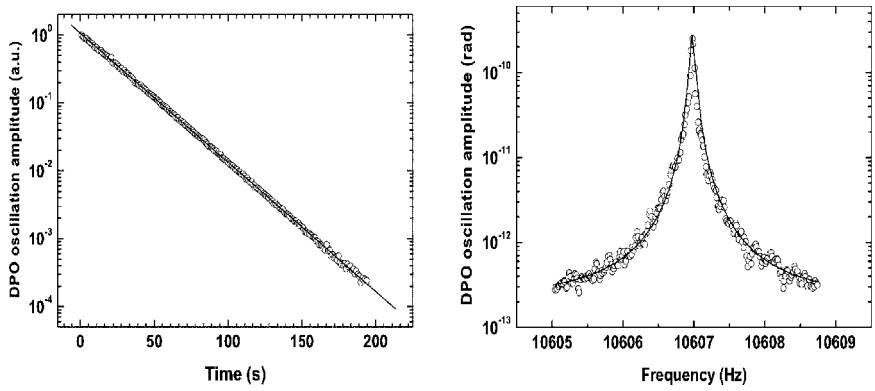

Figure 4.6: (a) Ringdown of the mode AS2 for a 500 μm DPO with a time constant of 23 s at room temperature, which corresponds to a Q factor of $7.7{\cdot}10^5$.(b) Spectrum of the same vibration mode due to thermal noise excitation (white noise).

4.3.2 Brownian noise of a DPO

Experimentally separating Brownian noise from other kinds of noise affecting a mechanical oscillator is a not trivial task. We will show how the use of the techniques and statistical tools presented in the previous chapter made the detection of Brownian noise and its characterization possible. In order to achieve this result, the DPO (#1 from previous section) was mounted on a passive vibration isolation. The measurements analyzed below were taken in several consecutive runs for a total of $3.4{\cdot}10^5$ s. The detection of the oscillator's angular displacement was perfomed by a digital dual-phase lock-in amplifier, with a local oscillator frequency set to allow measurement of the quadratures $X(t)$ and $Y(t)$. The bandwidth of the lock-in amplifier was set equal to 0.8 Hz (corresponding to a lock-in time constant of $\tau_L = 0.3\,\mathrm{s}$) and the data was acquired at a rate of 1 Hz. A run was divided into blocks and each block consisted of the following steps. First, the oscillator response was detected over 600s, while an external excitation was applied. The external excitation was then switched off and after waiting 100 s, necessary for the oscillator to reach equilibrium, a measurement without excitation was taken over 600 s. Then, the (slowly drifting) resonance frequency was determined by exciting the DPO with a fixed voltage at few different frequencies and fitting the measured amplitude to a Lorentz curve. Once this procedure was completed, the resonant excitation was modified, if necessary, and the next block started.

In order to determine the influence of the detection system noise, the quadrature $X(t)$ and $Y(t)$ were also measured in absence of external excitation and with the frequency of the local oscillator's frequency tuned 1 Hz below the DPO resonance. These measurements were performed in a single run with a duration of $2{\cdot}10^5$ s. The pressure in the vacuum vessel was constantly monitored throughout the complete duration of the measurement, since its variation could have changed the Q-factor of the DPO.

In order to characterize the measured oscillator deflection noise, we first analyzed the data taken in absence of external excitation. This data was considered as obtained all in a single measurement without dead time between the single runs [97]. Fig. 4.8 displays the statistic of the X quadrature for two different acquisition times, 2500 s and $1.7{\cdot}10^5$ s. In both cases the experimental data was fitted to Eq. (3.17),with the exponents as fit parameters. The plots of the fit residuals show how the agreement with theory improves for increasing measurement time, as expected. Also, the noise of the detection system was found to be approximately 50 times smaller than the thermal noise of the DPO, using the procedure described above. Assuming the statistics to be indeed due to Brownian noise, from the fits it is possible to obtain the torsion constant of the oscillator,

$D = (8.04 \pm 0.06) \cdot 10^{-2}$ Nm.

The torsion constant can also be approximately calculated from the oscillator's dimensions and is given by [84]

$$D_{sp} = \xi \frac{ab^3}{c} S, \tag{4.5}$$

where ξ is a parameter depending on the geometry of the oscillator, equal to 0.25 in our case, S is the shear modulus of silicon, a is the full width of the oscillator's head and is equal to 6.85 mm, b is the thickness, and $c = 1.09$ mm is the neck width. The calculated torsion constant is $D = 7.7 \cdot 10^{-2}$ Nm, in good agreement with the value obtained from the noise data. This confirms that the observed noise is Brownian noise.

In order to determine the torque sensitivity of the sensor, a small harmonic excitation was applied to the oscillator, as previously described. This was implemented by applying a small a.c. voltage at the sensor's resonance frequency to the piezoceramic actuator mounted on the vibration isolation system. The excitation voltage was generated by a frequency synthesizer phase-locked to the local oscillator used for the lock-in detection. In order to determine the correspondence between voltage and torque, the excitation was made large enough to produce an easily detectable deflection, which was converted into a torque by multipling it with the experimentally determined spring constant. In doing so, we made sure that the response of piezoceramic actuator was linear in the range used. In the following we used an external excitation corresponding to a torque $\Gamma_0 = 4.3 \cdot 10^{-18}$ Nm and its phase was chosen to be equal to the local oscillator phase. According to the theory of Section 3.2, this torque should be detectable for intergration times exceeding $1{\cdot}10^4$ s.

Fig. 4.9 shows the mean values of the X quadrature as a function of the averaging time. Note that the mean of the lock-in measurements is the time average of the Fourier amplitude of X at the DPO's resonance frequency. In calculating these mean values we assumed that the dead time between successive runs do not introduce any deviation, in analogy to the case previously illustrated. Since each sample was taken over 0.3 s, the "true" integration time corresponds to $5.1{\cdot}10^4$ s. The shown error bars are equal to ± 3 standard deviations of the mean value, calculated from the individual data points. The mean quadrature amplitude corresponds to, after subtracting the detection system noise, an excitation torque of $4.4{\cdot}10^{-18}$ Nm, in good agreement with the expected level.

For comparison, the figure also displays the mean X quadrature in absence of mechanical excitation. As can be seen, the presence of an external excitation is masked by noise for averaging times shorter than $7{\cdot}10^3$ s, whereas it is visible for longer averaging, in accordance with the above estimate. Statistical testing was done to determine if

the presence of the external signal resulted in a significant difference of the two sets of data. The result of a t-test for $2.5{\cdot}10^4$ samples indicated that the mean quadratures are statistically different with a significance level of 95%.

From the experimental data, we can estimate the minimum detectable torque as follows. The full data set is divided into 20 equally long subsets. The standard deviation of the subset mean values may be identified with the thermal amplitude noise, $1.3 \cdot 10^{-12}$ rad. As criterion for the minimum detectable torque we consider the torque equivalent to twice this deflection noise value, $1.3 \cdot 10^{-18}$ N m. This holds for an integration time of $2.5{\cdot}10^3$ s. Extrapolation to an integration time of $5.1 \cdot 10^4$ s (the whole data set length), yields $2.8 \cdot 10^{-19}$ N m. The theoretical value for this quantity, from Eq. (3.16) corrected by a factor $1/\sqrt{2}$ for the case of detection of a single quadrature, is $1.3{\cdot}10^{-18}$ Nm, a factor 5 larger than the extrapolated experimental value. The origin of this difference is unclear.

In conclusion, we have shown that it is possible to detect weak torques on the order of few 10^{-18} N m by using a macroscopic single-crystal oscillator (sensitive area of 12.5 mm^2), which can easily be fabricated in clean-room facilities. Moreover, we have experimentally reached the thermal-noise limited sensitivity of the detector. In particular, we showed that the measuremed noise level is in general agreement with Brownian noise theory. Thus, our apparatus represents a suitable approach for the detection of gravity-like new forces at short distances, a project studied in our laboratory. Moreover, the sensor could also be employed for the detection of classical, e.g. magnetic forces.

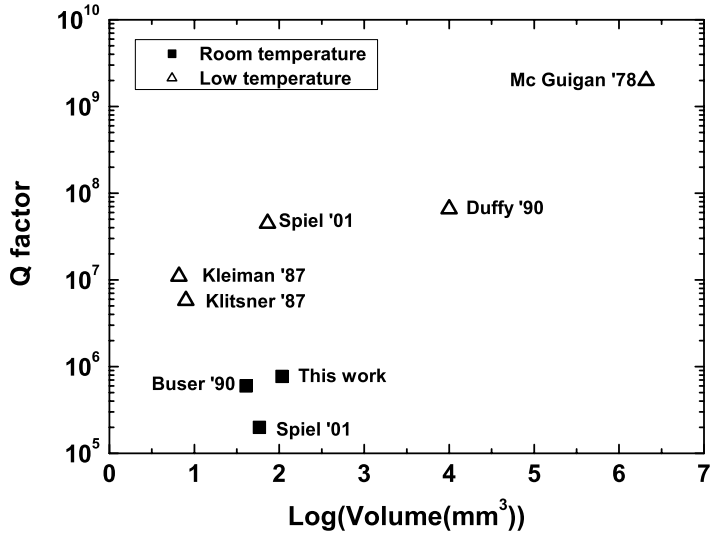

Figure 4.7: Comparison of the quality factors of different macroscopic mechanical oscillators[22, 78, 92, 93, 94, 95, 96]. (Picture adapted from Ref. [21].)

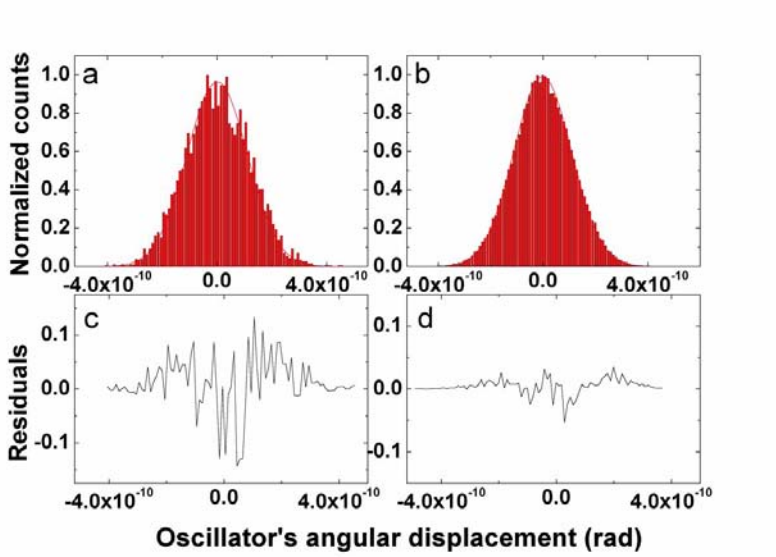

Figure 4.8: Histograms of the oscillator's X angular displacement quadrature measured at resonance and in absence of external excitation for two different measurement durations: (a) $2.5{\cdot}10^3$ s and (b) $1.7{\cdot}10^5$ s. The continuous curves represent Gaussian fits. (c) and (d) show the fit residuals.

4.3.3 Optical actuation

In the past, DPOs were mainly excited by electrostatic techniques. These require a metallic coating on the oscillator and the use of an electrode in the vacuum vessel [76]. In some applications, for example detection of small forces, optical actuation represents a suitable alternative. Although already used for different kinds of microoscillators [82], this approach has not previously been implemented for DPOs. The principle relies on the modulation of the intensity of a laser beam impinging on the oscillator. If the modulation is at the resonance frequency of the DPO, the periodic stress caused by the temperature modulation can couple to the oscillator mode. We used a He-Ne laser (spot size $\sim$ 1 mm^2) to excite the DPO. The beam was positioned on the DPO's wing or neck. An acousto-optical modulator, driven at the DPO resonance frequency by a signal generator, produced a sinusoidal amplitude modulation of the laser beam output power. The modulation depth was nearly 100%.

In Fig. 4.10(a) the response of the DPO to a rectangular optical excitation signal with a peak power of 10 μW is shown. Fig. 4.10(b) shows that the angular displacement of the oscillator head is proportional to the average power and to the power modulation amplitude of the laser beam. This measurement was for the laser beam impinging on the DPO wing. However, the efficiency of the excitation depends strongly on which part of the oscillator is illuminated. The strongest effect was measured when the laser beam was put on the bridge connecting neck and wings of the oscillator. This dependence allows, at least in principle, the use of previously calibrated DPOs as position sensitive photodetectors or as power meters. By comparing the signal and noise levels in Fig. 4.10(a), we can estimate that the minimum detectable power for a 300 μm thick DPO is 10 nW in a bandwidth of 0.1 Hz. Its sensitivity could be enhanced through a strongly absorbing coating on the DPO's most sensitive area, which, where appropriate, could be also chosen to widen the spectral range of the detector. Fig. 4.10(c) shows the effect of two counter-propagating beams impinging on opposite sides of the oscillator (see also Ref. 17). The angular oscillation amplitude of the DPO vanishes if the difference of the average power of the laser beams is equal to zero.

A second optical excitation method has also been studied. In this case the laser beam impinging on the oscillator had a constant average power, but its position was modulated. This was obtained by mounting a mirror on a piezoceramic actuator driven at the resonance frequency of the AS2 mode. The laser beam reflected by the oscillating mirror onto the DPO causes a position dependent temperature modulation, which excites the oscillator. The DPO oscillation amplitude as a function of the scan amplitude is

shown in Fig. 4.11(a). The laser optical power in this case was 5 mW. The DPO amplitude was found to be about 500 times larger than the thermal noise at room temperature. Fig. 4.11(b) shows that the DPO amplitude is proportional to the optical power of the laser beam used for the excitation.

The DPO can also be frequency-tuned by the laser. This was accomplished by illuminating the neck of the DPO with a laser beam, whose amplitude was not modulated. As shown in Fig. 4.11(c) the resonance frequency of a 300 μm thick DPO is a linear function of the laser beam average power. The measured frequency-power coefficient is -50 Hz/W. The optical power required to shift the DPO resonance frequency by the FWHM $\Delta\nu = \nu_R/Q = 0.03$ Hz is 0.6 mW.

The laser excitation enabled us to characterize and control the DPOs. The use of this technique can have major advantages in applications in which a remote excitation system is required, for example in a high-temperature environment.

4.4 Metal oscillators

Since our aim was to fabricate a sensor suitable for gravitational measurements, the possibility of manufacturing a metal oscillator, i.e. with an higher density than silicon, was investigated. Changing the material of the DPO, but not its geometry, affects the minimum detectable Yukawa force, since it has the following dependance on the material density and the Q factor (see for example Eq. (3.2))

$$\alpha \propto \rho^{-1} Q^{-1/2}. \tag{4.6}$$

Three different materials were tested: brass, copper and bronze. The best results were achieved with the copper oscillators. Their quality factor and resonance frequency are reported in Table IV. The measured quality factor is about one order of magnitude lower, compared to the one of the silicon oscillators. This was probably due to the dislocation motion, an effect that is not present in single-crystal silicon. Moreover, the measured quality factors showed the tendency to decrease over time. Such a phenomenon was probably due to the depinning of dislocation induced by mechanical stress [79]. If the damping is determined by the dislocation motion, it is possible that the change of Q is due to a variation of the dislocations mobility. The performances of the metal DPOs were not improved by thermal annealing at $300°C$.

Table IV. Resonance frequency and quality factor for three copper oscillators.

Material	Resonance frequency (kHz)	Q factor
Cu	2.0	$8{\cdot}10^3$
Cu	1.9	$1{\cdot}10^4$
Cu	1.8	$1.5{\cdot}10^4$

Defining α_{Si} and α_{Cu} as the minimum detectable Yukawa interaction for silicon and copper DPOs, the ratio $\alpha_{\mathrm{Si}}/\alpha_{Cu}$ is equal to about 1, . In conclusion, we have shown that the use of the metal oscillators fabricated in our laboratory cannot improve the sensitivity of our apparatus.

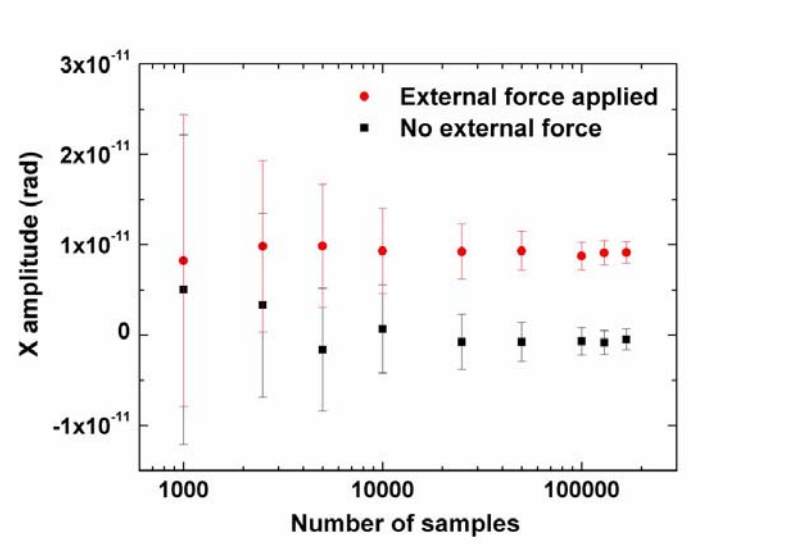

Figure 4.9: The mean values of the oscillator's X quadrature, measured with and without a small external mechanical excitation ($4.3{\cdot}10^{-18}$ Nm), as a function of integration time. Each sample corresponds to 0.3 s measurement time. The shown error bars correspond to ± 3 standard deviations of the mean values of the individual lock-in readings.

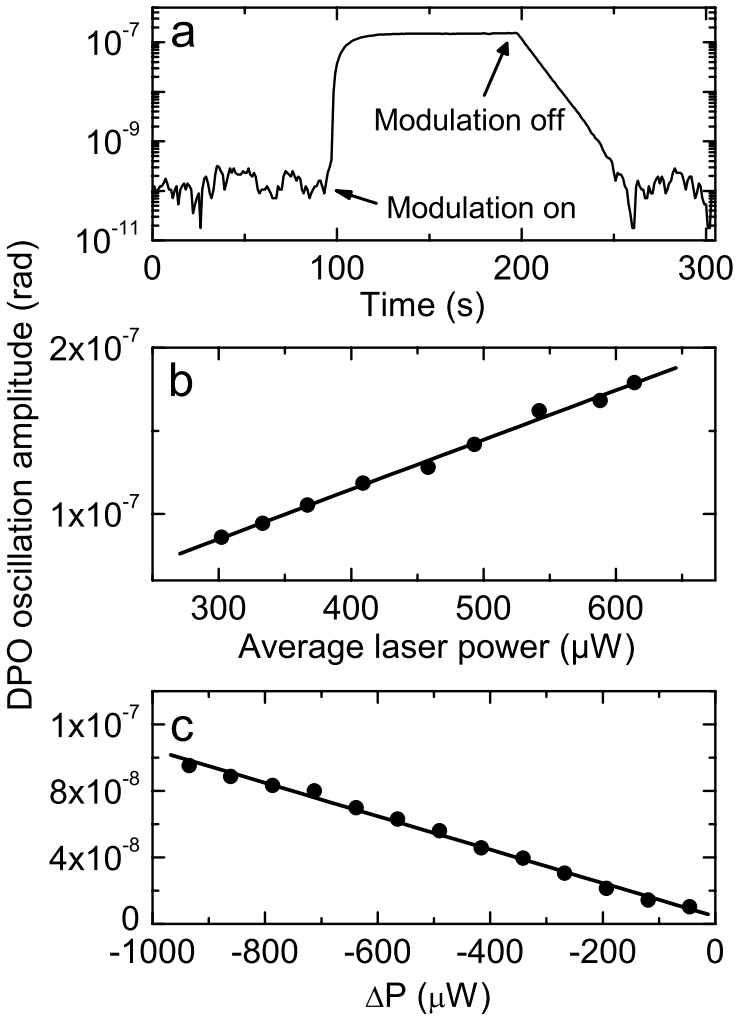

Figure 4.10: (a) Response of the oscillator to laser power modulation that was turned on at t = 93 s and off at t = 195 s. The fluctuations in the signal amplitude occuring when the laser is off, are due to Brownian noise of the oscillator. Lock-in time constant was 0.3 s. (b) Optical excitation of a DPO by a laser beam modulated at the oscillator's resonance frequency. (c) Optical excitation of a DPO by two counterpropagating laser beams, that impinge on the oscillator's wing. ΔP is the difference in the optical power of the beams.

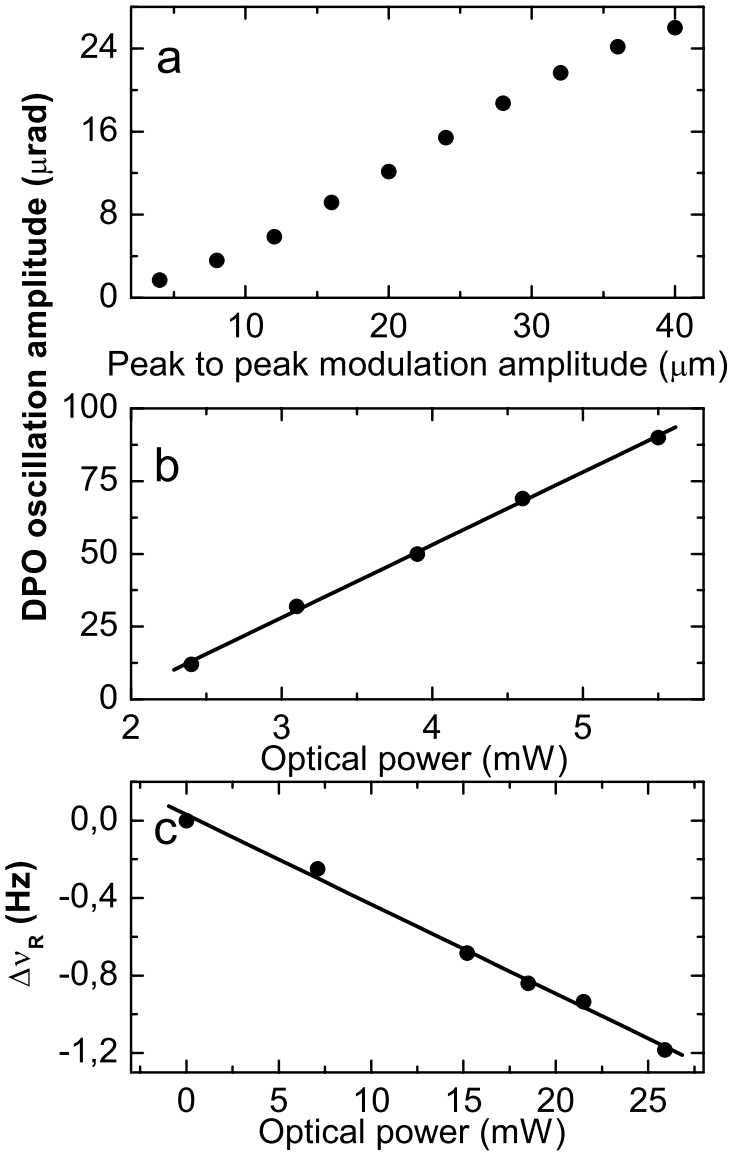

Figure 4.11: (a) Excitation of a DPO by a laser beam scanned on the region connecting the wings to the leg. The laser power was 5 mW. (b) DPO excited by a position modulated laser beam. Here the scan amplitude is constant (40 μm), but the laser power is varied. (c) Δv_R is the shift of the resonance frequency induced by a cw laser beam illuminating the neck of a 300 μm thick DPO.

Chapter 5

Gravitational excitation

There are two possible ways to produce a gravitational torque modulation in front of the sensor. In the first case the excitation is accomplished through position modulation of a source mass along the direction orthogonal to the sensor surface. This approach, used in other experiments [43], would have shown two main disadvantages, if implemented in our setup. Firstly, the mass motion could have transferred momentum to the oscillator through residual gas molecules excitation, even when the test masses had been operated under vacuum conditions. Secondly, the mass motion would have generated vibrations at resonance, that, if not appropriately damped, could have excited the sensor. An alternative approach is given by a periodic movement of the source mass along a direction parallel to the sensor's surface.

We followed this second scheme implementing the source mass motion through a rotating wheel made of a low density material, which held individual high density source masses. A sketch of the oscillator/wheel setup is shown in Fig. 5.1.

Both faces of the wheel can be machined flat in order to minimize their interaction with the residual molecules in the vacuum vessel. Moreover, the rotation frequency of the wheel was reduced by the use of several masses mounted on it. In this way the probability that the sensor was excited by the vibrations produced by the source masses was reduced. This approach overcomes also the practical difficulty in finding an actuator able to move a mass of the order of 10^{-2} g over a distance of some hundred micrometers and at a frequency of about 6 kHz.

In this chapter we describe the excitation system, which was designed to produce the resonant gravitational torque on the double-paddle oscillator. Using a numerical simulation based on a routine written by H. Wenz[1], it is shown how to optimize the

[1] M. Weingran obtained similar results with an independent simulation [98].

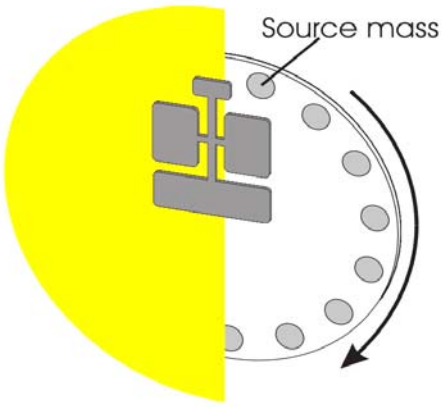

Figure 5.1: View of the oscillator and source masses attached to the wheel, together with half of the electrostatic shield (more details about this are given in Chapter 6).

dimensions of such an excitation system, in order to maximize the expected Newtonian and Yukawa torques on the sensor.

5.1 Calculation of the Newtonian and Yukawa torques

In the following calculations Cartesian coordinates are used, in which the torsion axis of the oscillator lies on the z axis, the long side of the DPO head is parallel to the y axis and the x axis is orthogonal to the DPO. The gravitational and Yukawa torque produced along the z direction by the elementary source mass dm_s on the oscillator mass dm_o, which is located at distance $\overrightarrow{r}_o = (x_o, y_o, z_o)$ from the torsion axis, is given by

$$\begin{aligned} d\Gamma_z &= [x_o\,(y_s - y_o) - y_o\,(x_s - x_o)] \times \\ &\quad Gdm_s dm_o \left(\frac{1}{|\overrightarrow{r}_o - \overrightarrow{r}_s|^3} + \alpha \left(1 + \frac{|\overrightarrow{r}_o - \overrightarrow{r}_s|}{\lambda} \right) e^{-\frac{|\overrightarrow{r}_o - \overrightarrow{r}_s|}{\lambda}} \right), \end{aligned} \tag{5.1}$$

where $\overrightarrow{r}_s = (x_s, y_s, z_s)$ is the distance of the elementary source mass dm_s from the origin of the coordinates system. In order to calculate the total torque acting upon the sensor the following six integrals are to be solved

$$\Gamma_z = \int_{V_o} \int_{V_s} d\Gamma_z, \tag{5.2}$$

where V_o and V_s represent the oscillator and source mass volume respectively. Two integrals were solved analytically [29], whereas the remaining four were calculated numerically using the function *NIntegrate* in Mathematica, which is based on Riemann sums that approximate the integral. In order to reduce the duration of the computation, the second term in the difference in squared brackets of Eq. (5.1) was neglected. From direct comparison between different calculations we estimated the error made under this assumption to be of the order of one percent, which was acceptable, considering that the experimental uncertainty on the wheel-distance was estimated to be larger than five percent.

A series of simulations was performed to determine the optimum size and position of the source masses on the wheel, under the assumption that their interaction is only due to Newtonian gravity. In this calculation we used the dimensions given in Fig. 4.1 for the DPO, its density $\rho_s = 2.3 \cdot 10^3$ kg/m^3, the wheel radius $R_w = 2.7 \cdot 10^{-2}$ m, the distance between the wheel center and a source mass center $r = 2.375 \cdot 10^{-2}$ m, and the density of the source masses $\rho_m = 20 \cdot 10^3$ kg/m^3 (Pt alloy). The radius of the wheel was chosen to be as large as possible while staying compatible with the dimensions of the experiment. This choice is due to the experimental need to rotate the wheel at a frequency which is not too large (below 500 Hz), in order to reduce the vibrational noise due to the motor.

Fig. 5.2 shows the results of a simulation, in which the radius of the source masses was varied between 1.5 and 4.5 mm. The maximum torque for an oscillator-wheel gap of 0.1 mm is achieved when the radius is equal to 3 mm, which corresponds to about half of the DPO's head. As a following step, the thickness of the source masses was varied in the range between 0.3 and 4.5 mm. We found that the Newtonian torque for thicknesses of the order of 2 mm reaches about 80% of its maximum value, as illustrated by Fig. 5.3. Setting the radius and thickness of the source masses equal to 2.5 and 2 mm respectively, we calculated the Newtonian torque as a function of time[2] as shown in Fig. 5.4. According to this result the time-dependence of the torque can be well approximated by a harmonic function.

Assuming, now, the existence of a Yukawa-like correction to Newton's gravity law, a slice of the source masses of thickness λ (interaction range of the correction) is expected to give the main contribution to the torque as illustrated in Chapter 3. This condition, confirmed by our calculations as shown in Fig. 5.5, is fulfilled in our experiment by

[2]The chosen dimensions are slightly smaller than the ones maximizing the Newtonian torque (see Fig. 5.3). When deciding upon the size of the source masses, we looked for a good compromise between maximum efficiency of the experiment and high costs due to the platinum masses.

the use of 2 mm thick source masses, since we focus attention on Yukawa-like forces with an interaction range of the order of 1 mm or smaller. Fig. 5.6 shows the distance dependence of the torque produced on the DPO by platinum or copper masses inserted into an alumium wheel provided with 15 sources masses. As a reference the expected Brownian noise level for an integration time of 600 s is shown. The torque produced by a plastic wheel with the same geometry, but without inserted disks, is also shown. Even if the momentum, in this case, is produced by the mass left after drilling the holes, our routine still gave the correct results under the assumption that the holes had a negative density. All three curves were fitted to exponential functions and it was found that their amplitude was reduced by a factor e^{-1} over a distance of 1.29 mm.

Since our aim was to test the predictions of the model by Arkani-Hamed, Dimopoulos and Dvali, we calculated, as an example, the Yukawa torque due to our excitation system (platinum source masses) in the case of the existence of two extra dimensions with a compactification radius of about 1 mm. In this case the non-Newtonian correction is expected to have an interaction range of the order of 1 mm and its amplitude, α, is expected to be in the range between 1 and 10. Fig. 5.7 shows the results of this simulation for $\alpha = 4$ and $\lambda = 1$ mm. The fact, that the existence of a Yukawa-like correction would change the distance dependence of the measured torque, suggests a possible strategy for our measurements. In fact, we could measure the distance dependence of the torque exerted by the source masses and compare it with the theoretical curve. The main advantage of this approach is that the distance dependence is not affected by the experimental uncertainties of the density of the masses, but is only determined by the geometry of the masses and by the analytical form of the interaction.

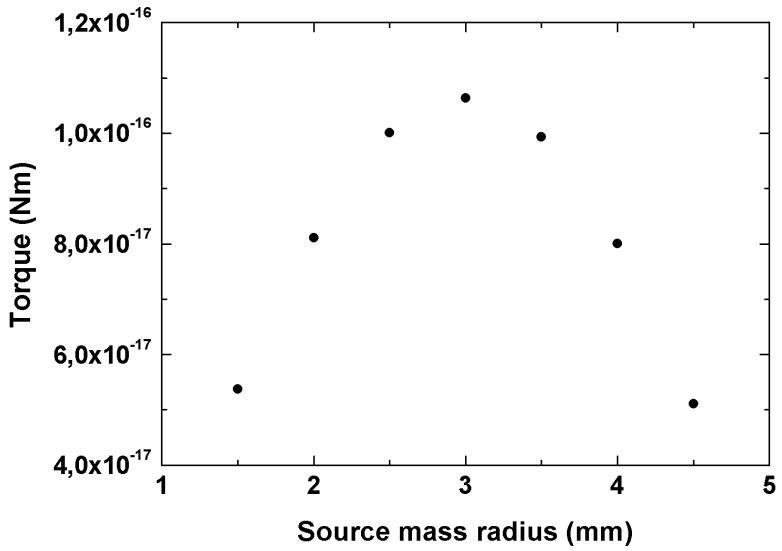

Figure 5.2: Calculated gravitational torque due to a platinum disk (thickness 2 mm) on the DPO as a function of the disk radius. Gap between oscillator and wheel: 100 μm.

5.2 Experimental aspects

The wheel was made of a high strength aluminium alloy, while the source masses were made of platinum or copper and filled the 15 equally spaced holes in the wheel. All dimensions have already given in the previous section. Using metal attractors to gravitationally excite a sensor was a natural choice in designing our experiment. It was not only due to the characteristic high density of some metals, but also a consequence of their low deformability under the mechanical stress induced by the wheel's rotation (rotation frequency $\sim$ 24000 rpm $\sim$ 400 Hz). Moreover, they can be machined to a high degree of precision in an ordinary workshop. In manufacturing the source masses, great attention was paid to the fact that both surfaces were flat, in order to minimize the interaction with the residual gases in the chamber. In addition, we performed the following test to prove the flatness of the wheel. A wheel without any inserted disks was mounted on a test motor and rotated. It was illuminated by a light source from one side, while a photodiode was put on the other side. The photodiode was adjusted so that its active surface was partially covered by the shadow of the rotating wheels and its signal was detected by a FFT analyzer. The same measurement was repeated once the disks were inserted into the wheel. A modulation of the photodiode's signal at the motor's rotation

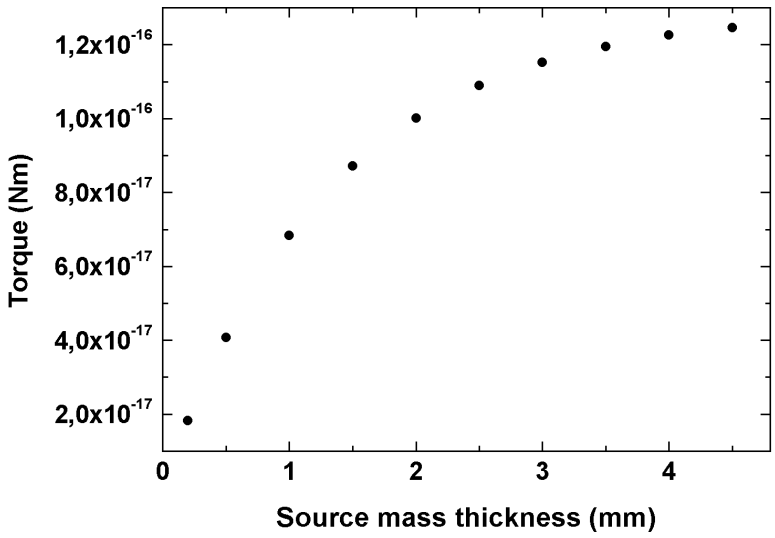

Figure 5.3: Influence of the disk thickness on the gravitational torque. The gap between oscillator and wheel is the same as in the previous case

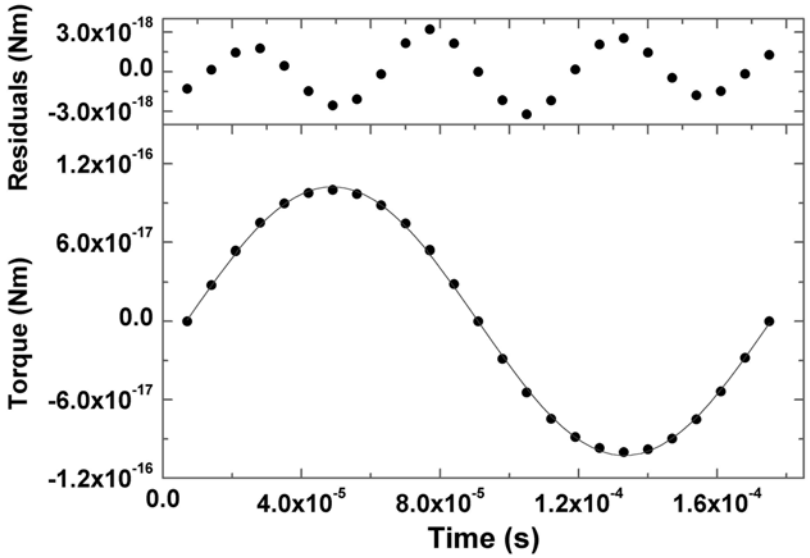

Figure 5.4: Lower diagram: Gravitational torque as a function of time (Disks: radius 2.5 mm, thickness 2 mm.) The line is a sinusoidal fit. Upper diagram: Fit residuals.

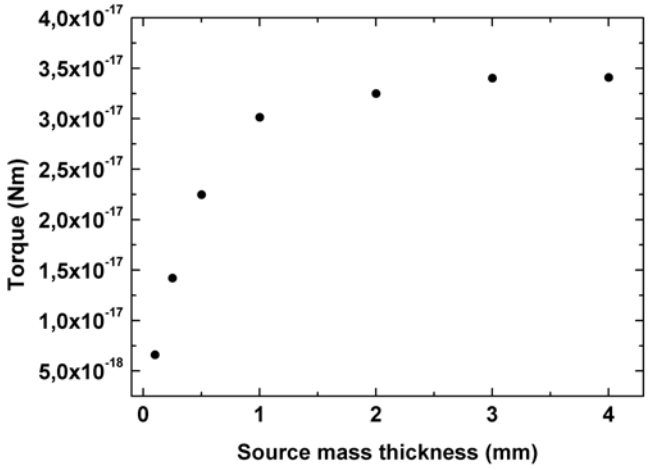

Figure 5.5: Calculated Yukawa torque as a function of the source mass thickness (simulation parameters: $\alpha = 1$, $\lambda = 500$ μm, gap 100 μm).

frequency was measured in both cases and its amplitude was not significantly changed by the insertion of the source masses. This result showed that the source masses did not introduce any change in the flatness of the wheel. The measured modulation can be associated with a small wobbling of the wheel, that was measured later with another method (see next chapter).

In the final setup the wheel was fixed on the axis of a small brushless DC-motor (Faulhaber 2036), which was commercially available in two different versions for standard and vacuum applications. We tested both motors in an auxiliary vacuum chamber (10^{-5} mbar) and we could observe that the standard version showed a shorter lifetime (noisy bearings), but its outgassing was relatively small. Nevertheless, all the following results where obtained using the vacuum-compatible motor, whereas a standard motor was used for tests at normal pressure. Since non-uniform mass distribution in the wheel could reduce the motor lifetime and increase the vibrational noise level, all wheels were balanced after being fixed to a motor. Hereby excess mass was removed from the wheels' back in order to preserve the flatness of the front side. For the first generation of wheels this removal of mass was performed by an external company, whereas at a later stage we were able to balance the wheels in our laboratory [98].

In order to provide an efficient excitation, the wheel rotation had to stay constant to within the oscillator linewidth ($\sim$ 35 mHz for a 300 μm thick oscillator). The frequency

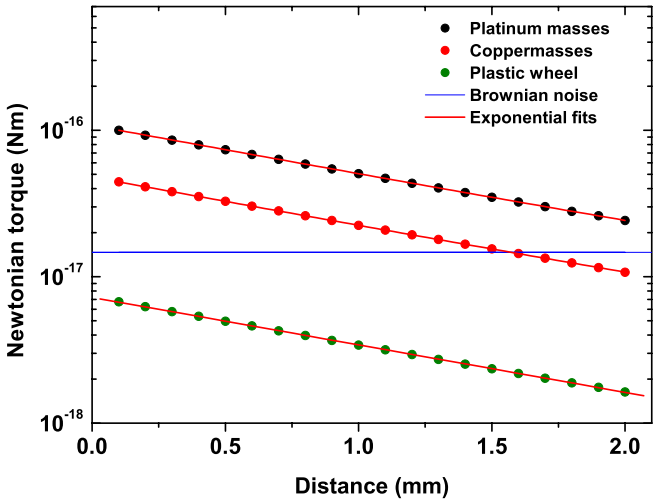

Figure 5.6: The gravitational torque due to three different attractors as a function of the gap between sensor and source masses. The upper curve represents the newtonian torque due to 15 platinum disks inserted into an aluminium wheel. Substituting them with copper disks, the torque decreases (middle curve). The lowest curve corresponds to the torque produced by a plastic wheel, whose holes are not filled. The three curves are fitted to exponential functions. The expected Brownian noise level is shown for an integration time of 600 s.

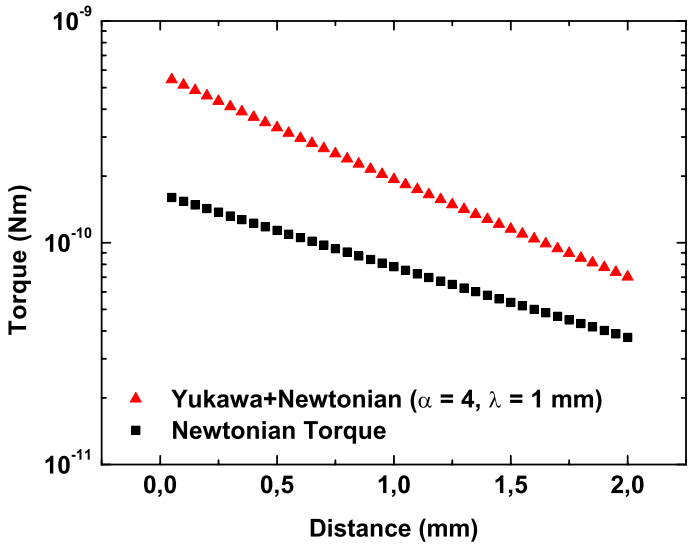

Figure 5.7: If a Yukawa-like correction to Newton's potential, due to two extra dimensions, existed (here we assumed that the correction has the form given by Eq. (2.5) $\alpha = 4$ and $\lambda = 1$ mm.), it could in principle be detected by our experiment, since it would change the distance dependence of the torque exerted on the oscillator.

stabilization servo system (Faulhaber BD-3502) delivered with the motor was not able to attain the level of stability required in our experiment. We could not find commercial driving electronics to satisfy this requirement. As a consequence, we developed our own stabilization system. In the first generation of this experiment the signal from a tiny home-built light-gate mounted on the motor was read out by a frequency counter (HP53181A) and sent to a computer, which controlled the motor's frequency through a LabView-based program developed by S. Schiller. In this way we achieved a linewidth of the order of 50 mHz over a few hours.

A significant improvement was obtained using a microcontroller based driver unit developed by M. Weingran [98], which was used in parallel to the commercial servo system. This stabilization unit relied on the principle of a phase-locked loop (PLL). The phase difference between a reference signal and the effective motor frequency, monitored through a Hall sensor in the motor, was calculated and an appropriate correction voltage was applied to the motor. Since the integration time span corresponded to many periods of the reference signal, a small frequency difference resulted in a large change in the phase of the signal. A disadvantage of this approach was that large frequency oscillations (> 1 Hz) made the loop unstable and, in this case, it was necessary to turn off the motor. Nevertheless, this was not a severe limitation to our experiment, since the typical frequency instability of the motor was of the order of some ten millihertz over several hours. A signal generator (SRS DS345, Stanford Research Systems) was used as a reference for the PLL, which had an accuracy of ± 5 ppm in the range between 20°C and 30°C. It corresponds, for a frequency of 6 kHz, to an uncertainty of about 30 mHz, which is comparable to the oscillator's linewidth.

In order to improve the stability of the reference, the signal generator was fed in with a 10 MHz signal from a function generator (Agilent E4422B) with an accuracy better than 1 ppm. Fig. 5.8 shows the improved stability obtained using the 10 MHz reference. Here, the PLL's reference signal and the motor signal at 341 Hz were measured by a FFT analyzer. The full width at half maximum of the motor was found to be smaller than 1 mHz over 4000 s. The almost perfect overlap of the motor and reference curve in Fig. 5.8 indicates that the measured frequency instability is due to the internal reference of the spectrum analyzer used in this measurement.

The calculated root Allan variance of the motor and reference signal, a hydrogen maser, is shown in Fig. 5.9 as a function of the integration time τ_0. The Allan variance of the motor signal scales like the inverse of the square root of the integration time ($\sim \tau_0^{-1/2}$) in the range from 10 s to 700 s, which is the typical dependence expected for noise with white spectrum. The achieved instability is of the order of $4{\cdot}10^{-9}$ for

an averaging time of 700 s. Since the frequency counter used in these measurements was not frequency locked to the hydrogen maser, the dependence of both curves on the integration time shown in Fig. 5.9 could have been affected by the instability of the internal reference of the frequency counter.

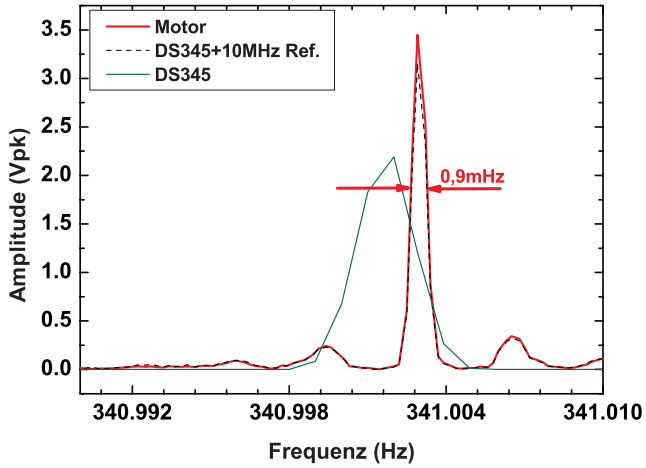

Figure 5.8: Spectrum of the motor signal (red) and of the reference frequency (externally controlled DS345 generator) used for stabilization (dashed black). For comparison, the spectrum of a lower stability frequency (from a DS345 generator without external reference) is also shown, in green.

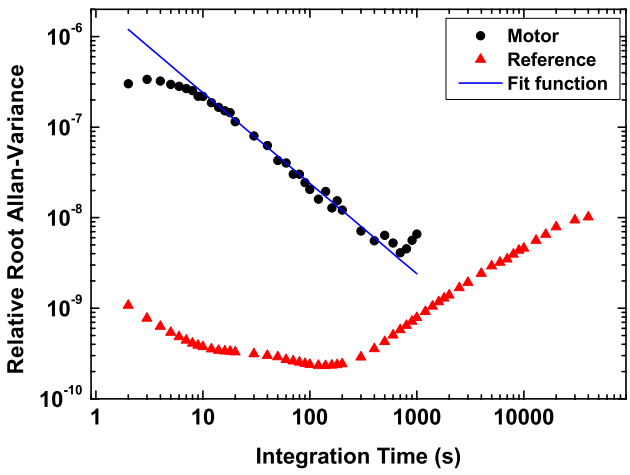

Figure 5.9: Root Allan variance of the motor signal (black) and of a hydrogen maser used as a refence for the motor stabilization electronics (red). The fit shows that in the range between 10 and 700 s the motor's stability is limited by noise with white spectrum. Both motor and maser signal show an instability, which could have been due to the internal reference of the frequency counter used for this measurement.

Chapter 6

The Experiment

The present chapter is devoted to a review of the apparatus we set up to test gravity with a DPO and the excitation system described in the previous chapters. Moreover, particular attention is paid to describing the data acquisition and the alignment of the test masses.

A view of the whole experiment, as it appeared during a typical measurement, is given in Fig. 6.1. The sketch in Fig. 6.2 shows a cross section of the vacuum chambers hosting the source and test masses. Our apparatus consisted of two stainless steel vacuum vessels, which rested on an optical table (mass 1.5 tons) provided with four pneumatic isolators having vertical frequency smaller than 1 Hz. The chamber on the left-hand side was of a high vacuum type, in which pressures of the order of 10^{-6} mbar were achieved using a turbo molecular pump (pumping speed 64 l/s). As shown in Fig. 6.2 this vessel contained the excitation system. This chamber was connected through two tubes of different diameters to a second vacuum chamber. In the lower tube, having a larger diameter, the motor-wheel system could be moved along the axis of the tube and adjusted with respect to the DPO (5.9 kHz resonance frequency). The end of this tube was closed by a thin metallic foil (brass, 25 μm thick) tightly stretched between two stainless steel rings, and, since it was grounded, could be used as an electrostatic shield. In the second connection between the vacuum vessels a valve was inserted, which allowed us to create a differential vacuum between the chambers and to avoid deformation of the thin electrostatic shield, due to pressure differences, during pumping down. The second vessel, which contained the oscillator, was of an ultra-high vacuum type, where a pressure of $1{\cdot}10^{-7}$ mbar was produced by a second turbo molecular pump (pumping speed 250 l/s). Both pumps were operated using oil free pre-pumps, in order to avoid contamination and degradation of the DPO's mechanical properties. Unscrewing the

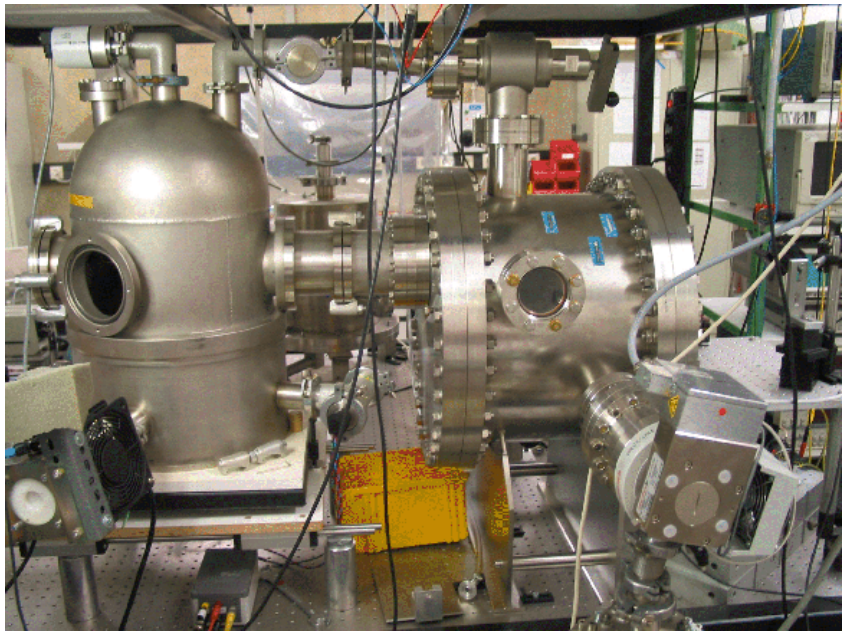

Figure 6.1: Side view of the apparatus.

ends of the two connections, it was possible to move the smaller chamber away from the larger one. For this purpose the high vacuum chamber was mounted on a system of rails, which allowed it to be moved with respect to the second vacuum vessel. This degree of freedom was required in order to align the two test masses, as explained in the next sections. Before describing each single component in more detail, we draw attention to another advantage of this experimental design. In our system the center of mass of the sensor-system could be kept far apart from that of the excitation system. In this way vibrations generated by the motor had to propagate over a long distance before they could reach the sensor. A disadvantage of this approach is that the relative adjustment of the wheel and the DPO, as later explained, is made more difficult.

6.1 The sensor system

The sensor's vacuum chamber was shaped like a cylinder with its main symmetry axis parallel to the surface of the optical table. Four brackets were welded inside it and a stainless steel plate was laid on them. A thin layer of elastomer was inserted between each bracket and the plate in order to reduce the transmission of mechanical vibrations. Brass weights (not shown in Fig. 6.2) were attached to the plate to lower its mechanical

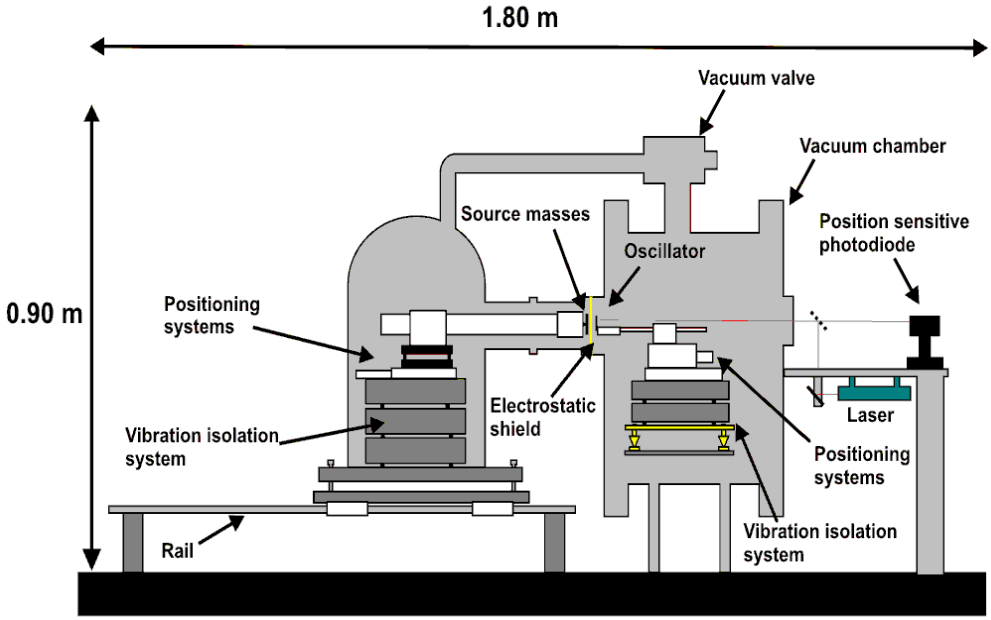

Figure 6.2: Cross section of the apparatus showing the major components of the experiment. Both vacuum vessels were equipped with vacuum gauges (not visible in this sketch). Dimensions of some components are not to scale.

resonance frequencies below 3 kHz. An electroshaker and an accelerometer (sensitivity 10 V/g, PCB Corp.) were placed on it for diagnostics. A second stainless steel plate was laid on the base plate, which was provided with three brass feet, shaped like upside down cones. This geometry was chosen in order to minimize the contact area between the two plates and to reduce the transmission of seismic noise to the upper stage. By unscrewing the feet it was possible to change the height of the second plate over a range of 8 mm. On this stage lay a passive vibration isolation consisting of two stainless steel disks (diameter 20 cm, thickness 5 cm), that were separated by soft elastomer springs. The springs were made of RTV 615, a material with a low Q-factor and well suited to vacuum operation. RTV can be modeled easily into any shape, since it is made by mixing two liquid components, that have to be then baked at 65°C for about 5 hours. To further improve the vibration isolation we added some graphite powder (6% by weight) to the liquid components [99], which increased the themoelastic losses in the elastomer, improving its damping properties. On the top of the vibration isolation system a precision alignment unit rested, which consisted of a linear stage, a tilt stage, and a goniometer (OWIS GmbH). While the first stage was hand-driven, the other two were motorized and driven by a computer. The resolution of the linear stage was 10 μm, while the minimum angular displacement due to both tilt stage and goniometer was smaller than 0.1 mrad. An aluminium rod (diameter 1 cm, length 25 cm) connected the oscillator holder to the alignment stage. Through the manual rotation of the rod around its symmetry axis, the oscillator could be turned parallel to the electrostatic shield. The oscillator was glued to an aluminium frame by using an epoxy (Stycast 1266) as already described in Chapter 4. In order to make the DPO resonance frequency constant, it is necessary to stabilize its temperature, as previously discussed. Therefore, a small electrical heater was glued to the bottom of the holder and a temperature sensor (PT100) was fixed near the DPO foot. The stabilization was achieved by a PID controller, which kept the temperature constant within 10 mK, corresponding to a frequency uncertainty of 2 mHz for the oscillator. In order to avoid that the cables connected to these elements could come into contact with the DPO, they were kept as short as possible and soldered to a connector, glued to one side of the holder, as shown in Fig. 6.3. The frame was also provided with four contact sensors used to determine the distance of the oscillator from the thin metallic membrane. They were connected to suited electronics, that mainly consisted of a sensitive ohmmeter and produced an acoustic signal if at least one of the contact sensors touched either the chamber or the electrostatic shield. Their cables were also connected to the connector on the aluminium frame. The holder was then mounted on a miniature linear stage (displacement range of 4.5 mm, OWIS GmbH),

which was driven by a piezo motor. On the bottom of it, a second hand-driven linear stage was connected, onto which an eddy-current sensor for distance measurements was placed. The resolution of this sensor was better than 1 μm in the range between 0 and 2 mm. Its calibration was performed by mounting it on a hand-driven linear stage and measuring the electrical signal generated at different distances from the electrostatic shield. All cables connecting the oscillator's holder to the external environment were soldered to a connector fixed on the bottom plate of the vibration isolation system. For this application, we chose thin and very flexible electrical wires, characterized by a low transmission of mechanical vibrations in the kHz range and by very low outgassing under vacuum operation. Once the chamber had been closed, the optical detection system was mounted on its side, as shown in Fig. 6.1. It consisted of a He-Ne laser, whose beam reflected by the DPO's head was detected by a split photodiode [98] (see also Chapter 4). Due to mechanical relaxation, for example of the elastomer springs, the position of the beam on the photodetector experienced a slow drift, which could influence the amplitude of the detected signal. In order to eliminate this problem, the photodiode was mounted on a motorized linear stage driven by a servo system, which moved the photodiode in the appropriate direction to compensate for the drift. This motion was performed over a time scale much longer than the vibration period of the DPO. Thus, the actual detection at 6 kHz was not affected by the position stabilization. Moreover, the temperature of the split photodiode was actively stabilized through a PID controller similar to the one used for the DPO, in order to avoid that fluctuation of its temperature could lead to variations in the sensitivity of the detection system.

6.2 The excitation system

The wheel and the motor were mounted in a holder equipped with four distance sensors, similar to the ones used for the oscillator. They can be partially seen in Fig. 6.4. The absence of contact with the chamber was monitored in a way similar to the one described in the previous section. The motor holder consisted of two aluminium cylinders of different dimensions. In the smaller one the motor was fitted, after being inserted into four thin viton rings that had the double function of protecting the motor while being inserted in the metal holder, and of reducing the amplitude of the vibration produced by the rotating wheel. This cylinder was then put in the bigger one and fixed with six aluminium screws, whose ends had been shaped like a tip in order to reduce the contact area and to damp, in this way, mechanical vibrations. Finally, a frame holding the distance sensors, made up of four micrometer screws, was mounted on the larger cylinder.

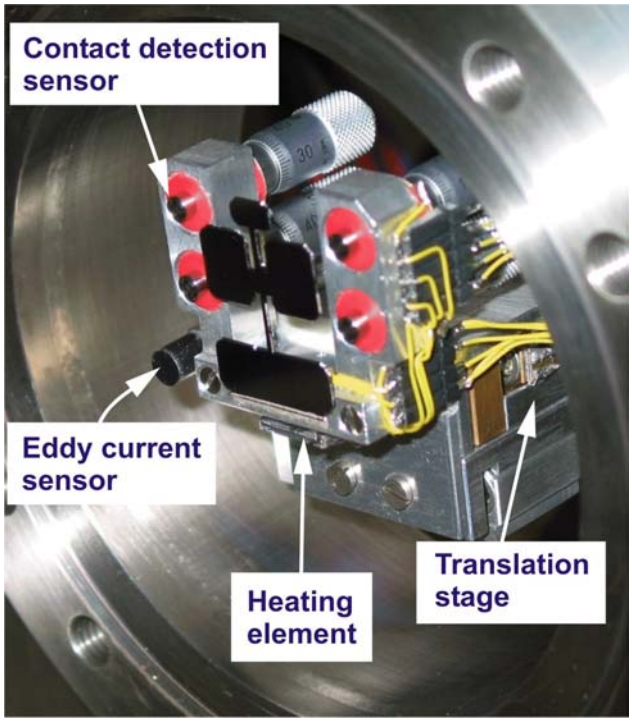

Figure 6.3: A view of the DPO mounted on its holder provided with distance sensors, temperature stabilization system, and positioning stage.

The motor holder was fixed on a longer aluminium tube, which was clamped on the top of the tower composed of the positioning systems and the vibration isolation (see Fig. 6.2). Also this tube was provided with a contact detector, whose output enabled us to determine if the motor holder or the tube itself touched the vacuum chamber laterally. All cables supplying the motor and the contact sensors were fed through the tube in order to avoid that they could propagate vibrations bypassing the isolation system. The positioning system consisted of two parts. The upper part integrated three hand-driven tilt stages, used for making the wheel parallel to the sensor, whereas a computer-driven linear stage allowed us to move the wheel in the direction parallel to the symmetry axis of the holder with submicrometric resolution. The system described above rested on a passive vibration isolation composed of three stainless steel stacks (diameter 25 cm, thickness 8 cm) and elastomer springs, as in the case of the DPO. Particular attention was paid to firmly fixing the electrical cables to the upper disk of the vibration isolation, before their ends were connected to an vacuum feedthrough. In the motor chamber two further sensors were integrated: a pressure gauge and an accelerometer (sensitivity 1

V/g, PCB Corp.).

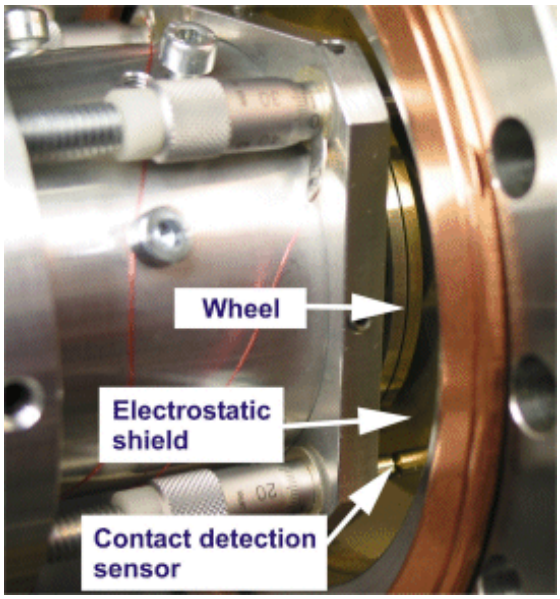

Figure 6.4: Side view of the motor holder, while being brought into contact with the electrostatic shield.

6.3 Data acquisition

Fig. 6.5 schematically shows our apparatus and the devices used for the data acquisition. For the sake of simplicity, the diagnostic units are not shown in the diagram. They consisted, as previously described, of accelerometers, contact detectors with their electronics, and an eddy current distance sensor. The signals were acquired through a commercial analog to digital board (National Instruments) inserted into a personal computer. The measured signal produced by the split photodiode was detected by a digital lock-in amplifier (SRS 830, Stanford Research Systems) using, as a local oscillator, the electrical signal generated by a Hall sensor mounted in the motor. Moreover, a spectrum analyzer (SRS 780) was available to determine Q-factor and resonance frequency of the DPO.

Since our goal was to perform measurements over a long integration time, it was convenient to automate the measurement procedure. We wrote a routine using the software LabView, which enabled us to perform a series of measurements independent of operator supervision. The structure of this routine was the following: first, it was

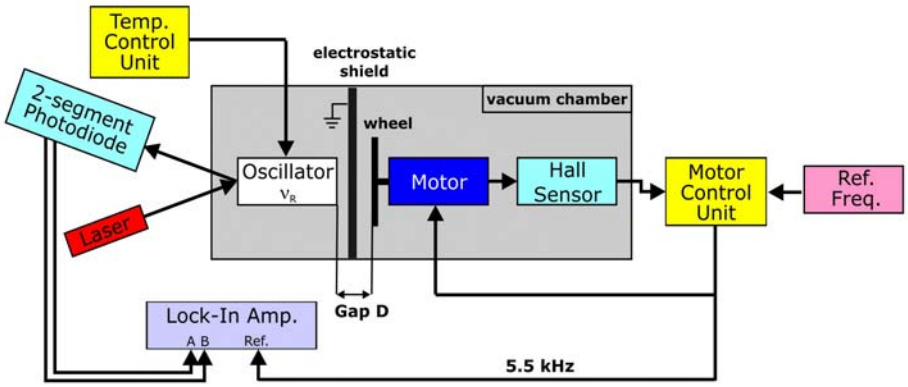

Figure 6.5: Schematic view of the apparatus

necessary to set the number of measurements n for each run, the repetition rate, and the number of times the procedure had to be repeated. Once the program had been started, it generated a file containing information about the status of the system, e.g. the distance between wheel and electrostatic shield. In a second file the date and time corresponding to the beginning of the measurement were recorded. Next, the lock-in amplifier, after being initialized, measured the amplitude and phase of the Brownian motion of the DPO. This data was stored in a single ASCII file. The motor was then turned on. Since it took about one minute before the motor reached the goal frequency, the next step was started only after the end of a two minute standby. At this point the motor frequency was measured two times consecutively within 10 s by a frequency counter (HP53181A). Both values were compared to the goal frequency. If the difference between the measured and goal values was larger than a specified amount set by the user, the motor was turned off and an error message was displayed. Otherwise, a new run of measurements with the lock-in was started. During the measurements the data was stored in the buffer memory of the lock-in amplifier, and only when the run was completed was it moved into a single file. At the end of this measurement, after the motor had been stopped, a pause of 2 minutes was implemented in order to give the DPO the possibility to reach equilibrium. While both data acquisition sessions (with and without gravitational excitation) were carried out, the temperature of the oscillator was measured, and its values were saved

to a file. It was crucial that during the measurement neither the oscillator nor the wheel touched the electrostatic shield. To avoid this occurence the signals coming from the contact sensors put on the motor's and oscillator's holders were constantly monitored. If one of the sensors had touched the shield, the computer would have immediately switched off the motor and stopped the measurement. The reaction time of this security system was estimated to be shorter than one second.

Two other optional routines could be run within this program. The first one was used to determine the resonance frequency of the oscillator. It required a frequency generator and a device to excite the oscillator (e.g. the electroshaker mounted in the DPO vacuum chamber). The parameters necessary to start the frequency search were the start frequency ν_i, the frequency range $\Delta\nu$, and the number of measurements to be performed N. Once this data was entered, the start frequency was given to the frequency generator, which supplied the piezoceramic actuator with an a.c. voltage. After a definite waiting time (four times longer than the oscillator ringdown time) the amplitude of the oscillator motion was measured and its mean value over 10 s was acquired. The same procedure was repeated at the frequency $\nu_{i+1} = \nu_i + \Delta\nu/N$. The difference between the amplitude measured at this frequency and the previous one was calculated. If it was positive, a new measurement was performed at $\nu_{i+2} = \nu_i + 2\Delta\nu/N$, otherwise the program was stopped and the frequency ν_{i+1} was returned as the new resonance frequency.

The second routine performed a ringdown measurement to determine the Q-factor of the oscillator. The DPO was excited by a piezoceramic actuator and after a certain time the excitation was switched off. The decaying amplitude of the oscillator's motion was measured by a lock-in amplifier for two minutes. Finally, the data was fitted to an exponential function and the quality factor was determined from the calculated ringdown time, as was shown in Chapter 4.

6.4 Alignment

Making two masses of macroscopic extension parallel is quite a challenging task if they are within a few hundred micrometers distance from each other. In our setup, the alignment was made even more difficult by the need of the two separate vacuum chambers for the DPO and the wheel, since during this procedure no optical access from the side was available. Besides its influence on the measurement results, a poor alignment could make the fast rotating wheel deform or even tear the electrostatic shield, causing the oscillator to break. The four micrometric screws, mounted on both oscillator and motor holder,

had the function to prevent such a possibility.

In the following we will describe a standard procedure to make the wheel parallel to the electrostatic shield at normal pressure. The motor holder was fixed on a separate support, outside the vacuum chamber, with the wheel being parallel to the plane of the optical table. The screws were adjusted so that all of them extended beyond the surface of the wheel. A thin aluminium plate, appropriately flat machined, was put on the screws' tip. Using an optical stereoscopic microscope (magnifying power 60x) equipped with a measuring scale in one of the oculars, it was possible to measure the width of the gap between the plate and the surface of the wheel. In this way the width of the gap was set to 0.1 mm and then the motor was put back in the vacuum chamber. First the wheel's chamber was connected to the DPO's vessel. Then the wheel and the motor were moved forward until one screw touched the electrostatic shield and produced an acoustical signal. If it had been, for example, the bottom one on the left, the motor holder would have been moved to the left until the right screw also touched the electrostatic shield. By iteratively repeating this procedure, it was possible to make all screws touch the foil at the same time, as in Fig. 6.4. Once this condition was achieved, the motor was moved until the wheel was at a definite distance from the electrostatic shield. Since the motor vibration could turn the micrometric screws, they were held in position from behind by screws with a plastic tip, as shown in Fig. 6.4. As observed in a previous section the motor tended to wobble when the wheel was rotated. To estimate the amplitude of this motion a small mirror was glued to the back of the motor. A laser beam impinging on it was reflected on a position-sensitive photodiode. In this way we observed that the gap between wheel and foil was periodically modulated and the peak-to-peak amplitude of this modulation was smaller than 5 μm.

An analogous alignment procedure was developed for the DPO. The major difference to the previously described procedure was given by the full motorized positioning systems, that enabled us to verify the DPO's alignment even when both vacuum chambers were evacuated We took advantage of this to test the stability of DPO's position after pumping down. In comparison with normal pressure, a slight tilt of the oscillator was observed in vacuum conditions, and the change it introduced in the shield-DPO distance was about 10 μm. The origin of this effect is still not known. Anyway, the DPO was re-aligned regularly after pumping down. No change in the wheel's position was determined by optical measurement analogous to that described to detect the wobbling of the wheel.

All contributions to the experimental uncertainty in the determination of the DPO-wheel separation are summarized in Table V. The total error made on the measurement

of the distance is of 42 μm in the alignment procedure, where the major contribution is due to the measurement with the optical microscope.

Table V. Experimental errors for the measurement of the wheel-DPO distance

Uncertainty due to	Δ (μm)
Motor's positioning	1
DPO's positioning	1
Optical microscope	25
Micrometer screws (Motor)	5
Micrometer screws (DPO)	5
Contact sensor	5
Wheel's wobbling (only during operations)	<5

Chapter 7

Experimental results

In this chapter we present the results of several runs of measurements performed using three different types of source masses: copper, platinum, and plastic. Several consistency check are also presented to determine the nature of the measured torque. Possible changes to the present setup, that could improve the sensitivity of this experiment to non-Newtonian forces, are also suggested. Lastly, constraints to the existence of a non-Newtonian interaction with Yukawa distance dependence are derived and compared to the present best limits.

7.1 Metal source masses

The distance dependence of the torque acting on the oscillator, when excited by copper and platinum masses, is shown in Fig. 7.1.

Each data point corresponds to a measurement duration of 1200 s. For both sets of source masses, the measured signal is notably larger than the expected Newtonian torque (blue and black lines in Fig. 7.1). Both data sets of data were fitted to exponential functions with the form $\eta \exp(-\varepsilon d)$, where d is the distance between wheel and DPO. A comparison of the fit parameters[1] with the theoretical expectation is given in Table VI.

[1] The measured signal was converted into a torque value by using Eq. (3.9) and Eq. (4.2)

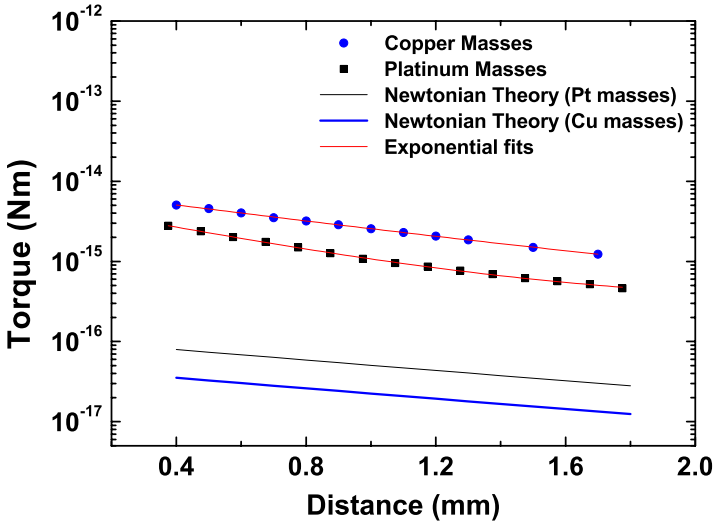

Figure 7.1: Torques measured with platinum and copper source masses compared to the expected gravitational signals (blue and black lines). The experimental data was fitted to exponential functions (solid red lines). Each data point was taken over 1200s

Table VI. Comparison between Newtonian theory and fit parameters

	η (Nm)	ε^{-1}(mm)
Expected value for Cu masses	$(4.7\pm0.1)\cdot10^{-17}$	1.288±0.002
Measured value for Cu masse	$(7.83\pm0.03)\cdot10^{-15}$	0.82±0.07
Expected value for Pt masses	$(1.1\pm0.1)\cdot10^{-17}$	1.288±0.002
Measured value for Pt masses	$(5.01\pm0.06)\cdot10^{-15}$	0.54±0.05

Surprisingly enough, the response of the oscillator, due to excitation by the platinum masses, about 45 times larger than the expected gravitational signal, is 1.6 times smaller than in the case of copper masses. This fact, together with the deviation between the expected and experimental distance dependence, rules out the possibility that the measured signal had a gravitational origin. Moreover, if this effect had been due to a non-Newtonian effect, it should have been detected in previous experiments [20, 43, 47]. In order to determine the nature of the unknown disturbance, which affected our measurements, a series of tests and consistency checks were carried out. In the following we report the results of these investigations.

7.1.1 Non-resonant disturbance

The measured signal showed a strong dependence on the rotation frequency of the wheel. Changing, for example, this frequency by 0.1 Hz, the amplitude of the measured signal was drastically reduced. In light of this result we can conclude that the measured signal was due to a resonant excitation.

7.1.2 Dependence of the signal on the DPO-photodiode distance

The results shown in Fig. 7.1 were obtained by varying the DPO's position, whereas the wheel was not moved. Therefore, it was coincevable that the distance dependence of the measured signal could have been due to the changed vertical position of the detection laser beam on the split photodiode. (A lateral misalignment was excluded by the active control on this degree of freedom we had implemented, as explained in the previous chapter.) To investigate this possibility, a run of measurements was performed, in which only the wheel's position was changed. The results were identical to the ones previously presented. Also moving both sensor and test mass did not cause any change in the distance dependence of the measured signal. As a further consistency check, we used a second lock-in amplifier to detect the split photodiode's signal at a frequency of 2 kHz. By repeating the complete measurement we could observe that this signal did not show any change when the distance wheel-DPO was changed. This confirmed that the measured effect was not due to deterioration of the laser beam alignment on the photodiode.

7.1.3 Distance dependence of resonance frequency or Q-factor

A distance dependent torque, as shown in Fig. 7.1, could also have been due to a position dependence of the resonance frequency and of the Q-factor of the DPO. Consequently, the distance dependence of these two parameters was investigated by changing the width of the gap between the DPO and the electrostatic shield. The resonance frequency showed a stability of about 10^{-6} over a distance of 1 mm. The Q-factor was found to be constant within 3% over the same distance range. We can conclude that neither a change of the resonance frequency nor a change in the Q-factor could to be responsible for the effect previously measured.

7.1.4 Pressure dependence of the measured torque

It was conceivable that the residual gas molecules accelerated by the wheel's motion could transfer momentum to the electrostatic shield. This mechanical vibration could have reached the DPO in different ways. The first test we performed to verify this hypothesis was the following. We repeated the measurement presented in Fig. 7.1 at different pressure. The response of the DPO resulted in being independent of the pressure in the vacuum chamber in the range 10^{-5}-10^{-8} mbar. Nevertheless, we also tried to measure a possible movement of the electrostatic shield. A small piece of polished silicon wafer (dimensions 10×10 mm) was glued to the foils and used as a mirror, which reflected a laser beam impinging on a split photodiode. No motion was detected either at the DPO's resonance frequency or at the motor rotation frequency. A final way of excluding any excitation through residual gases was given by using electrostatic shields with different thicknesses (0.025, 0.05, 0.1, 0.5 mm). The results of our measurements showed that all shields behaved the same manner and their thickness had no influence on the outcome of the experiment.

7.1.5 Electrical disturbances of the detection system

We performed several test measurements to determine whether the result could have been due to an electrical pickup. No evidence supporting this hypothesis was found.

7.1.6 Influence of mechanical vibrations

Both accelerometers, in the oscillator and in the wheel chambers, did not detect any accelereration at resonance frequency whilst the wheel was rotating. In addition, we observed the detected torque to be very sensitive to the relative position of sensor and source masses. With the center of the oscillator's head about 3 mm higher than the symmetry axis of the cylinder source mass, a strong reduction of about one order of magnitude in the torque signal was measured. Based on these results, the excitation of the DPO by vibrations produced by the motor could be excluded.

7.1.7 Excitation through higher harmonics

According to the results of the simulation presented in Chapter 5, it should be nearly impossible to excite the DPO with a frequency lower than the one used in our experiment. To verify this prediction, we reduced the motor rotation frequency by one half of its usual value. In this case we were still able to detect a torque only four times smaller than the

one shown in Fig. 7.1, whereas in the case of gravitational excitation a reduction by a factor of 100 was expected. Moreover, it was found that it was possible to excite the oscillator even by reducing the motor frequency to one third of its normal value. In this case a torque 30 times smaller than the previous one was measured.

7.1.8 Electrostatic interaction of the test masses

In light of the large differences in the strength of gravitational and electromagnetic forces it was conceivable that the measured torque could have an electrostatic origin. This possibility was thoroughly investigated, as reported in this section.

As a result of our first tests, the nature of the measured torque did change if the chamber or the oscillator's electrical potential was changed. In general, applying a d.c. potential (up to 10 V) to the DPO's holder, which was grounded during operations, did not cause any measurable change in the signal.

To test the effect of an a.c. voltage on the oscillator, we used a small copper electrode (about half the size of an oscillator's head) mounted in place of the motor. The electrode was aligned to be at the height of the DPO's head and to overlap one half of it. A resonant a.c. potential was then applied to it. No excitation could be detected for voltages up to 10 V. This result proved that the thin metallic membrane between wheel and oscillator provided a very effective shielding of electromagnetic fields. The importance of the electrostatic shield was also confirmed by the fact that the DPO could be excited by applying a resonant a.c. potential to the membrane. This effect was probably due to the imperfect parallelism between the DPO and the electrostatic shield. In order to exclude the possibility that the measured interaction was caused by surface potentials (patch effect), the wheel was coated with a thin graphite layer (thickness <1 μm). No change in the detected torque was observed, when the wheel was rotated.

7.1.9 Influence of magnetic fields

The electrode, as mentioned in the previous section, was replaced by a small coil to test if an a.c. magnetic field could interact with the sensor. In this case it was possible to detect an excitation of the oscillator, when an a.c. resonant current flowed through the coil. The amplitude of this motion was the same order of that shown in Fig. 7.1, when the coil generated a field of about 100 mG at the distance of 0.5 mm from the DPO. In contrast, the field modulation generated by the motor was found to have an amplitude of only 10 mG at the resonance frequency of the DPO, whereas the amplitude was of 3 G at the motor rotation frequency (about 390 Hz). These B-field measurements were

performed using a Hall sensor with a sensitivity of 3.125 mV/G and a measuring range of ±670 G. Since it was not possible to completely exclude the fact that the measured torque on the DPO was due to the motor's magnetic field, a careful investigation of the motor's magnetic properties was carried out. A motor similar to the one used in the experiment was mounted on a traslation stage, which allowed us to move the motor parallel and orthogonal to its axis. The Hall sensor was fixed in front of the motor. The distance dependence of the B-field was then measured. The magnetic field on the axis decreased exponentially and its amplitude was reduced to e^{-1} of its start value at a distance of 1 mm from the initial position. We performed the same measurement, having moved the Hall sensor laterally by 24 mm, which corresponded to the position of the oscillator's head during operations in the vacuum chamber. In this case the amplitude of magnetic field was reduced by a factor of about ten and its distance dependence was found to be linear (the slope was 50 mG/mm). To evaluate if the motor's B-field really had any influence on the oscillator, the motor axis was lengthened by 1 cm. Using this modified setup, a complete run of measurement was performed. No significant difference from the results in Fig. 7.1 could be determined. It is our opinion that this result excludes any contribution of the motor's magnetic field to the measured torque.

In our experiment we did not compensate in any way for the earth's magnetic field, which could have been modulated by the different magnetic permeability of copper, aluminium, and platinum. To measure how large this modulation would have been, we set up the following test apparatus. A permanent magnet with a field of 400 G was put just behind the wheel at the same height as the source masses (platinum). The Hall sensor was put at the same level, but on the other side of the wheel. The a.c. magnetic field measured at 5921 kHz was of 16 G. Since the earth's magnetic field is of the order of 0.3 G, its modulation through the rotation of the wheel would have produced a field with an amplitude of about 12 mG, which would have been about eight times too small to excite the DPO.

A deeper insight into the nature of the measured torque could be gained through the following test. A new aluminium wheel was machined, but no holes were drilled. It was then mounted on the motor, aligned with the oscillator and then rotated at the resonance frequency of the DPO. No torque due to the wheel was measured. This result confirmed that the effect we previously measured, was due to the inhomogeity introduced by the holes in the wheel. Next, 15 holes were drilled on the back of the wheel. They were left closed by a thin aluminium layer (about 100 μm thick). In this way the front side mantained the same geometry as in the previous test, but the missing mass produced a resonant modulation of gravity, when the wheel was rotated. This wheel produced

a torque on the DPO of the same order of magnitude as the one corresponding to the platinum inserts in Fig. 7.1. Lastly, the holes were drilled through the wheel completely. The measured torque did not change as compared with with the previous measurement. In the light of these results, we can come to following conclusions. The effect we measured was definitely due to the holes in the wheel. Since the holes were not filled with any metal inserts, it is possible to exclude that the torque we measured was mainly the result of electrical contact potentials. Moreover, the presence of platinum inserts did not seem to have any effect on the total torque. This confirms that the contribution of the modulation of the earth's magnetic field can be ignored, since platinum is paramagnetic and its magnetic permeability is about 10 times larger than in the case of aluminium.

Another phenomen that had to be taken into account in analyzing the results of our experiment was the induction of electromagnetic fields by accelerations in metals, which is a consequence of the electron inertia. The free electrons in the metal, pushed by the centrifugal forces, could accumulate at the periphery of the disk, where the holes, or the metal inserts, could make the charge distribution non uniform and cause the existence of an a.c. magnetic field. Similar effects were detected by Barnett [100], Tolman and Stewart [101] at the beginning of the last century. In a more modern experiment Beams observed a small radial electrical potential gradient along a spinning aluminium rotor [102]. Further investigations are required in order to test this hypothesis, since the fields measured in the cited works were quite small. In conclusion, the results of the measurements presented here confirm, in the author's opinion, that metal masses in gravitational experiments can give rise to disturbances, as already shown in a test of the Equivalence Principle by Fairbank and Witteborn [103].

7.2 Plastic source mass

The hypothesis that the anomalous torque was due to the distribution of electrons in the metal source masses could be tested by using an insulating material to make the attractor. In choosing the material for this new source mass we focused our attention on polymers. They offer the advantage of being machinable in an ordinary workshop and that they can easily be procured. However, they have also two main disadvantages: low density and low tensile strength. We chose Lexan, a polycarbonate resin, which is characterized by a relatively high tensile strength (75 MPa) and has a densitiy of 1.2 g/cm^3. The attractor's geometry was the same as used in the previous cases, but the holes were left open (no disks were inserted). Due to its low density, the wheel had a much smaller momentum of inertia than the aluminium wheel. Since the motor

stabilization loop had been designed for metal wheels, it was necessary to increase the momentum of inertia of the new attractor. This was achieved by mounting a brass ring on the back of the wheel. With this setup it was then possible to reach the same frequency stability as already mentioned in Chapter 5.

In Fig. 7.2 the results of a measurement with the new attractor are presented. The duration of the measurement for each data point was 13200 s. In this case the measured torque resulted in still being larger than expected from our simulations, but only two to five times, depending on the distance between DPO and wheel. The distance dependence in this case is not exponential and no definitive explanation was found for it. After performing these measurements, we could observe that a clear pattern having the form of the wheel was visible on the electrostatic shield. This was probably due to outgassing of Lexan and could be wiped off by using a clean room tissue. Since neither the wheel nor the contact sensors touched the metallic foil (its surface did not show any scratches and no contact was detected), we could exclude that the wheel had touched the electrostatic shield while rotating. This might explain the anomalous distance dependence of the measured torque: the molecules evaporating from the wheel surface could have transferred momentum to the metallic membrane, which could have excited the sensor mechanically or electrostatically (assuming a difference of potential between DPO and electrostatic shield.) In order to avoid further contamination of the vacuum chamber, we did not operate the plastic wheel any longer. Nevertheless, it is opinion of the author that the result of this last measurement shows the advantages of using a non-conductive material as a source mass, since the disturbance level relative to gravity was decreased. We think that it should be possible to measure gravity with our apparatus using a ceramic material for the source masses. A good candidate is zirconium dioxide, also known as zirconia, stabilized with magnesium oxide. This material has a densitiy of 5.74 g/cm^3 (almost five times larger than in the case of Lexan), a tensile strength larger than 300 MPa and can be machined with standard workshop tools. Moreover, it is much better suited to vacuum conditions than polycarbonate resin.

Finally, the constraints on the existence of a non-Newtonian force, based on our experimental results obtained with the plastic attractor, were compared with the previously cited experiment as shown in Fig. 7.3. Interestingly, all three experiments based on the use of high frequency mechanical oscillators (Stanford, Colorado and ours) could not provide as good results as the one performed at University of Washington, which was performed using a torsion pendulum as a force sensor. In our opinion, this difference is due to the fact that the use of kHz-oscillators in this kind of experiment is still relatively new, whereas a great deal of work over the last two centuries has been done with torsion

pendulums in gravitational physics.

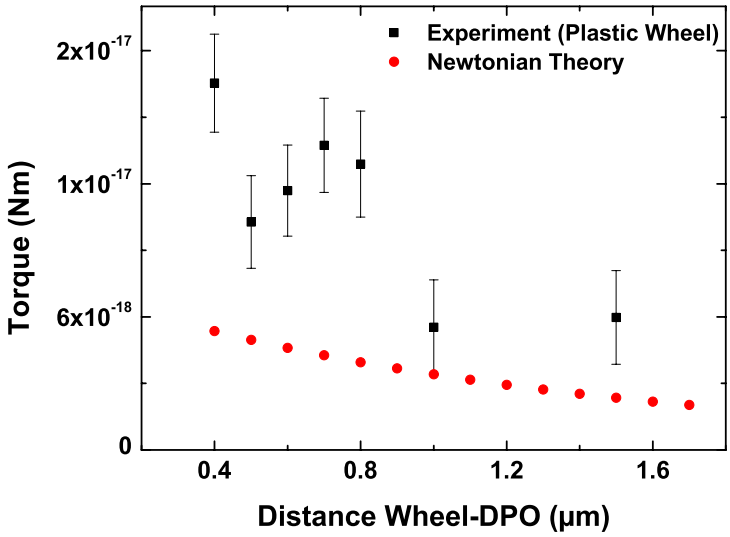

Figure 7.2: Torque produced by a Lexan wheel on the DPO compared to the expected gravitational signal. Each data point was taken over an integration time of 13200 s.

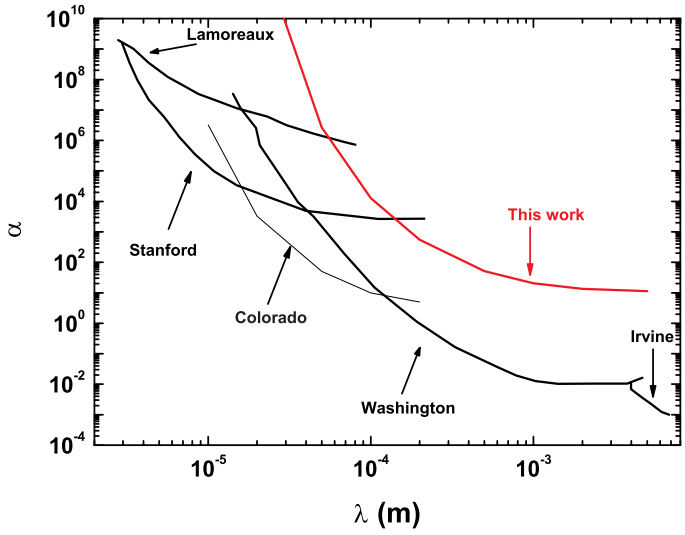

Figure 7.3: Upper limits to the strength of a non-Newtonian interaction relative to gravity from the experiment cited in Chapter 2 compared to our present results (red line).

Chapter 8

Search for non Newtonian gravity at ultra-short distance

As shown in Fig. 2.2, the existence of extra forces that couple to masses has been poorly constrained in the distance range below 100 μm. The major difficulties in performing an experiment at these distances are due to electrostatic and Casimir force. The impossibility to use a thin metallic plate as shielding, as done previously, requires the development of new concepts. Inspired by a work by Krause and Fischbach [64], we propose a new setup, that could improve the present limits in the range between 0.1 and 100 μm.

A view of the setup is shown in Fig. 8.1. The sensor is a torsional oscillator (labelled 3) similar to the one used in our experiment. The torsion axis is orthogonal to the picture plane. The gravitational excitation is provided by two source oscillators of the same type (labeled 1 and 2 in the picture), whose resonance frequencies are equal to ν_R[1]. All three oscillators are parallel. The source oscillators are aligned, while the test oscillator is shifted by one half of its width on one side as shown in Fig. 8.1. The source oscillators' heads are coated with a $s = 1$ μm thick gold layer on the inner side. The test oscillator is coated on one side with a $s = 1$ μm thick gold layer and on the other with 1 μm copper layer. The accesible part of the test oscillator is used to perform the optical detection of its motion. We assume here that the gap between each pair of masses is the same size.

The source masses are actuated sinusoidally in phase at the frequency ν_R, so that

[1]It is essential that the three DPOs have the same resonance frequency. Since it is very difficult to produce two oscillator with exactly the same geometry, their frequencies have to be tuned. This is possible by illuminating each with a different laser beam with an optical power suited to get the required ν_R (see Chapter 4).

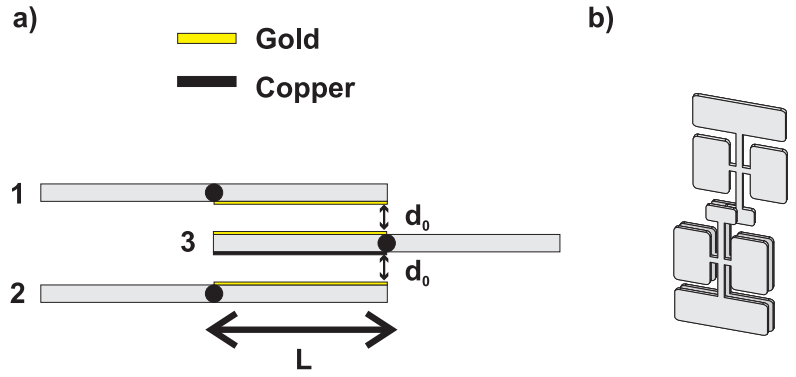

Figure 8.1: Proposed setup for testing gravity at ultra-short distance. a) Top view. Here d_0 is the gap width when all DPOs are at rest. b) 3D view

the gap width is given by

$$d\left(t\right) = d_0 + d_1 \cos\left(2\pi\nu_R t\right), \tag{8.1}$$

where d_1 represents the modulation amplitude. This can be accomplished by optical actuaction of the oscillators, as already demonstrated in Chapter 4.

The total torque acting on the sensor is then given by

$$\begin{aligned}\Gamma_{total} &= \Gamma_{gravitation} + \Gamma_{electrostatic} + \Gamma_{casimir} = \frac{L}{2} \times \\ &\left[\left(F_1^{gravity} - F_3^{gravity}\right) + \left(F_1^{electrostatic} - F_3^{electrostatic}\right) + \left(F_1^{casimir} - F_3^{casimir}\right)\right]\end{aligned} \tag{8.2}$$

where $F_i^{gravitation}$, $F_i^{electrostatic}$, and $F_i^{casimir}$ are the gravitational, electrostatic, and Casimir forces exerted by the oscillators i = 1 and 3 respectively and L is half the width of the DPO's head. Under the assuption that L >> d, the gravitational torque, which is due solely to the unequal films on oscillators 1 and 3, can be written in the simple form

$$\Gamma_{gravitation} = \pi G L^2 H s^2 \rho_{gold}\left(\rho_{gold} - \rho_{copper}\right)$$

Here G is the gravitational constant, the product L times H is the sensor area (equal to half of the DPO's head), s is the thickness of the metal layer, ρ_{gold} and ρ_{copper} are densities of the gold and copper layers. Using the values given in Table VII, it results that the gravitational torque $\Gamma_{gravitation}$ is equal to $2.1{\cdot}10^{-21}$ Nm.

Table VII. Parameters for the proposed experiment.

s	$1{\cdot}10^{-6}$	m
d_0	$2{\cdot}10^{-6}$	m
d_1	$1{\cdot}10^{-6}$	m
ρ_{gold}	$2{\cdot}10^{4}$	kg/m^3
ρ_{copper}	$9{\cdot}10^{3}$	kg/m^3

In order to suppress the electrostatic interaction due to charge excess on the metallic layer, a technique can be used that was developed for the spinning test masses of the GP-B satellite and relies on the use of photoemission effect [104]. The charges are removed through UV laser light exposition of all the test masses. Moreover, in a recent work it was shown that the use of metallic layers realized with plasma-enhanced chemical vapour deposition reduces the effect of surface potentials [105]. Therefore, it should be possible to make $\Gamma_{electrostatic}$ smaller than the gravitational torque using these two techniques.

If the metal layers were perfect mirrors, the Casimir force on the test oscillator would be perfectly balanced. Metals can be approximated as perfect mirrors at wavelengths larger than their plasma wavelengths, about 0.3 μm for copper and gold [106]. Therefore if the gaps between the oscillators are larger than a few times the plasma wavelength, the Casimir contributions of oscillator 1 and 3 should be equal and $\Gamma_{casimir}$ would vanish. Other background effects, such as the gravitational attraction between the oscillator mass (as opposed to the metal layer), the magnetic field generated by the acceleration of the metal films (Tolman-Stewart effect), and the pressure dependent effects, are expected to be perfectly compensated by the symmetry of the proposed setup.

Once all systematic effects are removed, the fundamental limit to the sensitivity of this apparatus is given by thermal noise. For this reason it is convienent to perform the experiment at liquid helium temperature, at which the quality factor of the oscillator reaches values of the order of 10^8 [80]. The Langevin thermal torque (see Chapter 4) is of the order of the gravitational torque for an integration time $\Delta t = 10^6$ s.

Assuming that a Yukawa-type correction to the Newtonian potential existed, it would act on the detector oscillator as a torque

$$\Gamma_{yukawa} = 2\pi\alpha G\lambda^2 LH\rho_{gold}\left(\rho_{gold} - \rho_{copper}\right)\left(1 - e^{-t/\lambda}\right)e^{-d/\lambda}\frac{L}{2}$$

Setting equal to one the ratio between the Yukawa torque and the thermal noise torque, we can express α as a function of the interaction range λ. The expected constraint on a deviation from Newton's law are plotted in Fig. 8.2, assuming $\Delta t = 10^6$ s and Q =

$6{\cdot}10^7$. The comparison with the present best limits shows that the proposed experiment could be able to strongly improve our knowledge of gravity in the distance range 0.1-100 μm.

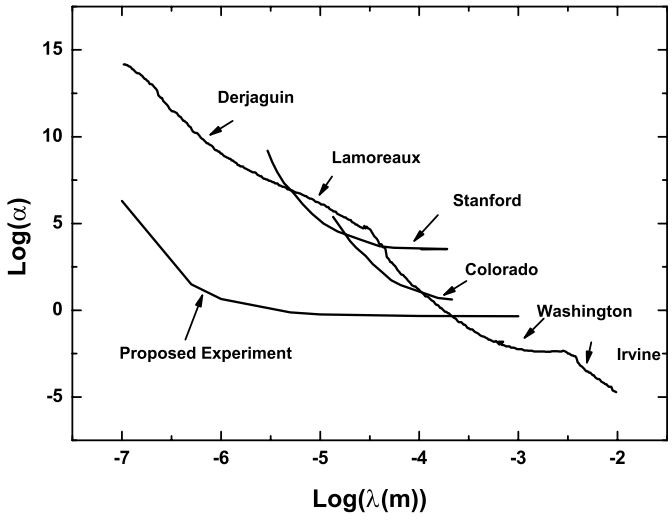

Figure 8.2: Present limits to the existence of a new gravity-like force as compared to the expected results from the proposed experiment.

8.1 Microfabrication of the test masses

In Fig. 8.3 a modified design of the DPOs, that could be used in the ultra-low distance experiment, is shown. The oscillator and its frame are made from the same single-crystal wafer. Two spacers (they could easily be made a using standard lift-off technique) are mounted on the sides of each frame, that are designed to be placed on each other and bonded to get the configuration of Fig. 8.1. The presence of the frame offers several advantages. First, it allows us to increase the distance of the DPO from the clamping points. As already mentioned, a part of its kinetic energy is contained in the upper part of the foot, making the clamping of the foot critical, and probably limiting the quality factor of the DPO. A second advantage is due to the sub-micrometric precision with which it is possible to fabricate the spacers that define the gap between the test masses. Moreover, the parallelism of the DPOs can also be extremely well controlled. In order

to test the dependence of the measured force on the distance, it would be necessary to produce more sets of this device with different gap widths between the test masses.

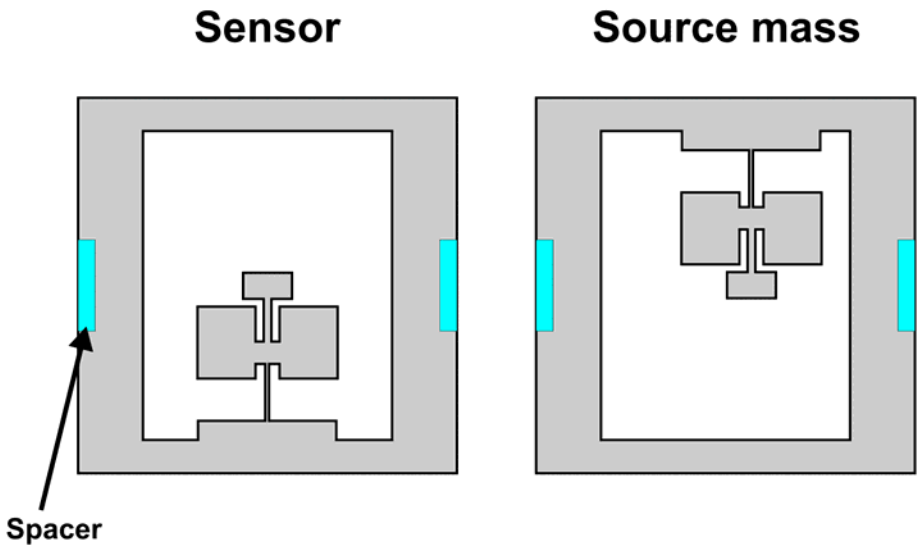

Figure 8.3: Left: The sensor DPO with its frame on which silicon nitride spacers are grown. Right: The source mass DPO is shifted by half an oscillator's head width to make the configuration shown in Fig.8.1 possible.

Chapter 9

Conclusions

In the present work we have shown that it is possible to set up a table-top experiment suited to test the predictions of modern string-based gravitational theories. At the heart of this setup there is the single-crystal double-paddle oscillator (DPO), which was used for the first time, to the author's best knowledge, to detect weak forces. We demonstrated a simple and versatile microfabrication procedure, which enabled us to manufacture oscillators with the highest measured quality factor, to date, at room temperature and in vacuum. Moreover, optical excitation was experimentally achieved by illuminating the DPO with a weak laser beam, whose amplitude was modulated at the oscillator's resonance frequency. This excitation method was used in the present work only for diagnostic measurements.

The ultimate limit to the torque-sensitivity of a DPO is given by Brownian noise. A characterization of this fundamental noise was given, and it was shown that its influence can be reduced by increasing the duration of the measurements. A detection limit of $2{\cdot}10^{-18}$ Nm in $5.4{\cdot}10^{4}$ s was demonstrated in the case of resonant excitation. For our measurements, the excitation was provided by cylindrical source masses moving in front of the oscillator. Due to the weakness of gravity compared to electromagnetic interaction, the two vacuum chambers containing the DPO and the source masses were divided by a thin conducting shield. Moreover, vibration isolation systems and a few sensors (e.g. accelerometers and contact sensors) were also used to control the influence of external background as vibrations.

Based on the results of our measurements, we can exclude the existence of a Yukawa-like interaction of 20 times gravitational strength with an interaction range of 1mm. A small disturbance (about 5 times stronger than gravity) affected the results of our measurements. Further improvements can probably be obtained by using a high density

non-conductive material for the test masses. Lastly, we showed the possibility of improving the present knowledge of gravity by a few orders of magnitude using a novel setup based on the optical excitation of DPOs at the liquid helium temperature.

Bibliography

[1] S. Weinberg, *Gravitation and Cosmology: Principles and Applications of the General Theory of Relativity*, J. Wiley and Sons, New York (1972)

[2] C. W. Misner, K.S. Thorne, and J. A. Wheleer, *Gravitation,* W. H. Freeman, San Francisco (1973)

[3] Y. Fuji, Nature, **234**, 5 (1971)

[4] D.R. Long, Nature **260**, 417 (1976)

[5] V. I. Panov and V. N. Frontov, Sov. Phys. JETP **50**, 852 (1979)

[6] H. T. Yu *et. al.,* Phys. Rev. D **20**, 1813 (1979)

[7] H. Hirakawa, K. Tsubono, and K. Oide, Nature **283**, 184 (1980)

[8] R. Spero, J. K. Hoskins, R. Newman, J. Pellam, and J. Schultz, Phys. Rev. Lett. **44**, 1645 (1980)

[9] H. A. Chan, M. V. Moody, and H. J. Paik, Phys. Rev. Lett. **49**, 1745 (1982)

[10] Y. Ogawa, K. Tsubono, and H. Hirakawa, Phys. Rev. D **26**, 729 (1982)

[11] J. K. Hoskins, R. D. Newman, R. Spero, and J. Schultz, Phys. Rev. D **32**, 3084, (1985)

[12] K. Kuroda and H. Hirakawa, Phys. Rev. D **32**, 342 (1985)

[13] E. Fischbach and C. Talmadge, Nature **356**, 207 (1992); E. Fischbach, G. T. Gillies, D. E. Krause, J. G. Schwan, and C. Talmadge, Metrologia **29**, 213 (1992)

[14] E. Fischbach, D. Sudarsky, A. Szafer, C. Talmadge, and S. H. Aronson, Phys. Rev. Lett. **56**, 3 (1986); E. Fischbach, D. Sudarsky, A. Szafer, C. Talmadge, and S. H. Aronson, Phys. Rev. Lett. **56**, 1427 (1986)

[15] N. Arkani-Hamed, S. Dimopoulos and G. R. Dvali, Phys. Lett. B **429**, 263 (1998)

[16] I. Antoniadis, N. Arkani-Hamed, S. Dimopoulos and G. R. Dvali, Phys. Lett. B **436**, 257 (1998)

[17] N. Arkani-Hamed, S. Dimopoulos and G. R. Dvali, Phys. Rev. D **59**, 086004 (1999)

[18] J. C. Price, *Gravitational Strength Forces below 1 cm,*Proceedings of the International Symposium on Experimental Gravitational Physics, ed. P. Michelson, H. En-ke, and G. Pizzella , D. Reidel, Dordrecht (1987)

[19] J. C. Long and J. C. Price, arXiv:hep-ph/0303057 (2003)

[20] C.D. Hoyle, U. Schmidt, B. R. Heckel, E. G. Adelberger, J. H. Gundlach, D. J. Kapner, H. E. Swanson, Phys. Rev. Lett. **86**, 1418 (2001)

[21] P. Mohanty, D. A. Harrington, K. L. Ekinci, Y. T. Yang, M. J. Murphy, and M. L. Roukes, Phys. Rev. B **66**, 085416 (2002)

[22] C. L. Spiel, R. O. Pohl, and A. T. Zehnder, Rev. Sci. Instrum. **72**, 1482 (2001)

[23] Gordon Kane, *Supersymmetry: Unveiling the Ultimate Laws of Nature*, Helix Books/Perseus Publishing (2000)

[24] T. Kaluza, Sitzungsber. Preuss. Akad. Wiss. Berlin, Math. Phys. **K1**, 966 (1921)

[25] O. Klein, Z. Phys. **37**, 895 (1926); O. Klein, Nature **118**, 516 (1926)

[26] M. Tegmark, Class. Quantum Grav. **14**, L69 (1997)

[27] M. Kaku, *Introduction to Superstrings and M-theory*, Springer-Verlag, New York (1999)

[28] E. Fischbach and C. Talmadge, *The Search for Non-Newtonian Gravity*, AIP Press/Springer-Verlag, New York (1999)

[29] Y. T. Chen and A. H. Cook, *Gravitational experiments in the laboratory*, Cambridge Univ. Press (1993)

[30] Kowalczyk *et al.*, *Constraint on Large Extra Dimensions*, unpublished

[31] L. Randall and R. Sundrum, Phys. Rev. Lett. **83**, 4690 (1999)

[32] D. J. H. Chung, L. Everett, H. Davoudiasl, Phys. Rev. D **64**, 065002 (2001)

[33] S. Dimopoulos and G. F. Giudice, Phys. Lett. B **379**, 105 (1996)

[34] I. Antoniadis, S. Dimopoulos, and G. Dvali, Nucl. Phys. B **516**, 70 (1998)

[35] J. Ellis, S. Kalara, K. A. Olive and C. Wetterich, Phys. Lett. B **228**, 264 (1989)

[36] T. R. Taylor and G. Veneziano, Phys. Lett. B **213**, 450 (1988)

[37] R. D. Peccei and H. Quinn, Phys. Rev. Lett. **38**, 1440 (1977)

[38] S. Weinberg, Phys. Rev. Lett. **40**, 223 (1978)

[39] F. Wilczek, Phys. Rev. Lett. **40**, 279 (1978)

[40] J. E. Moody and F. Wilczek, Phys. Rev. D **30**, 130 (1984)

[41] I. B. Khriplovich and G. G. Kirilin, arXiv:gr-qc/0207118v1 (2003)

[42] G. T. Gillies and R. C. Ritter, Rev. Sci. Instrum. **64**, 283 (1993)

[43] J. C. Long, H. W. Chan, A. B. Churnside, E. A. Gulbis, M. C. M. Varney, and J. C. Price, Nature **421**, 922-925 (2003)

[44] V. M. Mostepanenko, Braz. Jour. Phys. **34**, 211 (2004)

[45] R. S. Decca, E. Fischbach, G. L. Klimchiskaya, D. E. Krause, D. Lopez, and V. M. Mostepanenko, Phys. Rev. D **68**, 116003 (2003)

[46] S. K. Lamoreaux, Phys. Rev. Lett. **83**, 3340 (1999)

[47] J. Chiaverini, S.J. Smullin, A. A. Geraci, D. M. Weld, and A. Kapitulnik, Phys. Rev. Lett. **90**, 151101 (2003)

[48] B. Abbot *et a.l.,* D0 Collaboration, Phys. Rev. Lett. **86**, 1156 (2001)

[49] N. Arkani-Hamed, S. Dimopoulos and G. Dvali, Phys. Rev. D **59**, 086004 (1999)

[50] K. Hirata *et al.*, Phys. Rev. Lett. **58**, 1490 (1987)

[51] H. Cavendish, Phil. Trans. R. Soc. Lond. **17**, 469 (1798)

[52] J. Sinsky and J. Weber, Phys. Rev. Lett. **18**, 795 (1967); J. Sinsky, Phys. Rev. **167**, 1145 (1967)

[53] V. B. Braginsky, V. P. Mitrofanov, and V. I. Panov, *System with Small Dissipation*, The University of Chicago Press, Chicago (1985)

[54] L. D. Landau, and E. M. Lifshitz, *Theory of Elasticity*, Nauka, Moscow (1965)

[55] R. Buser, *Theoretical and Experimental Investigation n Silicon Single Crystal Resonant Structures,* PhD Thesis, University of Neuchatel (1989)

[56] W. Gerlach, Naturwiss. **15**, 15 (1927)

[57] G. E. Uhlenbeck and S. Goudsmit, Phys. Rev. **34**, 145 (1929)

[58] H. Nyquist, Phys. Rev. **32**, 110 (1928)

[59] H. B. Callen and T. A. Welton, Phys. Rev **83**, 34 (1951); H. B. Callen and R. F. Greene, Phys. Rev **86**, 702 (1952)

[60] R. C. Ritter, L. I. Winkler, and G. T. Gillies, Meas. Sci. Technol. **10**, 499 (1999)

[61] H. B. Chan, V. A. Aksyuk, R. N. Kleiman, D. J. Bishop, and F. Capasso, Phys. Rev. Lett. **87**, 211801 (2001)

[62] See for example: Proc. of the 6th International Conference on Noncontact Atomic Force Microscopy 2001 in Dingle, Ireland, published in: Nanotechnology 15, S40-S43 (2004)

[63] B. Ilic, H. G. Craighead, S. Krylov, W. Senaratne, C. Ober, and P. Neuzil, J. Appl. Phys. **95**, 3694 (2004)

[64] D. E. Krause and E. Fischbach, *Searching for Extra Dimensions and New String-Inspired Forces in the Casimir Regime*, in Gyros, Clocks and Interferometers...: Testing Relativistic Gravity in Space, edited by C. Lammerzahl, C. W. F. Everitt, and F. W. Hehl (Springer-Verlag, Berlin, 2001)

[65] L. Haiberger, M. Weingran, H. Wenz, and S. Schiller, *An Experiment to Detect Gravity at Sub-mm Scale with High Q Mechanical Oscillators*; to appear in Proceedings of the Tenth Marcel Grossmann Meeting on General Relativity, edited by M. Novello, S. Perez-Bergliaffa and R. Ruffini, World Scientific, Singapore (2005), [arXiv:hep-ph/0510211]

[66] Y. Hadjar, P. F. Cohadon, C. G. Aminoff, M. Pinard, and A. Heidmann, Europhys. Lett. **47**, 545 (1999)

[67] I. Tittonen, G. Breitenbach, T. Kalkbrenner, T. Müller, R. Conradt, S. Schiller, E. Steinsland, N. Blanc, and N. F. de Rooij, Phys. Rev. A **59**, 1038 (1999)

[68] P. R. Saulson, Phys. Rev. D **42**, 2437 (1990)

[69] V. B. Braginsky and A. B. Manukin, *Measurement of Weak Forces in Physics Experiments*, Chicago Press, Chicago (1997)

[70] C. W. McCombie, Rep. Prog. Phys. **16**, 266 (1953)

[71] V. B. Braginsky, C. M. Caves, and K. S. Thorne, Phys. Rev. D **15**, 2047 (1977)

[72] S. Chandrasekhar, Rev. Mod. Phys. **15**, 1 (1943)

[73] G. Meyer and N. M. Amer, Appl. Phys. Lett. **53**, 1045 (1988)

[74] Y. Martin and H. K. Wickramasinghe, Appl. Phys. Lett. **50**, 1455 (1987)

[75] B. E. White, and R. O. Pohl, Phys. Rev. Lett. **75**, 4437 (1995)

[76] P. Rösner, K. Samwer, R. O. Pohl, and S. Schneider, Rev. Sci. Instru. **74**, 3395 (2003)

[77] R. D. Biggar, and J.M. Parpia, Rev. Sci. Instrum. **69**, 3558 (1998)

[78] D. F. McGuigan, C. C. Lam, R. Q. Gram, A. W. Hoffman, D. H. Douglas, and H. W. Gutche, J. Low Temp. Phys. **30**, 621 (1978)

[79] R. N. Kleiman, G. K. Kaminsky, J. D. Reppy, R. Pindak, and D. J. Bishop, Rev. Sci. Instrum. **56**, 2088 (1985)

[80] X. Liu, J. F. Vignola, D. M. Photiadis, A. Sarkissian, B. H. Houston, R. D. Merithew, and R. O. Pohl, *Low Temperature Study of Loss Mechanism of Mechanical Oscillators*, presented at the Tenth International Conference on Phonon Scattering in Condensed Matter (2001)

[81] B. H. Houston, D. M. Photiadis, M. H. Marcus, J. A. Bucaro, Xiao Liu, and J.F. Vignola, Appl. Phys. Lett. **80**, 1300 (2002)

[82] See for example T. Kobayashi, T. Hara, J. Ohsawa, and N. Yamaguchi, Rev. Sci. Instr. **7**, 2651 (2002)

[83] X. Liu, S. F. Morse, J. F. Vignola, D. M. Photiadis, A. Sarkissian, M. H. Marcus, and B. H. Houston, Appl. Phys. Lett. **78**, 1346 (2001

[84] R. E. Mihailovich, *Low Temperature Mechanical Properties of Boron-Doped Single-Crystal Silicon,* PhD Thesis, Cornell University (1992)

[85] J. C. Greenwood, J. Phys. E: Sci. Instrum. **21**, 1114 (1988)

[86] I. Szabo, *Höhere technische Mechanik*, Springer, Berlin (1977)

[87] U. Hilleringmann, *Silizium-Halbleitertechnologie*, Teubner, Stuttgart-Leipzig-Wiesbaden (2002)

[88] Crystec GmbH, Berlin

[89] T. H. Metcalf, *Elastic Properties, Annealing , and Vapour Pressure of Neon and Argon Films*, PhD Thesis, Cornell University (2002)

[90] J. F. Vignola, X. Liu, S. F. Morse, B. H. Houston, J. A. Bucaro, M. H. Marcus, L. Sekaric, Rev. Sci. Instr. **73**, 3584 (2002)

[91] *Properties of Silicon,* EMIS Datareview Series No. 4, edited by T. K. Ning (INSPEC, New York 1988)

[92] W. Duffy, J. Appl. Phys. **68**, 5601 (1987)

[93] G. Agnolet (unpublished)

[94] T. Klitsner and R. O. Pohl, Phys. Rev. B **36**, 6551 (1987)

[95] R. N. Kleiman, G. Agnolet, and D. J. Bishop, Phys. Rev. Lett. **59**, 2079 (1987)

[96] R. A. Buser and N. F. de Rooij, Sens. Actuators A **21**, 323 (1990)

[97] D. W. Allan, IEEE Trans. Instr. Meas. **36**, 646 (1987)

[98] M. Weingran, Diploma Thesis, Düsseldorf (2004)

[99] M. V. Plissi, K. A. Strain, C. I. Torrie, N. A. Robertson, S. Killbourn, S. Rowan, S. M. Twyford, H. Ward, K. D. Skeldon, and J. Hough, Rev. Sci. Instrum. **69**, 3055 (1998)

[100] S. J. Barnett, Phys. Rev. **6**, 239 (1915); S. J. Barnett, Rev. Mod. Phys. **7**, 129 (1935)

[101] R. C. Stewart and T. D. Stewart, Phys. Rev. **8**, 97 (1916); R. C. Stewart and T. D. Stewart, Phys. Rev. **9**, 164 (1917)

[102] J. W. Beams, Phys. Rev. Lett. **21**, 1093 (1968)

[103] F. C. Witteborn and W. M. Fairbank, Phys. Rev. Lett. **19**, 1049 (1967)

[104] B. Lange, Phys.Rev. Lett. **74**, 1904 (1995)

[105] E. Moritz, PhD thesis (1999)

[106] A. Lambrecht and S. Reynaud, Eur. Phys. Lett. J. D **8**, 309 (2000)

[107] L. Haiberger, D. Jäger, and S. Schiller, Rev. Sci. Instrum. **76**,045106 (2005)

Appendix A

REVIEW OF SCIENTIFIC INSTRUMENTS 76, 1 (2005)

Fabrication and laser control of double-paddle silicon oscillators

L. Haiberger[a)]
Institut für Experimentalphysik, Heinrich-Heine-Universität Düsseldorf, Universitätsstrasse 1, 40225 Düsseldorf, Germany

D. Jäger
Zentrum für Halbleiter- und Optoelektronik, Universität Duisburg-Essen, Lotharstrasse 55, 47057 Duisburg, Germany

S. Schiller
Institut für Experimentalphysik, Heinrich-Heine-Universität Düsseldorf, Universitätsstrasse 1, 40225 Düsseldorf, Germany

(Received 10 August 2004; accepted 24 January 2005)

We describe a fabrication technique for double-paddle oscillators based solely on wet etching, resulting in quality factors up to $8 \cdot 10^5$ at room temperature and in vacuum. The quality factor achieved is the highest demonstrated so far at room temperature. The fabrication procedure, not involving any dry etching step, represents a valid and low cost alternative to the other techniques previously presented. Laser excitation and resonance frequency tuning is shown to be applicable to these resonant structures and to be a useful alternative to mechanical and electrical excitation methods used so far, especially for applications in which a remote excitation system is required (e.g., in a high-temperature environment). © *2005 American Institute of Physics.*
[DOI: 10.1063/1.1876972]

I. INTRODUCTION

Single-crystal mechanical oscillators have proved to be a powerful tool for different applications like magnetic force microscopy,[1] characterization of thin films at low temperature,[2] study of metallic films at high temperature,[3] torque magnetometry,[4] and investigation of quantum effects.[5] The key property is the very small damping (high quality factor) of these oscillators. In 1978 McGuigan and co-workers[6] measured a quality factor of about $2 \cdot 10^9$ for a longitudinal mode of a single-crystal silicon cylinder of mass 4.9 kg at 3.5 K. This result stimulated further efforts to improve the mechanical performances of microfabricated structures. An important development in this field was the double-paddle oscillator (DPO) by Kleiman and co-workers.[7] A further improvement in the quality factor of single-crystal oscillators was obtained by Pohl and co-workers at Cornell University, who produced and used DPOs to study elastic properties of thin metal films.[2] A typical DPO is shown in Fig. 1. Six different eigenmodes of this type of oscillator have been identified in the frequency range between 0.1 and 6 kHz.[8] One of them, an antisymmetric torsion mode, exhibits very small losses and insensitivity to thermal cycling. Its quality factor was found to be about $3 \cdot 10^5$ at 300 K and on the order of $8 \cdot 10^7$ at 4 K.[9] The difference between this result and the values reported by McGuigan and co-workers suggests that there could be still room for further improvements of the DPOs. Moreover, recent studies of the thermoelastic effect in single crystal micromechanical oscillators[10] have confirmed that the internal friction observed below 60 K cannot be explained in terms of thermoelastic losses.

Inspired by a proposal of Price,[11] we set up an experiment in which a DPO is used as a resonant sensor to detect the dynamical gravitational field generated by a mass, which is periodically moved in front of the oscillator. The goal of this experiment is to test the validity of Newton's gravity law at distances smaller than 1 mm.[12] In the present work we report on the fabrication of DPOs produced for this experiment, which differs from the standard procedures used in the previously cited works. We evaluate our fabrication method with respect to the oscillators' performance. We also show actuation of DPOs by means of a laser beam and control of their torsional constant. Optical actuation of resonant microstructures has been previously applied by different groups.[13] This technique has not yet been reported for DPOs. It does not require the DPOs to be conducting and does not need any electrodes in proximity of the DPOs unlike the electrostatic excitation.[8]

II. THE DOUBLE-PADDLE OSCILLATOR

A. Theoretical considerations

As shown in Fig. 1, a DPO consists of two masses, denoted by head and wings, that are connected by a torsion rod, the neck. The wings are connected to the base, the foot, by another torsion rod, the leg. This system can be modeled as a coupled oscillator consisting of two masses (head and wings) and of two springs (neck and leg). Since each spring can be twisted or bent in different directions, several vibration modes exist. In the present work we will restrict attention to an antisymmetric torsion mode, known in literature as AS2.[8]

a)Electronic mail: luca.haiberger@uni-duesseldorf.de

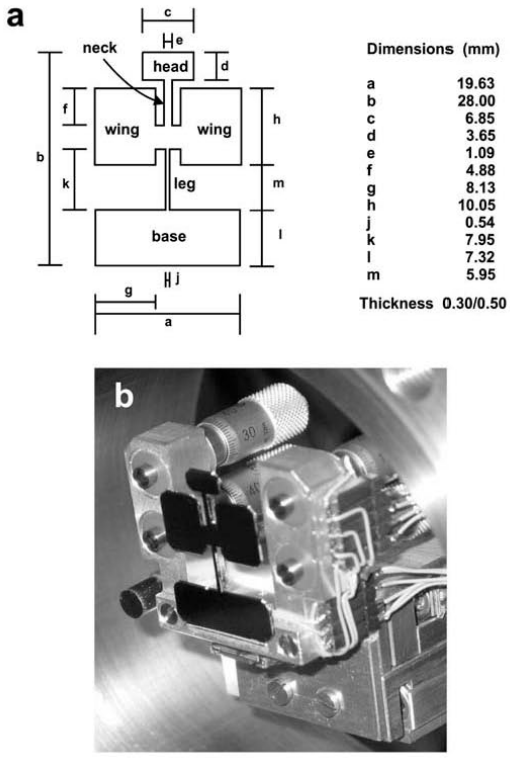

FIG. 1. (a) Dimensions of the double-paddle oscillator. (b) The DPO mounted on an aluminium holder, that is provided with a set of distance sensors used in our experiment to test gravity at small distances (see Ref. 12).

It consists of a twist of the neck around its length and a synchronous oscillation of the wings around an axis orthogonal to the DPO symmetry axis. The oscillations of head and wings are out of phase.[14] This mode is particularly interesting because of its very low internal losses.

The resonance frequency of the mode AS2 is given, to first approximation, by[15]

$$\nu_0 = \frac{1}{\pi}\sqrt{3}\sqrt{\frac{1}{c^3 d}gt^2\frac{\beta}{\rho f'}e}, \tag{1}$$

where c is the full width of the oscillator head, t is the oscillator thickness, f' is the neck length, e is the neck width, d is the height of oscillator head, $g=61.7$ GPa the shear modulus of silicon about the (100) orientation,[16] and β is a parameter, that depends weakly on the ratio t/e. In our calculations β is equal to 0.25.[17]

A parameter, which characterizes the damping losses for each mode, is the quality factor. It can be easily determined by exciting the oscillator at resonance, then turning off the excitation and following the decay of the oscillation amplitude. From this decay the ring-down time τ is determined. The quality factor is then given by the relation $Q=\pi\nu_0\tau$.

Even in absence of external drive, the oscillation amplitude does not vanish completely. This is due to thermodynamic fluctuations. Internal dissipation in silicon is the coupling mechanism between the microscopic fluctuations and the macroscopic state of motion of the oscillator as stated by the fluctuation-dissipation theorem.[18] This intrinsic noise can be quantitatively described using the theory of Brownian motion, in which a fluctuating thermal force, known as Langevin force, is responsible for the oscillator excitation. For a torsional oscillator, like the DPO, the power spectral density of the Langevin torque is given by

$$S_L = \sqrt{\frac{\pi k_B T m c^2 \nu_0}{3Q}}, \tag{2}$$

where m is the mass of the oscillator head and T is the temperature. The power spectral density of the oscillator angular deviation ϑ at resonance is then given by

$$S_\vartheta(\nu_0) = \frac{Q}{k}S_L, \tag{3}$$

where $k=(2\pi\nu_0)^2 I$ is the torsional spring constant of the oscillator and $I=\frac{1}{3}mc^2$ is its momentum of inertia around the vertical axis.

B. Fabrication technique

The DPO design we implemented is similar to the one developed by Pohl and co-workers.[8] Its dimensions are shown in Fig. 1(a).

The oscillators were fabricated from a 300-μm- (or 500-μm-) thick, float zone refined, double-side polished, ⟨100⟩ oriented, and p-doped silicon wafer with a room-temperature specific resistance larger than 10 kΩ cm. On each side a 80-nm-thick silicon nitride layer had been thermally grown (Crystec). The wafer was laid on a clean room wipe and a small notch was scratched with a diamond scriber in the direction parallel to the crystal axis ⟨100⟩. The scriber tip was then put in the notch and pressed firmly. In this way the wafer was split in more samples having an edge parallel to the crystal direction ⟨100⟩.[19] For cleaning, the sample was then immersed in boiling acetone and afterwards in boiling propanol for a few minutes. After blowing dry with nitrogen, the sample was put on a hot plate at 230 °C and at ambient pressure for 30 min in order to eliminate solvent residuals, that could degrade the quality of the sample surface. Since the most photoresists have bad adhesion on silicon nitride, a primer (Allresist, AR 300-80) was spun on each side of the sample. These thin layers were annealed at 170 °C for 3 min. Next, a positive photoresist (Allresist, AR 4040) was spun on both sides. The thickness of each layer was 1.4 μm. Baking at 95 °C for 3.5 min was required in order to temper the photoresist. To reproduce the oscillator pattern on the photoresist layer, the sample was put in contact with a chrome coated glass mask, on which the shape of the oscillator had been previously printed via scanning laser lithography. In order to minimize the mechanical losses of the DPO, it is important to carefully align the sample, so that the crystal axis ⟨110⟩ is parallel to the symmetry axis of the DPO.[8] The sample was then exposed for 12 s to light from a mercury

short-arc lamp, which produced a radiation in the wavelength range between 350 and 550 nm. The intensity required for the exposure of the resist layer was 70 mJ/cm^2. After developing in a 60% aqueous solution (by weight) of AR 3035 (Allresist) for 4 min, the sample was rinsed, blown dry and annealed at 110 °C for 10 min. The bare silicon nitride was then stripped in a H_3PO_4 solution (concentration 85% by weight in water) at 140 °C. Under these conditions an etch rate of about 1 nm/min was measured. After the conclusion of this step the nitride layer had been etched except in the area corresponding to the oscillator. In order to eliminate the residual photoresist, the sample was put in boiling N-methylpyrrolidone for about 15 min. The silicon etching was then performed in a KOH solution (30% concentration by weight in water) at 99 °C. The measured etch rate was about 3 μm/min. Next, the silicon nitride layer on the free standing structure was removed by HF solution (concentration 20% by volume in water) for 5 min. The oscillator was then rinsed and blown dry. The total time required to fabricate a DPO was about 5 h.

III. MEASUREMENTS AND RESULTS

A. Oscillator characterization

Since any coupling of the oscillator to the external environment would introduce mechanical losses, fastening it without degrading its mechanical properties is a crucial task. As suggested in Ref. 14, a small displacement during the oscillation takes place in the upper part of the foot. For this reason in our setup only the lower half of the oscillator foot was carefully glued with Stycast 1260 on an aluminium holder, as shown in Fig. 1(b). The oscillator holder was mounted on a piezoelectric transducer resting on a passive vibration isolation system to reduce the influence of seismic noise. This setup was operated in a high vacuum chamber (typical pressure 10^{-6} mbar and room temperature). In order to characterize the mechanical properties of the DPOs, an optical detection system was set up. A He–Ne laser beam was reflected by the DPO onto a split photodiode, which generated a photocurrent proportional to the amplitude of the angular displacement of the oscillator. This setup could detect a displacement of the laser beam of the order of 10^{-11} m in a bandwidth of 1 Hz. An electrical heater, mounted on the DPO support, allowed us to control the oscillator temperature. The temperature could be stabilized using an analog proportional integral differential controller. The measured temperature instability (in vacuum) was smaller than 10 mK over several hours.

The resonance frequency (and consequently the spring constant) is a function of the temperature of the oscillator. The temperature dependence of the resonance frequency has been measured, as shown in Fig. 2. The frequency-temperature coefficient, obtained from a linear fit, was found to be −169 mHz/K for a 300-μm-thick oscillator.

In order to determine the quality factor of the mode AS2, the oscillator was driven at resonance by the piezoelectric transducer. The excitation was then turned off. Using a lock-in amplifier the amplitude decay was measured. The result of a typical measurement is shown in Fig. 3(a). The

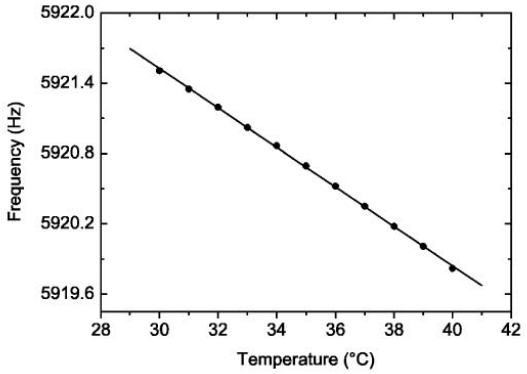

FIG. 2. Dependence of a 300-μm-thick DPO resonance frequency on the temperature.

experimental data were fitted by a single exponential function with a ring-down time τ=23 s, which corresponds to $Q=7.7\cdot10^5$ (oscillator thickness 500 μm). This value exceeds any measurement previously reported in literature. Houston *et al.*[10] have developed a model in which the quality factor of the mode AS2 is calculated assuming that the internal friction is due to the thermoelastic losses associated with a vibrational flexural component of this mode. Under this assumption the quality factor is given by

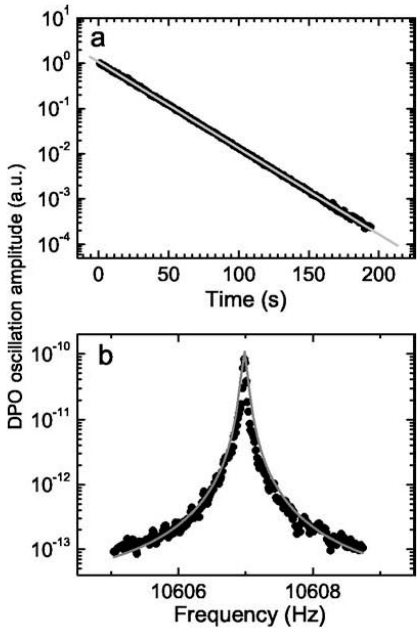

FIG. 3. (a) Ringdown measurement for a 500-μm-thick DPO at room temperature. The resulting decay constant is 23 s, which corresponds to a quality factor of $7.7\cdot10^5$. (b) Spectrum of the same oscillator excited by Brownian noise. The solid line represents a lorentzian fit. The linewidth (FWHM) is 13 mHz.

TABLE I. Experimental characterization of different DPOs. The theoretical resonance frequencies for the mode AS2 are derived from Eq. (1).

Oscillator	1	2	3	4	5
Thickness (μm)	300	300	500	500	500
Measured res. freq. (kHz)	5.9	5.2	8.6	8.9	10.6
Calculated res. freq. (kHz)	5.3	5.3	8.9	8.9	8.9
Q factor at 300 K and 10^{-6} mbar	$2.0\cdot10^5$	$1.3\cdot10^5$	$2.6\cdot10^5$	$3.0\cdot10^5$	$7.7\cdot10^5$

$$Q=\left[p\frac{E\alpha^2T}{\gamma}\frac{\omega_0\delta}{1+(\omega_0\delta)^2}\right]^{-1}, \tag{4}$$

where p is the modal participation factor and is equal to the ratio of vibrational flexural energy relative to total modal energy, E is the Young's modulus, α is the thermal expansion coefficient, γ is the specific heat, ω_0 is the angular frequency of the mode AS2, and δ is the thermal relaxation time is given by

$$\delta=\frac{t^2\gamma}{\pi^2\kappa} \tag{5}$$

with κ as the thermal conductivity. Substituting the material properties of silicon[20] in Eq. (4) and using Eq. (1), it is easy to show that the quality factor of the mode AS2 scales as t^{-3} and is about $2\cdot10^5$ for a 300- μm- thick DPO. This value is in good agreement with our results for the thin oscillators. For the thicker oscillators the measured values are significantly higher than expected from Eq. (4). A possible explanation is a strong reduction in the modal participation factor with increasing thickness, a reasonable assumption, which overcompensates the factor t^{-3}.

The use of a passive vibration isolation system allowed to measure the excitation due to thermal noise. As shown in Fig. 3(b) the resonance curve has a Lorentzian form and its witdth [full width at half maximum (FWHM)] is $\Delta\nu=0.013$ Hz, which implies a quality factor $Q=\nu_0/\Delta\nu=8\cdot10^5$ in good agreement with the results obtained from the ring-down measurement. The measured angular displacement due to the thermal noise is $6.2\cdot10^{-10}$ rad/Hz$^{1/2}$. Hereby, the electronic noise level of the detection system was $1.3\cdot10^{-11}$ rad/Hz$^{1/2}$. The expected value from Eq. (3) is $8.8\cdot10^{-10}$ rad/Hz$^{1/2}$ at resonance. The difference between these values is due to the uncertainty in the material parameters and to the approximations in Eq. (1).

Table I summarizes the results of the characterization of different oscillators. The discrepancies between the calculated and measured resonance frequency are due to variations in the fabrication process. For example photoresist underetching due to a longer duration of the etching step caused the higher resonance frequency of one of the thicker oscillators. A comparison of our oscillators with others described in the literature[21–25] is shown in Fig. 4.

B. Optical actuation

In the past, DPOs were mainly excited by electrostatic techniques. These require a metallic coating on the oscillator and the use of an electrode in the vacuum vessel.[3] In some applications, e.g., detection of small forces, optical actuation represents a suitable alternative. Although already used for different kinds of microoscillators,[13] this approach has not previously been implemented for DPOs. The principle relies on the modulation of the intensity of a laser beam impinging on the oscillator. If the modulation is at the resonance frequency of the DPO, the periodic stress caused by the temperature modulation can couple to the oscillator mode. We have used a He–Ne laser (spot size ~1 mm^2) to excite the DPO. The beam was positioned on the DPOs wing or neck. An acousto-optical modulator driven at the DPO resonance frequency by a signal generator produced a sinusoidal amplitude modulation of the laser beam output power. The modulation depth was nearly 100%.

In Fig. 5(a) the response of the DPO to a rectangular optical excitation signal with a peak power of 10 μW is shown. Figure 5(b) shows that the angular displacement of the oscillator head is proportional to the average power and to the power modulation amplitude of the laser beam. This measurement was for the laser beam impinging on the DPO wing. However, the efficiency of the excitation depends strongly on which part of the oscillator is illuminated. The strongest effect was measured when the laser beam was put on the bridge connecting neck and wings of the oscillator. This dependence allows, at least in principle, the use of previously calibrated DPOs as position sensitive photodetectors or as power meters. By comparing the signal and noise levels in Fig. 5(a), we can estimate that the minimum detectable power for a 300-μm-thick DPO is 10 nW in a bandwidth of 0.1 Hz. Its sensitivity could be enhanced through a strongly absorbing coating on the DPOs most sensitive area, which, where appropriate, could be also chosen to widen the spectral range of the detector. Figure 5(c) shows the effect of two counter-propagating beams impinging on opposite sides of

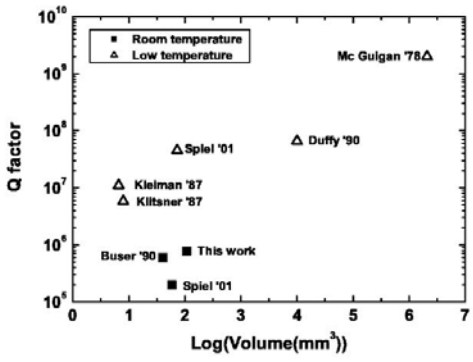

FIG. 4. Comparison of the quality factors of different macroscopic mechanical oscillators. (Picture adapted from Ref. 21.)

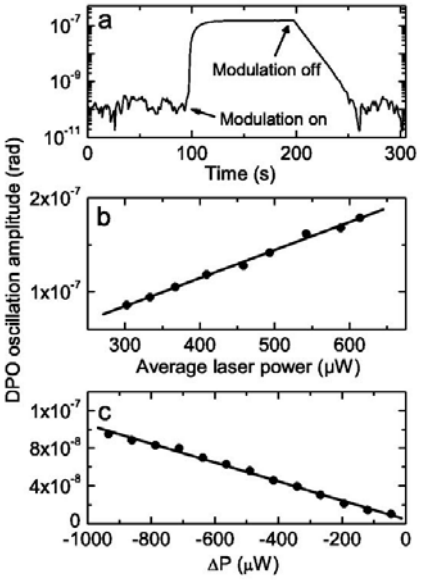

FIG. 5. (a) Response of the oscillator to laser power modulation, that was turned on at $t=93$ s and off at $t=195$ s. The fluctuations in the signal amplitude occuring when the laser is off, are due to Brownian noise of the oscillator. Lock-in time constant was 0.3 s. (b) Optical excitation of a DPO by a leaser beam modulated at the oscillator's resonance frequency. (c) Optical excitation of a DPO by two counterpropagating laser beams, that impinge on the oscillator's wing. ΔP is the difference in the optical power of the beams.

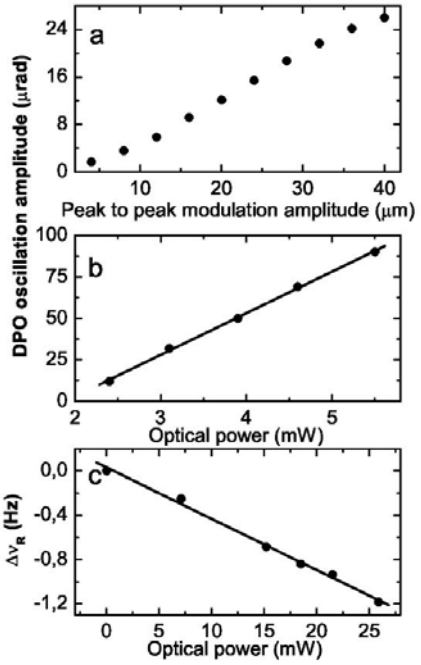

FIG. 6. (a) Excitation of a DPO by a laser beam scanned on the region connecting the wings to the leg. The laser power was 5 mW. (b) DPO excited by a position modulated laser beam. Here the scan amplitude is constant (40 μm), but the laser power is varied. (c) $\Delta\nu_R$ is the shift of the resonance frequency induced by a continuous wave laser beam illuminating the neck of a 300-μm-thick DPO.

the oscillator (see also Ref. 26). The angular oscillation amplitude of the DPO vanishes if the difference of the average power of the laser beams is equal to zero.

A second optical excitation method has also been studied. In this case the laser beam impinging on the oscillator had a constant average power, but its position was modulated. This was obtained by mounting a mirror on a piezoactuator driven at the resonance frequency of the AS2 mode. The laser beam reflected by the oscillating mirror onto the DPO causes a position dependent temperature modulation, which excites the oscillator. The DPO oscillation amplitude as a function of the scan amplitude is shown in Fig. 6(a). The laser optical power in this case was 5 mW. The DPO amplitude was found to be about 500 times larger than the thermal noise at room temperature. Figure 6(b) shows that the DPO amplitude is proportional to the optical power of the laser beam used for the excitation.

The DPO can also be frequency tuned by the laser. This was accomplished by illuminating the neck of the DPO with a laser beam with a constant output power. As shown in Fig. 6(c) the resonance frequency of a 300-μm-thick DPO is a linear function of the laser beam average power. The measured frequency-power coefficient is −50 Hz/W. The optical power required to shift the DPO resonance frequency of $\Delta\nu=\nu_0/Q=0.03$ Hz is 0.6 mW.

ACKNOWLEDGMENTS

The authors wish to thank M. Weingran, B. Sanvee (for their experimental help), Professor R. Pohl (for providing them with paddles in the initial phase of this work), C. L. Spiel (for helpful discussions), D. Püttjer, M. Schneider, the staff of the Center for Semiconductor and Optoelectronics (ZHO) of the University of Duisburg, P. Dutkiewicz, R. Gusek, H. Hoffmann, W. Kussmaul, and W. Röckrath (for their technical support). One of the authors (L.H.) gratefully acknowledges the DAAD for a fellowship and V. White for proofreading this manuscript.

[1] Y. Martin and H. K. Wickramasinghe, Appl. Phys. Lett. **50**, 1455 (1987).
[2] B. E. White and R. O. Pohl, Phys. Rev. Lett. **75**, 4437 (1995).
[3] P. Rösner, K. Samwer, R. O. Pohl, and S. Schneider, Rev. Sci. Instrum. **74**, 3395 (2003).
[4] R. D. Biggar and J. M. Parpia, Rev. Sci. Instrum. **69**, 3558 (1998).
[5] I. Tittonen *et al.*, Phys. Rev. A **59**, 1038 (1999).
[6] D. F. McGuigan, C. C. Lam, R. Q. Gram, A. W. Hoffman, D. H. Douglas, and H. W. Gutche, J. Low Temp. Phys. **30**, 621 (1978).
[7] R. N. Kleiman, G. K. Kaminsky, J. D. Reppy, R. Pindak, and D. J. Bishop, Rev. Sci. Instrum. **56**, 2088 (1985).
[8] C. L. Spiel, R. O. Pohl, and A. T. Zehnder, Rev. Sci. Instrum. **72**, 1482 (2001).
[9] X. Liu, J. F. Vignola, D. M. Photiadis, A. Sarkissian, B. H. Houston, R. D. Merithew, and R. O. Pohl, presented at the *Tenth International Conference on Phonon Scattering in Condensed Matter, 2001*.
[10] B. H. Houston, D. M. Photiadis, M. H. Marcus, J. A. Bucaro, X. Liu, and J. F. Vignola, Appl. Phys. Lett. **80**, 1300 (2002).
[11] J. C. Price, in *Proceedings of the International Symposium on Experimental Gravitational Physics*, edited by P. Michelson, H. En-ke, G. Pizzella, and D. Reidel, Dordrecht, 1987.
[12] L. Haiberger, M. Weingran, H. Wenz, and S. Schiller, in *Proceedings of the Tenth Marcel Grossmann Meeting on General Relativity*, edited by M.

Novello, S. Perez-Bergliaffa and R. Ruffini (in press).
[13] See for example T. Kobayashi, T. Hara, J. Ohsawa, and N. Yamaguchi, Rev. Sci. Instrum. **7**, 2651 (2002).
[14] X. Liu, S. F. Morse, J. F. Vignola, D. M. Photiadis, A. Sarkissian, M. H. Marcus, and B. H. Houston, Appl. Phys. Lett. **78**, 1346 (2001).
[15] R. E. Mihailovich, Ph.D. thesis, Cornell University, 1992.
[16] J. C. Greenwood, J. Phys. E **21**, 1114 (1988).
[17] I. Szabo, *Höhere Technische Mechanik* (Springer, Berlin, 1977).
[18] P. R. Saulson, Phys. Rev. D **42**, 2437 (1990).
[19] T. H. Metcalf, Ph.D. thesis, Cornell University, 2002.
[20] *Properties of Silicon*, EMIS Datareview Series No. 4, edited by T. K. Ning (INSPEC, New York, 1988).
[21] P. Mohanty, D. A. Harrington, K. L. Ekinci, Y. T. Yang, M. J. Murphy, and M. L. Roukes, Phys. Rev. B **66**, 085416 (2002).
[22] W. Duffy, J. Appl. Phys. **68**, 5601 (1987).
[23] T. Klitsner and R. O. Pohl, Phys. Rev. B **36**, 6551 (1987).
[24] R. N. Kleiman, G. Agnolet, and D. J. Bishop, Phys. Rev. Lett. **59**, 2079 (1987).
[25] R. A. Buser and N. F. de Rooij, Sens. Actuators, A **21**, 323 (1990).
[26] O. Marti, A. Ruf, M. Hipp, H. Bielefeldt, J. Colchero, and J. Mlynek, Ultramicroscopy **42–44**, 345 (1992).

Appendix B

A highly sensitive silicon crystal torque sensor operating at the thermal noise limit

L. Haiberger, M. Weingran, S. Schiller

Institut für Experimentalphysik, Heinrich-Heine-Universität Düsseldorf, Universitätsstrasse 1, 40225 Düsseldorf, Germany

December 6, 2006

Abstract

We describe a sensitive torque detector, based on a silicon single-crystal double-paddle oscillator (DPO). The high Q-factor ($\sim 10^5$ at room temperature and in vacuum) makes DPOs well suited for the detection of weak forces. The limiting sensitivity of a sensor is given by Brownian (thermal) noise if all external disturbances are eliminated. In this case, the minimum detectable force can be decreased by measuring over a time significantly longer than the oscillator's relaxation time. We demonstrate operation in this regime, with integration times of up to 14 hours. A resulting torque sensitivity of $2 \cdot 10^{-18}$ Nm is reached. Tests are performed to show that the sensor is only affected by thermal noise. The present sensor is well suited for measurements of extremely weak forces, e.g. of gravitational attraction between laboratory masses.

1 Introduction

One of the first measurements of the Brownian motion of a mechanical oscillator goes back to Gerlach in 1927, who studied the torsional Brownian noise of a small mirror attached to a very fine wire [1]. A theoretical analysis of this phenomenon was provided by Uhlenbeck and Goudsmith in 1929 [2]. A deeper understanding of the origin of Brownian noise was developed by Nyquist, who pointed out the existence of a connection between stochastic motion and the internal mechanical loss of the material [3]. A further generalization of this concept was given by Callen and Welton, through the Fluctuation-Dissipation Theorem [4].

In the last decade the relevance of mechanical oscillators for precision measurements of weak forces has steadily grown [5]. The detection of the Casimir force [6], 3D-microscopy with sub-nm resolution [7] and attogram mass detection [8] are some of the most recent examples of the results achieved by the use of mechanical oscillators in high precision experiments. Particularly challenging applications of ultrasensitive force sensors are tests of Newton's law at small distance [9, 10, 11, 12, 13, 14] and optical measurements of small displacements [15, 16]. In many cases, Brownian noise of the detector represents the desirable ultimate limit to their sensitivity. A review of the measurement and data analysis strategies, developed to improve the sensitivity of these detectors, can be found in the work by Ritter *et al.* [17].

In the present work we report on a torque sensor based on a single crystal silicon oscillator, the double-paddle oscillator (DPO). This sensor type, originally developed to measure internal friction of thin films [25, 26], is very well suited to the measurement of weak forces because of its high Q-factor. Under vacuum operation and at room temperature, it is possible to detect and characterize its Brownian motion, which is due to the scattering of phonons.

The paper is structured as follows. We briefly review the theory of Brownian motion for a torsional oscillator, relevant for comparing the measured force sensitivity with the thermal noise limit. Based on this theory we discuss the measurement procedure for detection of a weak time-harmonic force in presence of stochastic noise. Then, we review the main properties of the microfabricated DPOs and describe the experimental apparatus. The experimental results are given in the last section, which also describes tests that demonstrate that the measured noise is consistent with Brownian noise.

2 Theory of Brownian noise

A simple model can describe the angular fluctuations of a torsional oscillator due to Brownian noise and is suitable for characterizing the sensitivity of a variety of precision experiments, e.g. weak force sensors and gravitational wave detection [18].

The equation of motion of a harmonic torsional oscillator driven by Brownian noise is

$$I\ddot{\vartheta} + \beta\dot{\vartheta} + D\vartheta = M(t) \ , \tag{1}$$

where I is the moment of inertia around the torsion axis, ϑ is the angular deflection of the oscillator, β is the damping coefficient, D is the spring constant, and M is a fluctuating torque. Eq. (1) is a Langevin equation for a simple harmonic oscillator of frequency $\omega_R^2 = D/I$. We assume that $M(t)$ has the following properties:

i) zero mean value,

ii) its variance is a constant in time: $\overline{M^2(t)} = const.$,

iii) its values at two different times are uncorrelated.

The angular fluctuations of an oscillator excited by such a stochastic torque do not obey the statistics of pure random noise. This is a consequence of the correlations introduced by the oscillator. If the oscillator's deflection at time t_0 is $\vartheta(t_0)$, the probability distribution of its deflection at a later time t is given by [19]

$$P\left[\vartheta(t) \mid \vartheta(t_0)\right] = \frac{\vartheta(t)}{\overline{\vartheta^2}(1-e^{-2t/\tau})} I_0\left(\frac{\vartheta(t)\vartheta(t_0)e^{-t/\tau}}{\overline{\vartheta^2}(1-e^{-2t/\tau})}\right) \exp\left[-\frac{\vartheta^2(t)+\vartheta_0^2(t)e^{-t/\tau}}{2\overline{\vartheta^2}(1-e^{-2t/\tau})}\right], \tag{2}$$

where $\tau = 2I/\beta$ is the mechanical relaxation time of the oscillator, $\overline{\vartheta^2}$ is the mean square deflection, and I_0 is the modified Bessel function.

If the oscillator is excited by an external harmonic torque at the oscillator's resonance frequency, $\Gamma = \Gamma_0 \sin(\omega_R t)$, the minimum detectable torque amplitude can be derived using Eq.(2) and is given by [19, 20, 21]

$$(\Gamma_0)_{\min} = \pi\sqrt{\frac{k_B T I}{\tau \Delta t}} = \pi\sqrt{\frac{k_B T I \omega_R}{2Q\Delta t}}, \tag{3}$$

if the measurement time Δt is smaller than the oscillator relaxation time τ. Here, the Q-factor has been introduced through $\tau = 2Q/\omega_R$. The improvement of torque sensitivity with increasing measurement time can easily be pictured. During the measurement time the response of the oscillator to the external force increases steadily due to the phenomenon of resonance, whereas the response due to Brownian noise fluctuates. This is the

regime in which the most sensitive torsion pendula operate [21], whose relaxation times are of the order $10^6 \div 10^9$ s. A detailed analysis of the sensitivity of torsion pendula can be found in the book by Chen and Cook [22].

Increasing the measurement time Δt beyond τ does not lead directly to an improved torque sensitivity unless an appropriate data analysis is performed [5, 22]. Following Uhlenbeck and Goudsmit [2], it is necessary to develop the measured angular displacement in a Fourier series, $\vartheta(t) = \sum_k \vartheta_k(t)$, where the index $k = 0, ..., \infty$ denotes the frequency harmonics $\omega_k = 2\pi k/\Delta t$. We first consider the oscillator motion in absence of external torque. The term k' of the series at the oscillator's resonance frequency is the one of interest. The time average of $(\vartheta_{k'}(t))^2$ depends on the measurement time as

$$\overline{\vartheta_{k'}^2} = \frac{4\, k_B T Q}{I \omega_R^3 \Delta t} \,. \tag{4}$$

Each quadrature amplitude of $\vartheta_{k'}$ then also averages to zero, as $(\Delta t)^{-1/2}$ for $\Delta t \gg 4Q/\omega_R$. A similar result can be obtained applying Nyquist's theorem [18]. The potential energy of the oscillator, in absence of external excitation, can be calculated from Eq. (4) and, as shown in Ref. [2], is constant and independent of the observation time as expected from the equipartion theorem.

The signal-to-noise ratio of a measurement of a resonant torque of amplitude Γ_0 is defined as the ratio between the corresponding steady-state oscillator amplitude and the Brownian noise amplitude given by Eq. (4). Setting this ratio equal to unity yields the minimum detectable torque in the case $\Delta t \gg \tau$,

$$(\Gamma_0)_{\min} = \sqrt{\frac{4\, k_B T I \omega_R}{Q \Delta t}}. \tag{5}$$

Thus, the minimum detectable torque decreases with the square root of the measurement duration. The validity of this analysis is limited to the case of noise with white spectrum. An example of weak (gravitational) force detection using detection of the oscillator amplitude at the resonance frequency is given in ref. [9].

It is interesting to consider the statistical properties of the oscillator's response. In the following analysis we assume that the deflection of the oscillator is measured by a lock-in technique where the local oscillator is tuned to the oscillator's resonance frequency. This yields the slowly varying amplitude $r(t)$ and phase $\psi(t)$ of the oscillator's deflection $\vartheta(t) = r(t)\cos(\omega_R t - \psi(t))$. The quadrature amplitudes $X(t) = r(t)\cos\psi(t)$ and $Y(t) = r(t)\sin\psi(t)$ can then be calculated. In steady-state, the probability distribution function

for these two quantities is given by $W(X,Y) = W(X)W(Y)$, where [23]

$$W(X) = \left(\frac{I\omega_R^2}{2\pi k_B T}\right)^{\frac{1}{2}} \exp\left(-\frac{I\omega_R^2}{2k_B T}X^2\right). \tag{6}$$

From Eq. (6) it follows that both quadratures have vanishing mean value, while their variance is equal to $k_B T/I\omega_R^2$, as expected from the equipartion theorem.

3 Experimental results

3.1 Description of apparatus

Single-crystal silicon has low internal friction and a large knowledge exists concerning its fabrication into appropriate geometries. These two properties make it the favourite material for mechanical sensors in many reasearch fields. Our oscillator was developed for an experiment to detect gravity at short (< 1 mm) distances [14]. The design we used was developed by Kleiman and coworkers [25] and later improved by Pohl and cowokers [26], who used it for characterizing the elastic properties of thin films. The oscillator is shown in Fig. 1. It was fabricated from a 300 μm thick, float-zone refined, double-side polished, $\langle 100 \rangle$- oriented, p-doped silicon wafer with a room-temperature specific resistance larger than 10 kΩ·cm. The fabrication procedure was developed in our group and is based on wet etching [27]. The sensor consists of two masses, head and wings, connected by a torsion rod, the neck. The wings are themselves connected to a base (foot) by a thinner rod, the leg. The vibrational modes of this structure have been fully characterized in the range between 0.1 and 10 kHz [26]. In the present work a torsional mode, denoted by AS2 in the literature, was used. In this mode the head oscillates twisting the neck, while the wings' motion is out of the oscillator's plane around an axis orthogonal to the neck length. The resonance frequency ν_R of the AS2 mode of the oscillator was $\nu_R = (5921.303 \pm 0.003)$ Hz and its quality factor was $Q = (1.86 \pm 0.02) \cdot 10^5$, which corresponds to a relaxation time τ =10 s. The full width of the resonance curve at half-power was $\Delta\nu = \nu_R/Q = 0.033$ Hz. In our experiment the oscillator's base was glued on an aluminium holder, which contained a heating element, a temperature sensor, and a set of distance detectors. The DPO holder rested on a passive vibration isolation stage made of alternating steel disks and silicon gel dampers. The use of this vibration isolation system allowed us to strongly reduce the influence of external disturbances on the oscillator, e.g. seismic noise. A piezoceramic actuator, mounted on the lowest stage of the vibration isolation system, was used for

excitation and permitted diagnostics (determination of resonance frequency and Q-factor) and sensitivity studies. The apparatus was operated in a vacuum chamber at a pressure of about 10^{-7} mbar. The pressure in the vacuum vessel was constantly monitored during the complete duration of the measurement, since its variation could have induced a change the Q-factor of the DPO.

The detection of the angular deflection of the DPO's head was performed by an optical lever. It consisted of a He-Ne laser beam that was reflected by the oscillator head onto a position-sensitive (split) photodiode. The resolution of this detection system was about $3{\cdot}10^{-11}$ rad in a 1 Hz measurement bandwidth. As shown in our previous work [27], the stabilization of the DPO temperature is necessary in order to minimize oscillator frequency drift and thus maximize the effects of an external constant-frequency excitation. Using a PID controller, we reduced the temperature instability to the level of 0.08 K over several hours, which corresponds to a resonance frequency instability of about 0.01 Hz.

The measurements analyzed below were taken in several consecutive runs for a total of $3.4{\cdot}10^5$ s. The detection of the oscillator's angular displacement was perfomed by a digital dual-phase lock-in amplifier, with a local oscillator frequency set to allow measurement of the quadratures $X(t)$ and $Y(t)$. The bandwidth of the lock-in amplifier was set equal to 0.8 Hz (corresponding to a lock-in time constant of $\tau_L = 0.3$ s) and the data was acquired at a rate of 1 Hz. A run was divided into blocks where each block consisted of the following steps. First, the oscillator response was detected during 600 s, while an external excitation was applied. The external excitation was then switched off and after waiting 100 s, necessary for the oscillator to reach equilibrium, a measurement without excitation was taken over another 600 s. Then, the (slowly drifting) resonance frequency was determined by exciting the DPO with a fixed voltage at a few different frequencies and fitting the measured amplitude to a Lorentz curve. Once this procedure was completed, the resonant excitation was modified, if necessary, and the next block started.

In order to determine the influence of the detection system noise, the quadratures $X(t)$ and $Y(t)$ were also measured in absence of external excitation and with the local oscillator frequency tuned 1 Hz below the DPO resonance. These measurements were performed in a single run with a duration of $2{\cdot}10^5$ s.

3.2 Characterization of thermal noise

In order to characterize the measured oscillator deflection noise, we first analyzed the data taken in absence of external excitation. This data was considered as taken all in a single measurement without dead time between the single runs [24]. Fig. 2 displays the statistics of the X quadrature for two different acquisition times, 2500 s and $1.7{\cdot}10^5$ s. In both cases the experimental data was fitted to Eq. (6), with the exponents as fit parameters. The plots of the fit residuals show how the agreement with theory improves for increasing measurement time, as expected. Also, the noise of the detection system was found to be approximately 50 times smaller than the thermal noise of the DPO, using the procedure described above. Assuming the statistics to be indeed due to Brownian noise, from the fits it is possible to obtain the torsion constant of the oscillator, $D = (8.04 \pm 0.06) \cdot 10^{-2}\,\mathrm{Nm}$. The torsion constant can be also be calculated approximately from the oscillator's dimensions and is given by [28]

$$D = \xi \frac{ab^3}{c} G, \tag{7}$$

where ξ is a parameter depending on the geometry of the oscillator, equal to 0.25 in our case, $a = 6.85\,\mathrm{mm}$ is the full width of the oscillator's head, $b = 0.3\,\mathrm{mm}$ is the thickness, and $c = 1.09\,\mathrm{mm}$ is the neck width. The calculated torsion constant is $D = 7.7 \cdot 10^{-2}\,\mathrm{Nm}$, in good agreement with the value obtained from the noise data. This confirms that the observed noise is Brownian noise.

3.3 Detection of weak torques

In order to determine the torque sensitivity of the sensor, a small harmonic excitation was applied to the oscillator, as previuosly described. This was implemented by applying a small ac voltage at the sensor's resonance frequency to the piezoceramic actuator mounted on the vibration isolation system. The excitation voltage was generated by a frequency synthesizer phase-locked to the local oscillator used for the lock-in detection. In order to determine the correspondence between voltage and torque, the excitation was made large enough to produce an easily detectable deflection, which was converted into a torque value by multipling it with the experimentally determined spring constant. In doing so, we made sure that the piezo actuator's response was linear in the range used. In the following we used an external excitation corresponding to a torque $\Gamma_0 = 4.3 \cdot 10^{-18}\,\mathrm{Nm}$ and its phase was chosen equal to the local oscillator phase. According to the theory of section II, this torque should be detectable for integration times exceeding approx. $1{\cdot}10^4$

s.

Fig. 3 shows the mean values of the X quadrature as a function of the averaging time. Note that the mean of the lock-in measurements is the time average of the Fourier amplitude of X at the DPO's resonance frequency. In calculating these mean values we assumed that the dead times between successive runs do not introduce any deviation, in analogy to the case illustrated in the previous section. Since each sample was taken over 0.3 s, the "true" total integration time corresponds to $5.1{\cdot}10^4$ s. The shown error bars are equal to ± 3 standard deviations of the mean value, calculated from the individual data points. The mean quadrature amplitude corresponds to, after subtracting the detection system noise, an excitation torque of $4.4{\cdot}10^{-18}$ Nm, in good agreement with the expected level.

For comparison, the figure also displays the mean X quadrature in absence of mechanical excitation. As can be seen, the presence of an external excitation is masked by noise for averaging times shorter than $7{\cdot}10^3$ s, whereas it is visible for longer averaging, in accordance with the above estimate. Statistical testing was done to determine if the presence of the external signal resulted in a significant difference of the two sets of data. The result of a t-test for $2.5{\cdot}10^4$ samples indicated that the mean quadratures are statistically different with a significance level of 95%.

From the experimental data, we can estimate the minimum detectable torque as follows. The full data set is divided into 20 equally long subsets. The standard deviation of the subset mean values may be identified with the thermal amplitude noise, $1.3 \cdot 10^{-12}$ rad. As criterion for the minimum detectable torque we consider the torque equivalent to twice this deflection noise value, $1.3 \cdot 10^{-18}$ N m. This holds for an integration time of $2.5{\cdot}10^3$ s. Extrapolation to an integration time of $5.1 \cdot 10^4$ s (the whole data set length), yields $2.8 \cdot 10^{-19}$ N m. The theoretical value for this quantity, from Eq. (5) corrected by a factor $1/\sqrt{2}$ for the case of detection of a single quadrature, is $1.3{\cdot}10^{-18}$ Nm, a factor 5 larger than the extrapolated experimental value. The origin of this difference is unclear.

In conclusion, we have shown that it is possible to detect weak torques on the order of few 10^{-18} N m by using a macroscopic single-crystal oscillator (sensitive area of 12.5 mm^2), which can easily be fabricated in clean-room facilities. Moreover, we have experimentally reached the thermal-noise limited sensitivity of the detector. In particular, we showed that the measuremed noise level is in general agreement with Brownian noise theory. Thus, our apparatus represents a suitable approach for the detection of gravity-like new forces at short distances, a project studied in our laboratory. Moreover, the sensor could also be employed for the detection of classical, e.g. magnetic forces.

Acknowledgements

We thank Prof. D. Jäger and the staff at the Center for Solid-State Electronics and Optoelectronics of the Universität Duisburg-Essen for generously supporting the fabrication of the DPO used in this work. This work was supported by the Gerhard-Hess program of the German Science Foundation.

References

[1] W. Gerlach, Naturwiss. **15**, 15 (1927)

[2] G. E. Uhlenbeck and S. Goudsmit, Phys. Rev. **34**, 145 (1929)

[3] H. Nyquist, Phys. Rev. **32**, 110 (1928)

[4] H. B. Callen and T. A. Welton, Phys. Rev **83**, 34 (1951); H. B. Callen and R. F. Greene, Phys. Rev **86**, 702 (1952)

[5] R. C. Ritter, L. I. Winkler, and G. T. Gillies, Meas. Sci. Technol. **10**, 499 (1999)

[6] H. B. Chan, V. A. Aksyuk, R. N. Kleiman, D. J. Bishop, and F. Capasso, Phys. Rev. Lett. **87**, 211801 (2001)

[7] See for example: Proc. of the 6th International Conference on Noncontact Atomic Force Microscopy 2001 in Dingle, Ireland, published in: Nanotechnology 15, S40-S43 (2004).

[8] B. Ilic, H. G. Craighead, S. Krylov, W. Senaratne, C. Ober, and P. Neuzil, J. Appl. Phys. **95**, 3694 (2004)

[9] Y. Ogawa, K. Tsubono, and H. Hirakawa, Phys. Rev. D **26**, 729 (1982)

[10] D. E. Krause and E. Fischbach, "*Searching for Extra Dimensions and New String-Inspired Forces in the Casimir Regime*," in *Gyros, Clocks and Interferometers...: Testing Relativistic Gravity in Space*, edited by C. Lammerzahl, C. W. F. Everitt, and F. W. Hehl (Springer-Verlag, Berlin, 2001)

[11] C.D. Hoyle, U. Schmidt, B. R. Heckel, E. G. Adelberger, J. H. Gundlach, D. J. Kapner, H. E. Swanson, Phys. Rev. Lett. **86**, 1418 (2001)

[12] J. C. Long, H. W. Chan, A. B. Churnside, E. A. Gulbis, M. C. M. Varney, and J. C. Price, Nature **421**, 922-925 (2003)

[13] J. Chiaverini, S.J. Smullin, A. A. Geraci, D. M. Weld, and A. Kapitulnik, Phys. Rev. Lett. **90**, 151101 (2003)

[14] L. Haiberger, M. Weingran, H. Wenz, and S. Schiller, *An Experiment to Detect Gravity at Sub-mm Scale with High Q Mechanical Oscillators*; to appear in Proceedings of the Tenth Marcel Grossmann Meeting on General Relativity, edited by M. Novello, S. Perez-Bergliaffa and R. Ruffini, World Scientific, Singapore (2005), [arXiv:hep-ph/0510211]

[15] Y. Hadjar, P. F. Cohadon, C. G. Aminoff, M. Pinard, and A. Heidmann, Europhys. Lett. **47**, 545 (1999)

[16] I. Tittonen, G. Breitenbach, T. Kalkbrenner, T. M üller, R. Conradt, S. Schiller, E. Steinsland, N. Blanc, and N. F. de Rooij, Phys. Rev. A **59**, 1038 (1999)

[17] G. T. Gillies, and R. C. Ritter, Rev. Sci. Instrum. **64**, 283 (1993)

[18] P. R. Saulson, Phys. Rev. D **42**, 2437-2445(1990)

[19] V. B. Braginsky and A. B. Manukin, *Measurement of Weak Forces in Physics Experiments*, Chicago Press, Chicago (1997)

[20] C. W. McCombie, Rep. Prog. Phys. **16**, 266 (1953)

[21] V. B. Braginsky, C. M. Caves, and K. S. Thorne, Phys. Rev. D **15**, 2047 (1977)

[22] Y. T. Chen and A. H. Cook, *Gravitational experiments in the laboratory*, Cambridge Univ. Press (1993)

[23] S. Chandrasekhar, Rev. Mod. Phys. **15**, 1 (1943)

[24] D. W. Allan, IEEE Trans. Instrum. Meas. **IM-36**, 646 (1987)

[25] R.N. Kleiman, G.K. Kaminsky, J.D. Reppy, R. Pindak, and D.J. Bishop, Rev. Sci. Instrum. **56**, 2088 (1985)

[26] C.L. Spiel, R.O. Pohl, and A.T. Zehnder, Rev. Sci. Instrum **72**, 1482 (2001)

[27] L. Haiberger, D. Jäger, and S. Schiller, Rev. Sci. Instrum. **76**, 045106 (2005)

[28] R. E. Mihailovich, *Low Temperature Mechanical Properties of Boron-Doped Single-Crystal Silicon,* PhD Thesis, Cornell University (1992)

Figure 1: The single-crystal silicon double-paddle oscillator used in this work. The thickness is approx. 300 μm.

Figure 2: Histograms of the oscillator's X angular displacement quadrature measured at resonance and in absence of external excitation for two different measurement durations: (a) $2.5{\cdot}10^3$ s and (b) $1.7{\cdot}10^5$ s. The continuous curves represent Gaussian fits. (c) and (d) show the fit residuals.

Figure 3: The mean values of the oscillator's X quadrature, measured with and without a small external mechanical excitation ($4.3{\cdot}10^{-18}$ Nm), as a function of integration time. Each sample corresponds to 0.3 s measurement time. The shown error bars correspond to ± 3 standard deviations of the mean values of the individual lock-in readings.

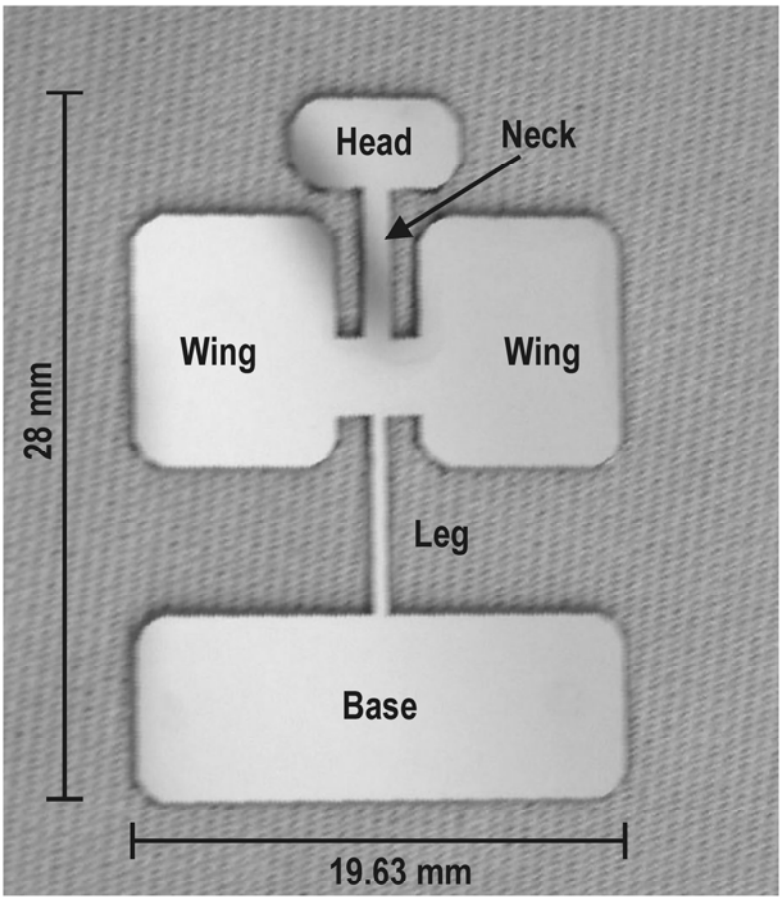

Figure 1

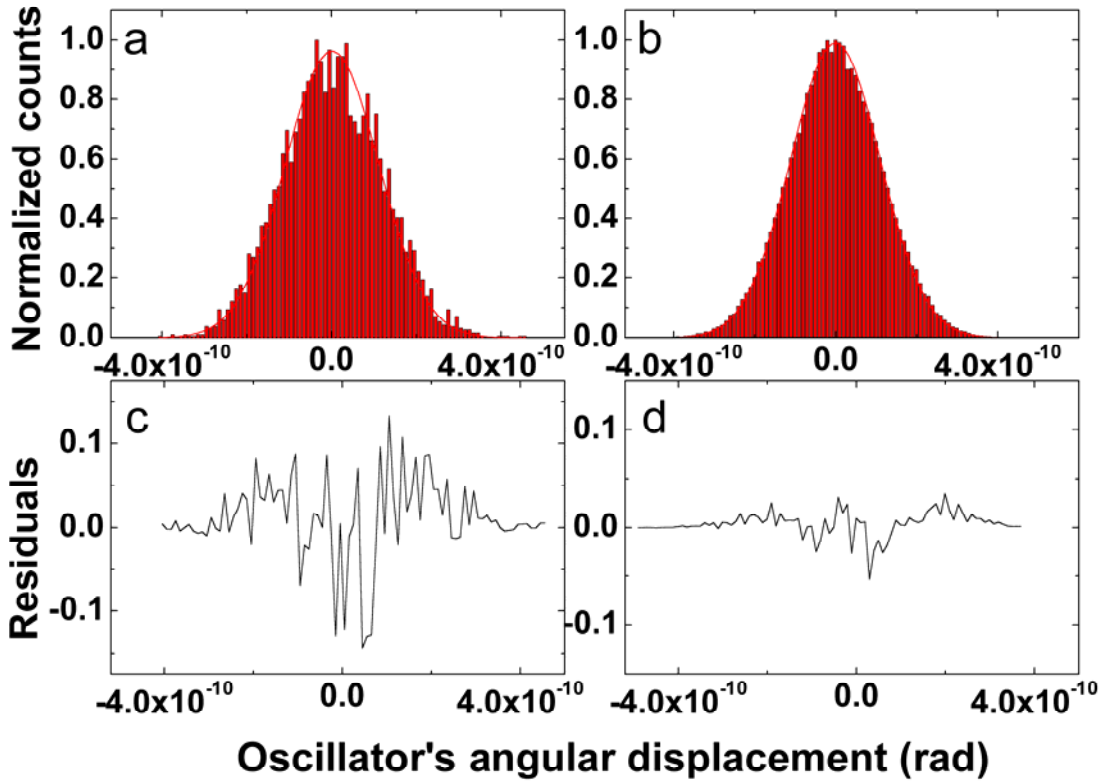
Normalized counts
a
b
c
d
Residuals
1.0
0.8
0.6
0.4
0.2
0.0
0.1
-0.1
-4.0x10-10
0.0
4.0x10-10
Oscillator's angular displacement (rad)

Figure 2

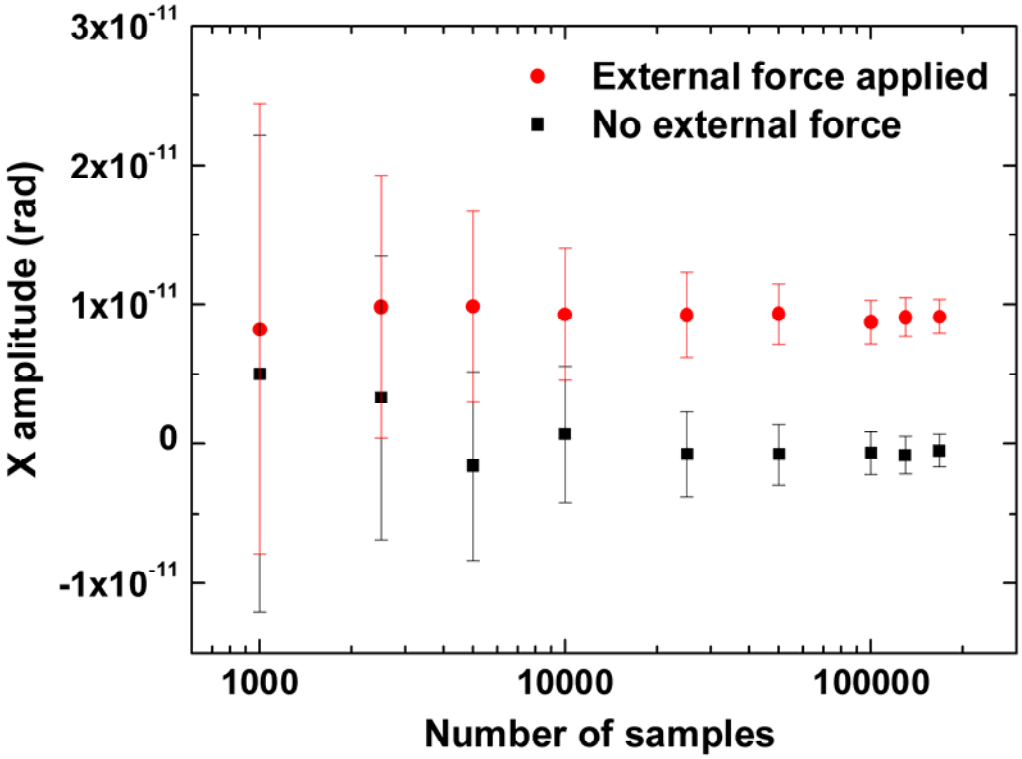
3x10-11
2x10-11
1x10-11
0
-1x10-11
X amplitude (rad)
External force applied
No external force
1000
10000
100000
Number of samples

Figure 3

Acknowledgements

This work was made possible through the contributions of many people, who I would like to thank personally.

Firstly, I would like to thank Prof. Stephan Schiller for giving me the opportunity of working on an interesting and challenging project. During the years spent in his group I was able to benefit from his great knowledge of both experimental and theoretical physics. I also feel privileged to have had the possibility of attending various different international conferences.
For a pleasant working atmosphere, many interesting discussions and useful suggestions, I would like to thank the current and former scientific staff of the Institute of Experimental Physics of the University of Düsseldorf, especially Ulf Fröhlich, Alexander Ostendorf, Piergiorgio Antonini, Bernhard Roth, Roland Wilke, Claus Lämmerzahl, Frank Müller, Hartmuth Borawksi, Ertan Göklü, Pino Ruoso, and Ingo Ernsting.
A special thanks also goes to Rita Gusek, Jens Bremer, Peter Dutkiewicz, Heinrich Hoffman, and Waldemar Kussmaul for their valuable technical help.
I am grateful to Norbert Lümmen for helping me in the crucial start-up phase of this experiment, and for being the first diploma student to work on this project.
The excellent work of Michael Weingran also deserves a special mention. The electronics he developed for this experiment, together with his commitment (not to mention his sense of humor!) enabled us to make some valuable progress in our research.
Prof. D. Jäger and the staff of the ZHO (Zentrum für Halbleiter- und Optoelektronik, Universität Duisburg-Essen) also deserve a mention for giving me the opportunity to microfabricate the DPOs.
A significant contribution to this work was given by Prof. Robert O.Pohl, who provided us with the first DPOs, and introduced me to Christoph L. Spiel, who I would like to thank for his precious advice on the microfabrication of the DPOs.
I wish to extend a special thanks to Benjamin Sanvee and Götz Lehmann for much experimental work, and for making many 3D sketches of our experiment.
Prof. J. Mlynek and the many members of his group, especially Jürgen Schoser and Dominik Schneble, gave me a lot of support during my stay at the University of Konstanz, greatly enhancing my first experiences of German university life.
I would like to thank the DAAD for helping to finance this work with a grant.
Last but not least, without the loving support and encouragement of Victoria and my family, none of this would have been possible.
My apologies go to all the people I may have forgotten to mention here, but who contributed in some way to this project.

Die hier vorgelegte Dissertation habe ich eigenständig und ohne unerlaubte Hilfe angefertigt. Die Dissertation wurde in der vorgelegten oder in ähnlicher Form noch bei keiner anderen Institution eingereicht. Ich habe bisher keine erfolglosen Promotionsversuche unternommen.

Düsseldorf, den 15.12.2006

(Luca Haiberger)